DOE/NASA/0004-79/1

NASA-CR-159654

DDA EDR 9790

SINGLE SHAFT AUTOMOTIVE GAS TURBINE ENGINE CHARACTERIZATION TEST

R. A. Johnson
Detroit Diesel Allison
Division of General Motors Corporation

September 1979

(NASA-CR-159654) SINGLE SHAFT AUTOMOTIVE GAS TURBINE ENGINE CHARACTERIZATION TEST Final Report (Detroit Diesel Allison, Indianapolis, Ind.) 103 p HC A06/MF A01 CSCL 13F G3/85

N79-32129

Unclas
35753

Prepared for

NATIONAL AERONAUTICS AND SPACE ADMINISTRATION
Lewis Research Center
Under Contract DEN 3-4

For
U. S. DEPARTMENT OF ENERGY

Conservation and Solar Applications
Office of Transportation Programs

DOE/NASA/0004-79/1
NASA CR-159654
DDA EDR 9790

SINGLE SHAFT AUTOMOTIVE GAS TURBINE ENGINE CHARACTERIZATION TEST

R. A. Johnson
Detroit Diesel Allison
Division of General Motors Corporation
Indianapolis, IN 46206

September 1979

Prepared for
NATIONAL AERONAUTICS AND SPACE ADMINISTRATION
Lewis Research Center
Cleveland, Ohio 44135
Under Contract DEN 3-4

For
U.S. DEPARTMENT OF ENERGY
Conservation and Solar Applications
Office of Transportation Programs
Washington, D.C. 20545
Under Interagency Agreement EC-77-A-31-1040

FOREWORD

Work accomplished on this contract was performed by a large group of people at Detroit Diesel Allison Division of General Motors Corporation. Principal contributors to this work were:

Design Activities:	B. C. Hall, Leonard Lindgren, David Decker
Test Activities:	E. S. Barc, David Hall, Donald Wilson
Materials:	Donald Schreiner, D. R. Betner
Controls Activities:	Dennis Schroff, Robert Nelson, Wayne Waggoner
Performance Analysis:	James Wooten, Terry Knickerbocker
Program Administration:	W. Southard, Joseph Rees
Program Management and Reporting:	R. E. Cutler, Richard Johnson, James Stieff

TABLE OF CONTENTS

TABLE OF CONTENTS (cont)

LIST OF ILLUSTRATIONS

LIST OF ILLUSTRATIONS (cont)

LIST OF TABLES

SUMMARY

AGT-2 is a single-shaft, variable geometry automotive gas turbine engine, which was designed and built by Detroit Diesel Allison (DDA) during 1973-1974. This corporate-funded engine was sized at 167.8 kW (225 hp) for application in future General Motors' (GM) automobiles. The program was carried to the point of initial engine test, but then it was suspended because the energy crisis indicated that engine power was too large for replanned future cars. Although undeveloped, the engine was an asset because of its unique single-shaft configuration and variable geometry components. To utilize this asset for gaining information valuable to the future Department of Energy (DOE) automotive gas turbine program, the National Aeronautics and Space Administration (NASA) and DDA agreed to conduct a performance characterization test.

Under NASA Contract DEN 3-4 the engine was rebuilt in a nonrecuperative configuration and was tested for approximately 49 hr between June and December 1978. The purpose of this testing was to characterize the performance of a single-shaft engine incorporating wide-range, variable geometry components. Additionally, the test results were to be used to verify engine modeling techniques using a digital computer program with component rig rest performance maps. They were also used to compare component performance in the engine with their performance in rig testing. The test program explored the following areas:

- o Inlet guide vane mapping
- o Best specific fuel consumption (SFC) mapping
- o Idle optimization
- o Low power performance
- o Simulated fixed geometry

Results of the testing revealed the following:

- o Significant engine performance improvements are available through the use of variable compressor diffuser vanes and variable turbine vanes. These improvements are particularly significant at part-power conditions. For example, a variable geometry to fixed geometry performance comparison at 14.9 kW (20 shp) demonstrated a reduction in fuel flow that ranged from 27.4% at 70% engine speed to 29.8% at 100% engine speed. It should be noted, however, that these comparisons do not take into account the leakage effects around the vanes, which would not be encountered in a true fixed geometry engine using the adjusted model simulation of 926.7°C (1700°F) turbine inlet temperature (TIT) and 8% surge margin diffuser vane (DV) to turbine vane (TV) schedule.
- o Compressor variable inlet guide vanes (IGV) had minimal effect on the AGT-2 engine performance. This was expected as a result of the compressor rig test, which showed the variable diffuser vanes to be superior to the variable inlet guide vanes for extending the compressor flow range of stable operation. The configuration of the AGT-2 compressor inlet may have caused an adverse flow distribution that reduced the effectiveness of the inlet guide vanes. Also, it was noted that the inlet guide vanes had little effect in the engine low speed range. Although their effect in the high speed range on the engine was not checked, earlier testing on the compressor rig had indicated that they were somewhat effective in the high

speed range. It is probable that this phenomenon is a result of the fact that the compressor inducer is probably stalled at low speeds, thereby nullifying the inlet guide vane effects.

- o There is an optimum schedule of compressor diffuser vanes to turbine vanes to achieve best performance while maintaining adequate compressor surge margin. In general, the flow settings of each component should be paired; e.g., the turbine geometry should be set in a low-flow setting when the compressor is also set in a low-flow setting.
- o The contractor's current engine modeling techniques using component rig test performance maps are sufficiently accurate to predict the overall performance of a gas turbine having variable geometry components and a single-shaft configuration.
- o Adjustment to the engine model to simulate test data indicated engine air flow to be 0.08 kg/s (0.17 lbm/sec) higher than rig flow at 0.18 kg/s (0.4 lbm/sec) rig flow and decreasing to 0.07 kg/s (0.15 lbm/sec) lower than rig flow at 1.36 kg/s (3.0 lbm/sec) rig flow. The ratio of engine compressor efficiency to rig efficiency ranged from 1.0 at 0.15 kg/s (0.34 lbm/sec) rig flow to 1.057 at 1.36 kg/s (3.0 lbm/sec) rig flow. The ratio of engine turbine efficiency to rig efficiency was 0.98 at all turbine conditions. Because of errors in reported turbine geometry settings, engine turbine flow capacity was assumed equal to the rig values.

INTRODUCTION

This test program was a part of an overall study of gas turbine fuel consumption improvements being managed by the Lewis Research Center of the National Aeronautics and Space Administration under sponsorship of the Department of Energy. The program, reported herein under Contract DEN 3-4, involved testing of a single-shaft gas turbine with wide-range variable geometry to obtain information that would assist in modeling and evaluating this type of engine.

The AGT-2 is a single-shaft, variable geometry automotive gas turbine engine which was designed and built by DDA during 1973-1974. This corporate-funded engine was sized at 167.8 kW (225 hp) for application in future GM automobiles. The program was carried to the point of initial engine test, but then it was suspended because the energy crisis indicated that engine power was too large for replanned future cars. The AGT-2 was designed with the following objectives:

1. Maximize fuel economy
2. Meet government emission standards
3. Ensure safety under all operating conditions
4. Guarantee producible and cost-competitive automobiles in quantities
5. Provide acceptable automotive performance
6. Represent minimum vehicle controls and driving technique changes
7. Present minimum change to basic automobile design
8. Develop maintenance capability with current industry skill and facilities

Acceleration, fuel economy, braking, gradability, and emissions requirements were established with the aid of computer simulations using integrated city and highway driving cycles.

The AGT-2 engine design incorporates wide-range, variable geometry components. The compressor has variable angle inlet guide vanes and a variable area diffuser. The combustor has variable geometry to produce low emissions. The turbine has variable area nozzles. These variables give the components very wide airflow range (hence "wide range"). For example, airflow can be varied significantly even at a constant speed. This component capability allows the AGT-2 engine to possess severaly highly desirable characteristics:

- o Operation at a constant turbine temperature over most of the power range strongly contributes to maintaining a low and flat SFC characteristic.
- o At very low power levels, airflow is lower and the cycle pressure ratio is higher than with a conventional turbine engine. These two factors allow the fuel flow to be reduced substantially below that of a fixed geometry engine.
- o From a given steady-state condition, large power increases are possible by simply moving the variable geometry elements into their high-flow settings. This can be accomplished virtually instantaneously, thus immediate power response is available.
- o Idle speed is higher than for conventional turbine engines; thus, the speed range required to accelerate from idle to maximum speed is reduced.

The objective of the program described herein was, by further running of the AGT-2 engine, to establish the effect of variable component geometry on power and fuel consumption over a range of steady-state conditions as well as on the acceleration and braking characteristics of the engine. A second objective was to determine the adequacy of engine performance computer modeling techniques.

The program consisted of the following major tasks:

1. The engine and spare parts retained from the 1974 program were removed from storage, and the engine was examined to determine areas requiring modification.
2. The engine was modified to allow testing of the engine in a nonrecuperative configuration. This modification resulted in a lower cost program while still affording attainment of the basic objective of characterizing the performance of a single-shaft, variable geometry automotive turbine.
3. A performance test was conducted, and the data were analyzed. This testing and analysis included:
   - o Determination of the engine performance at various variable geometry settings throughout the engine operating spectrum
   - o Comparison of the engine test data with an existing computer model that was in turn based on existing rig test component characteristics
   - o Evaluation of the performance of engine components based on test results

The data collected and reported during this test program contribute to the overall studies of the gas turbine as an automotive power plant. In particular, they provide previously unavailable information on the performance characteristics of a unique type of gas turbine. The results of this study should prove useful in the evaluation of engines utilizing the wide-range, variable geometry concept.

ENGINE DESCRIPTION

ORIGINAL ENGINE

The AGT-2 engine was originally designed and built for passenger car use in 1974. At that time it was tested for 14 hr. It had two novel features. First, it had a single-shaft configuration. Secondly, it used variable geometry aerodynamic components extensively. This feature allowed the cycle to be adjusted so that optimum operating conditions could be maintained over a wide range of power levels. Exploration of the performance characteristics of these features was one of the major aims of the current test program.

Figure 1* illustrates the method by which variable geometry was utilized to optimize performance on the original engine. For each performance curve shown, the diffuser vane setting was coordinated (by means of a cam and linkage arrangement) with a specific turbine vane setting to give an 8% (or greater) compressor surge margin.

The mode of control may be explained by examining the method by which power was reduced from maximum.

At 1 038°C (1900°F) and a diffuser vane throat area of 100%, the surge margin, as noted previously, was 8%. Power was reduced from this point (holding DV = 100%) by reducing fuel flow until a turbine inlet temperature of 927°C (1700°C) was reached. Below this line, TIT was held constant at 927°C (1700°F), and power was reduced by decreasing airflow (via DV and TV modulation) until a DV of 40% throat area was reached. Below this point, DV and TV areas were again held constant, and further power reduction was achieved by reducing fuel flow and, as a result, TIT.

Figure 2 is a schematic of the engine configuration showing major components. Although the engine rating of 167.8 kW (225 hp) is large compared to current requirements, its characteristics are applicable to smaller engines. Figures 3 and 4 show a cross section and cutaway view, respectively, of the engine as originally designed. Figure 5 is a photograph of a mock-up of the engine as originally designed. Figures 3 and 4 show that the engine utilized a centrifugal-type compressor with variable inlet guide vanes and variable exit diffuser vanes. Air entered the compressor through twin ports in the reduction gearbox casting and flowed through an inlet annulus that provided constant acceleration to the impeller. Air from the variable diffuser was discharged into a constant velocity compressor scroll and was directed to a recuperative heat exchanger through two diffuser transfer tubes. The airflow from the heat exchanger was fed to a combustor manifold that fed the combustor. The combustor was a low emission type featuring variable geometry in the primary zone. The heated air flowed from the combustor through a transition section to a bifurcated turbine scroll. The gas was fed to the radial inflow tubine through variable turbine vanes and was discharged to an exit diffuser where air was directed to the low pressure side of the recuperator. After flowing through the recuperator, the air was discharged through twin exhaust ports.

*Figures 1 through 91 can be found in Appendix B.

The engine variable geometry utilized a single actuator to operate the compressor and turbine systems. A second actuator modulated the burner variable geometry.

The engine rotor was designed such that the turbine shaft acted as a tie bolt to clamp the compressor impeller as well as to provide the input drive to a single-stage reduction gearbox through a pinion gear. The rotor thrust was taken by a ball bearing located between the turbine wheel and the compressor impeller. The pinion gear was supported by two roller bearings and drove into a single-step reduction gear.

A roller bearing was provided on the rotor between the thrust bearing and the two front roller bearings, which supported the pinion gear (ref Figure 2). The accessories and starter were driven through a chain connecting the accessory gear shaft with the bull gear. The engine oil pump supplied oil to the engine as well as providing hydraulic power to operate the variable geometry actuators.

Pertinent specifications of the original engine are shown in Table I.

TABLE I. - AGT-2 DESIGN SPECIFICATION--ORIGINAL ENGINE

	Maximum	Maximum continuous
Turbine inlet temperature (maximum)	1 037.8°C (1900°F)	926.7°C (1700°F)
Rotor speed	53,000 rpm	53,000 rpm
Output shaft speed	3969 rpm	3969 rpm
Pressure ratio	4.5:1	4.43:1
Turbine expansion ratio	3.39:1	3.37:1
Airflow at seal level static, 15°C (59°F)	1.37 kg/s (3.02 lbm/sec)	1.39 kg/s (3.07 lbm/sec)
Power at sea level static, 15°C (59°F)	167.8 kW (225 hp)	127.3 kW (170.7 hp)
Compressor tip speed	154.1 m/s (1659 ft/sec)	154.1 m/s (1659 ft/sec)
Turbine tip speed	181.1 m/s (1949 ft/sec)	181.1 m/s (1949 ft/sec)
Size and Weight		
Bare engine weight	275.2 kg (606.8 lbm)	
Box dimensions	937 mm long x 767 mm wide x 724 mm high (36.9 in. long x 30.2 in. wide x 28.5 in. high)	
Equivalent rotor inertia (polar moment)	0.0084 kg m^2 (28.86 lbm-$in.^2$)	

ENGINE COMPONENT DETAILS

Variable Inlet Guide Vanes

The prewhirl angle of the air entering the compressor inducer section was controlled by 21 variable inlet guide vanes installed in the inlet annulus (ref Figures 3 and 24). Each of the vanes consisted of a cambered blade 32.4 mm (1.275 in.) long by 25.7 mm (1.010 in.) high by 2.0 mm (0.0772 in.) maximum thickness. They were all actuated to the same angle relative to a radial line through the engine centerline (ref Figure 24) by means of a control ring driven by a hydraulic actuator. These vanes were made of die cast aluminum.

Compressor Impeller

The compressor impeller was cast in high purity C-355 aluminum. Table II lists its pertinent physical characteristics.

TABLE II. - AGT-2 COMPRESSOR IMPELLER ASSEMBLY

Number of blades	30
Inlet hub radius	18.1 mm (0.714 in.)
Inlet shroud radius	51.8 mm (2.04 in.)
Axial distance rotor inlet to hub end	53.3 mm (2.10 in.)
Exit width	8.4 mm (0.332 in.)
Tip diameter	182.2 mm (7.175 in.)
Design tip speed	154.1 m/s (1659 ft/sec)
Design rotational speed	53,000 rpm
Weight	1.27 kg (2.81 lbm)
Inertia	0.002 kg·m^2 (7.11 lbm-in.^{2})
Pressure ratio	4.5:1

Diffuser

The diffuser passage was formed by a variable vane portion and a stationary vane extension (ref Figures 3 and 26). The variable vanes were used to satisfy the aerodynamic requirements at the idle point. The variable vanes and the vane extension were combined to form the optimum passage at the full power condition.

The 26 variable vanes for the initial engine were fabricated from SAE 4140 steel. Each vane was supported by a cylindrical section attached to the leading edge. The vanes tapered in width from 0.4 mm (0.015 in.) at the leading edge to 10.1 mm (0.398 in.) at the downstream edge. Each vane was 72.6 mm (2.860 in.) long and 7.9 mm (0.3098 in.) high. As in the case of the inlet guide vanes, the diffuser vanes were all actuated together by means of a control ring driven by a hydraulic actuator.

The vane extension, or fixed portion of the diffuser, was also fabricated from SAE 4140 steel. It consisted of two plates that formed the diffuser wall and of fixed vane details with tabs that extended through the plates. The tabs were folded over, and the entire assembly was completed by brazing (see Figure 26).

Combustor

The low pressure drop combustor used for the AGT-2 engine was made of Hastelloy X material. It featured a prechamber with fixed swirl vanes plus variable geometry in the form of a slotted rotating band that modulated airflow into the prechamber by changing the area of prechamber side-wall slots. The rotating band was actuated by a controlled hydraulic cylinder and appropriate linkage. The combustor featured a single "air assist" fuel nozzle, which utilized an external air supply. It also had a single igniter. Both fuel nozzle and igniter were mounted in the combustor dome, and both could be removed independent of the dome. The schematic of this combustor is shown in Figure 6.

Variable Turbine Vanes

The turbine variable geometry consisted of 20 movable vanes as shown in Figure 28. These vanes were made of SAE J467b-X40 steel. Each vane was 48.8 mm (1.923 in.) long by 13.4 mm (0.527 in.) high and had a thickness of 8.6 mm (0.340 in.) at the maximum airfoil section. The movable vanes operated in the turbine inlet annulus formed by the turbine shroud and the turbine outer seal. They were all actuated by control arms, which supported cam rollers. These rollers matched with a cam slot in the turbine vane actuating ring. The ring was rotated by means of a hydraulic actuator.

Turbine Assembly

The AGT-2 turbine section consisted of an inlet scroll that accepted burner outlet gas and bifurcated the flow, a variable geometry vane-type nozzle, and a radial inflow turbine rotor. In the original design configuration, the rotor produced a maximum of 461 kW (618 hp) at an expansion ratio of 3.39 and an average inlet temperature of 1 037.8°C (1900°F).

The original turbine wheel was an integral investment casting composed of Inco 713LC material and was inertia welded to a shaft made of SAE 4140 material. Stress-rupture life at the maximum rating temperature was limited, and for this test program additional castings made of Mar-M246 were procured to provide additional life.

The turbine specifications and performance parameters are listed in Table III.

TABLE III. - AGT-2 TURBINE SPECIFICATIONS AND DESIGN POINT PARAMETERS

Tip diameter	214.0 mm (8.426 in.)
Length--wheel and shaft	392.2 mm (15.440 in.)
Number of blades	14
Number of vanes	20
Vane inlet total temperature	1 311.1 K (2360°R)
Vane inlet total pressure	410.6 kP (59.55 psia)
Vane inlet gas flow	1.352 kg/s (2.980 lbm/sec)
Rotational speed	53,000 rpm
Specific work	340 992 J/kg (146.6 Btu/lbm)
Total to total expansion ratio	3.39
Original efficiency goal	
Total-static	0.810
Total-total	0.855
Specific speed	84.5

Figure 7 shows the turbine wheel and shaft assembly with the compressor impeller and associated bearings and seals. This entire assembly constituted the complete engine rotor.

ENGINE MODIFICATIONS BEFORE TEST

In order to run the current test program, a number of design modifications to the engine were made prior to the first engine build, based upon the initial design and test experience in 1974. In addition, several less extensive design changes were made as required during the course of the engine running.

The original configuration of the engine has been previously described. The changes to this configuration prior to the first engine build are described in detail below.

Transfer Tubes and Exhaust Diffuser

Because of its state of development and lack of supporting hardware, the recuperator represented a significant risk to attaining the test objectives. It was, therefore, decided to operate the engine without its recuperator. In place of the recuperator, additional ducting arrangements were required to route compressor discharge air to the combustor manifold and to direct the exhaust gas flow from the engine. A pair of transfer tubes were designed to duct flow from the compressor scroll outlet ports to corresponding ports on the burner manifold. Flanges for attachment of these tubes were welded to the manifold and pressed and pinned to the compressor scroll because the material was not weldable. Four compliant "E" seals were used to provide sealing and to resolve some of the thermal growth and mechanical stack. Figure 8 depicts this arrangement.

A single annular exhaust diffuser (ref Figure 9) was designed to provide uniform turbine exit conditions. The diffuser design featured a centerbody cross keyed to the outer shell, utilizing four alignment pins. To simulate the effect of the recuperator core pressure loss, a restrictor consisting of a plate containing multiple orifices was mounted downstream of the diffuser in the test cell ducting. The restrictor caused a pressure drop equal to 10.3% of the pressure immediately upstream of the plate.

Variable Geometry

A number of minor modifications were required to the variable geometry linkage to provide independent actuation of the inlet guide vanes, the compressor diffuser vanes, the turbine inlet vanes, and the combustor geometry. Two additional hydraulic actuators were used, and the same relationship between actuator travel and vane position was maintained as existed on the original engine. Figures 23, 25, and 27 are calibration curves relating actuator position to vane position and throat area. Figures 24, 26, and 28 depict the meaning of the respective vane positions with respect to the actual engine components.

Turbine

The turbine wheel on the original AGT-2 engine was made of Inco 713LC material. Late in the 1974 program, an analysis of the wheel based on revised metal temperature predictions revealed a lower than desired stress-rupture life at the design point condition. To ensure adequate life, new castings were procured for the NASA/DOE program using Mar-M246 material.

Another part that was redesigned was the bolt that spans the flow path and secures the turbine shroud to the support as shown in Figure 10. Review of the engine after the 1974 tests showed considerable yielding of these bolts, which were made of A286 material. The bolts were changed to Waspaloy material and increased in diameter from 4.83 mm (0.190 in.) to 6.35 mm (0.250 in.). This change required modification of the surrounding hardware and fabrication of larger diameter spacers (Figure 11).

A similar problem was found in the turbine outer seal (backplate). Analysis of the turbine outer seal (backplate) using test data and temperature estimates indicated a probable creep and/or low cycle fatigue problem. The backplate material was changed from Hastelloy S to HS188 to ensure satisfactory life.

Also noted during the initial testing was high leakage in the turbine section. Distortion of the turbine inlet scroll halves at the slip joint was evident after the initial running. For the NASA/DOE test program, these halves were secured using an added flange bolt (ref Figure 9).

Evidence of leakage was also noted around the turbine vane shafts. Sealing washers were added around the shafts, and a ground mating surface was provided on the backplate to minimize this problem. The vane shafts had a slight change in the machining definition, and the backplate insulation had radial slots added to accommodate the washers (ref Figure 12).

For increased reliability, the turbine vanes were changed from percussion-welded vane and shaft assemblies to available integrally cast X-40 assemblies. Previous testing had shown weakness at the weld joint.

Distortion and leakage witness lines were evident on the face seal behind the turbine backplate after the initial AGT-2 testing. These indications emanated from the radial slots in the bore of the backplate. These slots were sealed using welded shim stock.

Evaluation of components after the first AGT-2 test also revealed a local rub on the turbine shroud. The blade tips were not damaged, but the combination of local frictional heating and mechanical interference caused the shroud to crack. An abradable coating was, therefore, added to the shroud to allow rubbing without serious consequences.

Combustor

Removal of the recuperator resulted in significant changes in the combustor operating environment. The temperature of the air entering the combustor was reduced from about 593.3°C (1100°F) to about 204.4°C (400°F). This caused a reduction in the liner pressure drop and a significant increase in the fuel required to achieve a given burner outlet temperature. The primary zone also had to be operated at a considerably higher temperature since mixing was done with substantially cooler dilution air.

An evaluation of combustor requirements for the nonrecuperative operation was made. As a result of these studies, the dilution hole area was reduced. This resulted in an increased liner pressure drop, as well as decreased fuel-to-air ratio in the primary zone and lower liner wall temperatures. The flow passages of the fuel nozzle were increased to accommodate the increased fuel flow, and flow checks of the modified nozzle were conducted to verify spray characteristics.

Because of distortion of the combustor cover during the initial AGT-2 test, a doubler flange was added for improved stiffness (ref Figure 9). The recuperator and combustor support was also changed from 321 SS material to Hastelloy X to minimize a yielding problem encountered on the first test.

Bump Stop Arrangement

During the initial AGT-2 test, the vibration response exceeded desired limits above 70% rated engine speed. The dynamic response frequencies noted in the initial test were simulated by adjusting of the rotor dynamic analysis model. The results indicated a probable critical speed occurring within the engine operating range. The roller bearing aft of the compressor impeller was, therefore, replaced with an oil-lubricated bump stop arrangement. Details are depicted in Figure 13.

Modified Engine Configuration

The overall engine configuration including the changes described previously is shown in Figure 9.

ENGINE MODIFICATIONS DURING TEST

As a result of mechanical problems encountered during the current program, two design changes were made during the course of testing. The first of these consisted of adding a speed pickup within the engine to allow a more direct measurement of engine rotor speed. This change necessitated minor changes to the compressor impeller sleeve.

The second change consisted of a redesign in the bump stop area to provide for an additional separate external oil supply to the bump stop, thus giving a higher oil flow than had been available from the engine oil pump. This design also introduced a one-piece bump stop and locknut arrangement, which was later rejected in favor of the original design, although the external oil supply feature was retained. This effort also added two shaft-whip pickups designed to measure turbine shaft deflection during engine operation.

INSTRUMENTATION

The instrumentation installed in the engine and adjacent test equipment during the test is listed in Table IV.

TABLE IV. - AGT-2 TEST INSTRUMENTATION

Location	Number of probes			Remarks
	T	P_t	P_s	
Primary flow stream				
Inlet duct				
1. Airflow	---	---	---	Standard ASME orifice
2. Compressor inlet	2x2 ele rake	3x3 ele* rake	2*	X2 ducts (2 spare probes per duct)
Compressor				
1. Scroll	---	---	1	X2 scrolls
2. Transfer tube	1x5 ele rake	2x3 ele* rake	3	X2 tubes
Combustor				
1. Inlet	1	---	1*	X2 (fore and aft in case)
2. Exit	3	3*	3*	
Turbine				
1. Scroll	20x1 ele			20 performance T/C's + (4 spare performance probes)
2. Rotor inlet	---	---	3*	X2 (shroud and backplate)
Diffuser				
1. Inlet			4 inner*	
o Basic	1x5 ele rake	5-Kiel	4 outer*	
2. Exit	---	---	4	
Exhaust orifice plate				
1. Exit	2	---	2*	
Secondary flow stream				
Cavity, compressor Scroll and turbine	---	---	1	
Cavity, ring seal, fwd	1	---	---	
Cavity, ring seal, aft	1	---	1	
Cavity, turbine shroud seal, inner	---	---	1	

TABLE IV. (cont)

Location	Number of probes			Remarks
	T	P_t	P_s	
Lube oil				
No. 1 bearing inlet	1	---	1	
No. 1 bearing outlet	1	---	1	
No. 1 bearing race	2	---	---	
Main oil	2	---	1	
Bump stop oil	---	---	1	
Main oil flow	---	---	---	Flowmeter
Mechanical				
Compressor and turbine vibration	---	---	---	Front vertical, rear vertical, front horizontal
Compressor and turbine rub pins	---	---	---	3 at compressor tip; 3 at each of turbine tip, knee exducer
Burner skin	3	---	---	7 spares
No. 1 bearing outer race	1	---	---	1 spare
Seal plate	2	---	---	1 upper, 1 lower
Compressor shroud	2	---	---	1 spare
Compressor scroll	3	---	---	
Miscellaneous				
Control ambient	1	---	---	
Airflow orifice	---	---	8	4 upstream; 4 downstream
Airflow reference	1	---	---	
x Speed	---	---	---	Engine rotor; dynamometer
x Torque	---	---	---	
Fuel flow	---	---	---	Flowtron flowmeter
Inlet guide vane position	---	---	---	Linear pontentiometer
x Compressor diffuser	---	---	---	Linear pontentiometer
Vane position	---	---	---	
x Turbine inlet vane position	---	---	---	Linear pontentiometer
x Burner position	---	---	---	Linear pontentiometer
Compressor vibration	---	---	---	Vertical + 2 accelerometers
Turbine vibration	---	---	---	Horizontal + vertical
x Fuel nozzle ΔP	---	---	---	ΔP transducer
x Fuel valve current	---	---	---	
Shaft whip	---	---	---	2 pickups

*Denotes manifolding

A majority of these parameters were recorded automatically by a central recording system during testing. Certain critical parameters were observed continuously by test personnel during operation. Those parameters in the list above marked (x) were recorded continuously on the test cell by strip-chart recorders or x-y plotters. Parameters marked (*) were recorded continuously on engine builds 8 and 9 as functions of discrete frequency values and time.

The airflow was measured with a standard ASME sharp-edged orifice. The temperatures were measured using chromel-alumel thermocouples having $\pm$0.5% accuracy at maximum temperature capacity and were recorded on the Systems Engineering Laboratory (SEL) digital data acquisition system. The full-scale accuracy of the temperature acquisition system was $\pm$0.173%. The pressures were measured with Rosemount transducers or Rosemount ΔP transducers and recorded on the SEL digital data acquisition system. Full-scale accuracy of the pressure acquisition system was $\pm$0.25%. The fuel flow was measured by a Flowtron mass flowmeter with a full-scale accuracy of $\pm$0.58%. Speed was measured with an ATEC counter. Accuracy of this system was $\pm$0.002%. Torque was read by means of a Lebow Associates Model 7521 transducer digital indicator and was also recorded on the SEL digital data acquisition system. The full-scale accuracy of this system was $\pm$0.26%. The vane angles of the variable geometry components versus actuator travel were measured during the engine buildup. Repeatability of these measurements cold was $\pm$0.25%. The actuator travel was set at the "idle" and "full power" positions with mechanical stops. During engine running, the travel was recorded on the SEL data acquisition system, and the full-scale accuracy of this system was $\pm$0.17%.

Figure 14 shows details of the instrumentation installed within the engine assembly. Figure 15 shows, in schematic form, the location of the installed instrumentation within the engine assembly, while Figure 16 shows, in greater detail, the location of the various pressure and temperature probes within the primary flow stream.

TEST FACILITIES

TEST CELL ARRANGEMENT

Test Cell 894 was modified for the AGT-2 test as shown in Figure 17. A welded base was designed and built to support the engine torquemeter and a step-down gearbox. The latter provided a speed reduction ratio of 1.84:1 between the engine output shaft and the dynamometers. A single shaft utilizing two flexible couplings joined the output of the gearbox and the dynamometers. A safety shield supported by two posts surrounded this shaft. The load consisted of two coupled 372.8-kW (500 hp) motoring dynamometers. The two dynamometers were used because converting of the test cell (controls, shafting, etc) for use as a single unit would have resulted in considerable added expense. For starting, the engine was driven by the dynamometers, and they, conversely, absorbed power during engine operation. Air for the engine was drawn from the test cell through a filter fitted to the end of an inlet pipe. This pipe contained the airflow measurement orifice and associated instrumentation. Air from this pipe entered the engine on both sides through a bifurcated duct arrangement, each branch of which contained the engine air inlet instrumentation. The engine exhaust discharged through an insulated duct. An external hydraulic system consisting of a supply tank, motor-driven pump and regulator provided 2 068.4-kPa (300 psig) pressure for the engine variable geometry actuators. As noted previously, a separate external oil supply for the bump stop was also provided on engine builds 8 and 9.

Figure 18 shows the instrumented engine, torquemeter, and reduction gearbox mounted on their base prior to the initial test cell installation. Figures 19 through 21 show the engine installed and the test cell. In Figure 19, the airflow orifice can be seen in the air inlet pipe at the upper left. At the lower left is the external hydraulic supply. In Figure 20, details of the inlet duct instrumentation can be seen in the rectangular duct on the right-hand inlet.

CONTROLS

For the NASA/DOE test, the engine control system was modified, as noted previously, to allow each of the engine variable geometry elements to be controlled individually. The circuit boards, which had previously been used to calculate variable geometry positions, were replaced with new circuit boards designed for individual geometry actuation.

A test console, shown by Figure 22, was designed to interface with the electronic control noted previously. This console allowed the operator to change each of the engine geometry positions as well as the turbine inlet temperature by means of sliding potentiometers. Digital readouts for each of these parameters were also provided.

The modified control retained the closed-loop turbine inlet temperature mode of controlling engine fuel flow.

RESUME OF TESTING

The engine installation on Test Cell 894 and associated instrumentation have been described previously. The test plan called for evaluation of the following areas:

- o Inlet guide vane mapping
- o Best SFC mapping
- o Idle optimization
- o Low power performance
- o Stabilized braking
- o Simulated fixed geometry

The oil used during testing on engine builds 2 through 7 was MIL-L-7808. In an effort to eliminate bump stop failures, an increased viscosity oil (MIL-L-23699) was used on builds 8 and 9. Diesel No. 2 fuel was used for all running.

Because of mechanical problems encountered during the initial testing, the test plan described here was modified to obtain a maximum of important data in a minimum of engine operating time. A universal test control, designed for operation of various engines through use of an electronic fuel valve, was utilized for control of fuel flow during part of the test when the control box became inoperative.

DATA OBTAINED

Table V lists the test settings at which specific data were collected during the 48:34 hr of testing. Because of mechanical problems that will be discussed later, no data were obtained at 100% rpm and maximum power. The only test phase not attempted was that which characterizes airflow transients. Initial attempts to obtain motoring data requested by NASA were unsuccessful, and because these data were considered to be of lower priority than other testing, they were not obtained prior to termination of testing by a major mechanical failure. Table VI is a listing of the data obtained (or calculated) from the test settings listed in Table V.

MECHANICAL PROBLEMS

Prior to the current performance test program, the AGT-2 engine had not undergone mechanical development. As a result, certain unpredictable parts failures occurred during operation.

Build 2 was dedicated to determining gearbox, bearing, and windage losses by motoring the engine with the dynamometer and measuring the heat input to the engine oil. After 47 min of motoring, it was discovered that the turbine rotor shaft was broken in torsion 47.8 mm (1.88 in.) from the aft end of the shaft. Investigation revealed that the failure was caused by excessive shaft torque encountered when the turbine rotor rubbed the turbine shroud. The rub occurred because inadvertent backward rotation of the dynamometer produced rotor thrust loading in an unexpected direction.

TABLE V. - ENGINE TEST SETTINGS

Reading No.	Category	$N_G/\sqrt{\theta}$ %	TIT/θ °C	TIT/θ °F	IGV actuator mm	IGV actuator in.	Throat area %	DV actuator mm	DV actuator in.	Throat area %	TV actuator mm	TV actuator in.	Throat area %
3593	IGV MAPPING	66.09	738	1361	23	.92	22.2	1	.03	33.5	24	.95	53.0
3642		65.98	733	1351	15	.61	17.8	1	.03	33.5	24	.96	52.5
3691		66.05	733	1351	9	.35	12.1	1	.03	33.5	24	.96	52.5
3740		65.59	739	1363	4	.15	6.3	1	.03	33.5	24	.96	52.5
3789		65.56	746	1354	1	.04	2.8	1	.03	33.5	24	.96	52.5
3512		66.16	742	1368	23	.92	22.2	16	.64	73.0	15	.61	75.0
3256		66.66	777	1430	23	.92	22.2	24	.96	97.0	3	.11	119.0
3305		66.65	771	1419	15	.61	17.8	24	.96	97.0	3	.11	119.0
3355		66.43	768	1415	9	.35	12.1	24	.96	97.0	3	.11	119.0
3408		66.56	760	1400	4	.15	6.3	24	.96	97.0	3	.11	119.0
3457		66.52	757	1394	1	.03	2.5	24	.96	97.0	3	.11	119.0
4072		76.26	778	1433	23	.92	22.2	24	.96	97.0	3	.11	119.0
4121		76.22	777	1431	15	.61	17.8	24	.96	97.0	3	.11	119.0
4170		76.18	779	1435	9	.35	12.1	24	.96	97.0	3	.11	119.0
4219		76.23	770	1418	4	.15	6.3	24	.96	97.0	3	.11	119.0
4274		76.18	773	1423	1	.04	2.8	24	.96	97.0	3	.11	119.0
3080		95.39	837	1539	14	.56	16.6	24	.96	97.0	3	.10	119.0
1358	SFC MAPPING*	69.65	797	1467	1	.02	2.0	0.3	.01	32.3	0	0.0	130.0
1260		69.94	802	1475	0.3	.01	1.6	5	.18	42.6	0	0.0	130.0
1162		69.74	798	1468	0.3	.01	1.6	9	.35	53.2	0	0.0	130.0
1064		69.69	779	1435	3	.10	4.7	16	.63	72.2	0	0.0	130.0
893		69.92	771	1420	22	.86	21.5	24	.95	96.2	0	0.0	130.0
966		70.30	767	1412	22	.85	21.4	24	.95	96.2	0	0.0	130.0
230		70.46	749	1380	22	.86	21.5	24	.95	96.2	0.3	.01	129.0
1407		69.82	798	1468	1	.02	2.0	0.3	.01	38.0	3	.10	119.9
1309		69.77	806	1483	1	.02	2.0	5	.18	42.6	3	.10	119.9
1211		70.05	796	1465	0.3	.01	1.6	9	.35	53.2	3	.10	119.9
1113		69.98	786	1447	3	.10	4.7	16	.63	72.2	3	.10	119.9
1015		69.95	775	1427	22	.85	21.4	24	.95	96.2	3	.10	119.9
1617		69.77	786	1446	1	.02	2.0	2	.06	35.4	8	.30	101.0
1554		70.36	779	1434	1	.02	2.0	5	.18	42.6	8	.30	101.0
1505		69.28	774	1426	1	.02	2.0	9	.35	53.2	8	.30	101.0
1456		70.19	757	1395	3	.01	4.7	16	.63	72.2	8	.30	101.0
1812		69.58	802	1475	1	.02	2.0	0.3	.01	38.0	17	.68	69.8
1715		69.38	796	1464	1	.02	2.0	5	.18	42.6	17	.68	69.8
1666		69.93	794	1461	1	.02	2.0	9	.35	53.2	17	.68	69.8
1861		68.85	807	1484	1	.02	2.0	1	.02	32.7	24	.94	53.5
3423	SFC MAPPING	69.79	966	1590	22	.87	21.7	24	.96	97.0	3	.10	119.9
3374		69.65	861	1581	22	.87	21.7	24	.96	97.0	3	.10	119.9
2282		70.07	858	1576	2	.08	4.0	16	.64	73.0	11	.42	90.6

TABLE V. (cont)

Reading No.	Category	$N_G/\sqrt{\theta}$ %	TII/θ °C	°F	IGV actuator mm	in.	Throat area %	DV actuator mm	in.	Throat area %	TV actuator mm	in.	Throat area %
2380	SFC MAPPING	69.86	901	1654	- 0.3	-.01	1.0	9	.34	52.5	18	.69	68.9
2744	↓	70.07	926	1699	- 0.3	-.01	1.0	4	.17	42.2	21	.81	61.4
2796	↓	69.79	877	1610	- 0.3	-.01	1.0	0	0.0	31.9	24	.94	53.5
2331	SFC MAPPING*	70.13	736	1356	2	.08	4.0	16	.64	73.0	11	.42	90.6
2695	↓	70.22	756	1392	- 0.3	-.01	1.0	4	.17	42.2	21	.81	61.4
2184	↓	68.88	630	1166	23	.92	22.2	24	.96	97.0	- 0.3	-.01	131.0
314	↓	57.73	790	1454	1	.02	2.0	9	.35	53.2	0	0.0	130.0
177	↓	57.99	754	1390	22	.87	21.7	24	.95	96.2	0	0.0	130.0
363	↓	57.75	793	1460	1	.02	2.0	9	.35	53.2	0.3	.10	119.9
539	↓	59.79	762	1403	1	.02	2.0	16	.63	72.2	0.3	.10	119.9
265	↓	57.83	771	1419	22	.87	21.7	24	.95	96.2	0.3	.10	119.9
642	↓	60.41	777	1431	1	.02	2.0	9	.35	53.2	8	.30	101.0
588	↓	60.25	755	1391	3	.11	5.0	16	.63	72.2	8	.30	101.0
665	↓	76.88	761	1401	22	.87	21.7	24	.95	96.2	3	.10	119.9
752	↓	77.01	776	1428	3	.10	4.7	16	.63	72.2	11	.42	90.6
807	↓	77.00	793	1459	0.3	.01	1.6	9	.35	53.2	17	.68	69.8
856	↓	76.94	803	1478	0.3	.01	1.6	5	.18	42.6	20	.80	61.9
905	↓	76.99	796	1464	0.3	.01	1.6	0.3	.01	38.0	24	.94	53.5
2535	SFC MAPPING	77.17	877	1610	22	.87	21.7	24	.96	97.0	2	.09	121.2
2478	↓	77.16	897	1646	2	.08	4.0	16	.63	72.2	11	.42	90.6
2429	↓	77.20	914	1678	- 0.3	-.01	1.0	9	.34	52.5	18	.69	68.9
2894	↓	77.39	882	1620	- 0.3	-.01	1.0	4	.17	42.2	21	.81	61.4
2845	↓	77.28	893	1639	- 0.3	-.01	1.0	0	0.0	31.9		.94	53.5
1106	SFC MAPPING*	90.18	754	1390	22	.86	21.5	24	.95	96.2	3	.10	119.9
1155	↓	90.32	772	1422	3	.10	4.7	16	.63	72.2	11	.42	90.6
1204	↓	90.28	797	1466	1	.02	2.0	9	.35	53.2	17	.68	69.8
3276	SFC MAPPING	89.69	875	1607	22	.87	21.7	24	.96	97.0	3	.10	119.9
3031	↓	90.40	838	1541	22	.87	21.7	24	.96	97.0	3	.10	119.9
2584	↓	90.05	882	1620	2	.08	4.0	16	.64	73.0	11	.42	90.6
2646	↓	89.79	944	1731	- 0.3	-.01	1.0	9	.34	52.5	18	.69	68.9
1910	LOW POWER	69.28	700	1292	1	.02	2.0	0.3	.01	38.0	24	.94	53.5
1959	↓	69.20	565	1049	1	.02	2.0	0.3	.01	38.0	24	.94	53.5
2008	↓	69.47	421	790	1	.02	2.0	0.3	.01	38.0	24	.94	53.5
1488	FIXED GEOM.	58.16	671	1239	24	.94	22.5	24	.98	98.5	0	0.0	130.0
2233	↓	70.02	842	1548	22	.87	21.7	24	.96	97.0	2	.09	121.2
279	↓	70.41	757	1394	22	.87	21.7	24	.95	96.2	3	.10	119.9
334	↓	70.15	675	1247	22	.86	21.5	24	.95	96.2	3	.10	119.9
606	↓	69.90	669	1237	22	.86	21.5	24	.95	96.2	3	.10	119.9
384	↓	70.08	547	1016	22	.87	21.7	24	.95	96.2	3	.10	119.9
536	↓	69.52	544	1012	22	.87	21.7	24	.95	96.2	3	.10	119.9
487	↓	70.03	544	1011	22	.87	21.7	24	.95	96.2	3	.10	119.9
433	↓	70.02	450	842	22	.87	21.7	24	.95	91.2	3	.10	119.9

TABLE V. (cont)

Reading No.	Category	$N_G/\sqrt{\theta}$ %	TIT/θ °C	°F	IGV actuator mm	in.	Throat area %	DV actuator mm	in.	Throat area %	TV actuator mm	in.	Throat area %
959	FIXED GEOM.	77.02	654	1209	22	.86	21.5	24	.95	96.2	3	.10	119.9
1008		77.05	528	983	22	.86	21.5	24	.95	96.2	3	.10	119.9
1057		76.89	485	905	22	.86	21.5	24	.95	96.2	3	.10	119.9
3325		79.95	860	1580	22	.87	21.7	24	.96	97.0	3	.10	119.9
1253		90.48	665	1229	22	.86	21.5	24	.95	96.2	3	.10	119.9
1302		90.54	523	973	22	.86	21.5	24	.95	96.2	3	.10	119.9
1351		90.48	428	803	22	.86	21.5	24	.95	96.2	3	.10	119.9
3227		94.96	878	1612	14	.55	16.6	24	.96	97.0	3	.10	119.9
3178		95.06	804	1480	14	.56	16.6	24	.96	97.0	3	.10	119.9
3129		95.06	703	1297	14	.56	16.6	24	.96	97.0	3	.10	119.9
3472		99.49	684	1264	14	.55	16.6	24	.96	97.0	2	.09	121.2

*Also low power, idle, and braking resulting from low TIT level.

TABLE VI. - AGT-2 ENGINE TEST DATA
Sea level 15.6°C (60°F)

Reading No.	$W_a\sqrt{\theta}/\delta$ kg/s	$W_a\sqrt{\theta}/\delta$ lbm/sec	R_c	η_c %	$(\Delta P/P)_{C-T}$ %	R_e	η_T* %	$(\Delta P/P)_{T-E}$ %	Shaft power kW	Shaft power hp	Fuel flow kg/h	Fuel flow lbm/hr	η_T ratio** eng/rig
3593	.208	.459	1.794	46.05	-	1.789	-	-	- 9.3	-10.0	14.2	32.3	-
3642	.210	.462	1.794	46.77	-	1.790	-	-	- 7.1	- 9.5	14.5	32.0	-
3691	.209	.461	1.798	47.45	-	1.792	-	-	- 6.8	- 9.1	14.6	32.1	-
3740	.202	.446	1.786	47.70	-	1.782	-	-	- 5.9	- 7.9	14.7	32.3	-
3789	.197	.437	1.780	47.73	-	1.776	-	-	- 6.0	- 8.0	14.5	32.0	-
3512	.343	.756	2.042	64.69	-	1.985	-	-	9.8	13.1	24.0	52.9	-
3256	.512	1.129	2.028	68.23	-	1.884	-	-	23.3	31.2	37.5	82.6	-
3305	.509	1.122	2.015	68.74	-	1.874	-	-	23.1	32.0	36.9	81.4	-
3355	.500	1.103	1.992	68.93	-	1.857	-	-	22.7	30.5	36.5	80.5	-
3408	.502	1.106	1.991	69.55	-	1.859	-	-	22.3	29.9	36.1	79.5	-
3457	.499	1.100	1.890	69.21	-	1.837	-	-	21.9	29.4	35.5	78.3	-
4072	.674	1.486	2.431	69.38	-	2.169	-	-	30.6	41.0	44.9	98.9	-
4121	.669	1.475	2.420	70.35	-	2.155	-	-	31.5	-2.3	44.8	98.7	-
4170	.666	1.468	2.409	71.25	-	2.134	-	-	32.5	43.6	44.8	98.8	-
4219	.663	1.462	2.395	71.63	-	2.125	-	-	31.4	42.1	44.0	97.0	-
4274	.655	1.444	2.379	71.45	-	2.116	-	-	31.4	42.1	44.0	96.9	-
3080	1.155	2.546	3.409	68.88	9.39	2.741	82.72	9.81	51.1	68.6	69.6	153.5	.982
1358	.252	.555	1.421	25.80	-	-	-	-	-23.6	-31.7	17.7	39.1	-
1280	.328	.722	1.551	34.50	-	-	-	-	-17.1	-22.9	23.4	51.6	-
1162	.401	.884	1.703	44.72	-	-	-	-	- 6.5	- 8.7	28.4	62.6	-
1064	.529	1.166	1.978	63.37	-	-	-	-	15.3	20.5	37.3	82.2	-
893	.623	1.373	2.127	69.81	-	-	-	-	22.8	30.6	41.8	92.1	-
966	.626	1.381	2.144	70.16	-	-	-	-	23.9	32.1	42.3	93.2	-
230	.504	1.112	2.148	69.86	-	-	-	-	22.2	29.8	40.7	89.7	-
1407	.251	.554	1.429	26.10	-	-	-	-	-22.9	-30.7	17.8	39.2	-
1309	.326	.719	1.563	35.19	-	-	-	-	-15.6	-21.0	23.2	51.2	-
1211	.402	.886	1.729	45.84	-	-	-	-	- 5.3	- 7.1	28.4	62.7	-
1113	.525	1.157	2.022	65.06	-	-	-	-	16.8	22.6	36.4	80.2	-
1015	.577	1.272	2.157	69.90	5.62	1.949	81.48	3.05	24.2	32.5	39.5	87.0	.990
1617	.269	.592	1.567	33.91	-	-	-	-	-15.1	-20.3	18.9	41.6	-
1554	.325	.717	1.716	43.31	-	-	-	-	- 9.4	-12.6	22.2	49.0	-
1505	.390	.859	1.904	55.51	-	-	-	-	3.6	4.8	26.4	58.2	-
1456	.469	1.035	2.140	68.12	-	-	-	-	15.7	21.1	30.4	67.0	-
1812	.238	.525	1.773	43.09	-	-	-	-	- 8.4	-11.3	17.0	37.4	-
1715	.300	.661	2.046	57.97	-	-	-	-	2.4	3.2	20.9	46.1	-
1666	.329	.726	2.187	64.18	1.10	2.117	72.83	1.85	7.8	10.4	22.6	49.9	.975
1861	.218	.480	1.987	52.18	0	1.984	65.42	-0.14	- 4.3	- 5.8	15.6	34.3	1.016
3423	.673	1.483	2.112	68.30	6.52	1.877	81.32	4.19	29.1	39.0	48.1	106.1	1.009
3374	.670	1.477	2.101	67.10	6.56	1.870	82.70	4.19	28.3	38.0	47.4	104.6	1.027
2282	.476	1.050	2.143	66.74	4.16	2.003	78.88	1.91	21.5	28.8	34.7	76.4	.972
2380	.359	.792	2.088	60.06	2.29	2.013	76.63	1.05	12.0	16.1	27.9	61.4	.989
2744	.272	.600	1.829	45.63	1.69	1.741	75.08	2.33	- 2.4	- 3.2	23.5	51.9	.985
2796	.205	.453	1.628	34.05	1.05	1.591	66.00	0.91	-13.6	-18.2	16.3	36.0	.979
2331	.489	1.078	2.125	66.89	4.52	1.939	75.46	3.83	10.8	14.5	28.3	62.5	.914
2695	.275	.607	1.823	45.92	1.89	1.732	66.38	2.30	-11.7	-15.7	17.1	37.6	.916

TABLE VI. (cont)

Reading No.	$w_a\sqrt{\theta}/\delta$ kg/s	$w_a\sqrt{\theta}/\delta$ lbm/sec	π_c	η_c %	$(\Delta P/P)_{C-T}$ %	π_e	η_T* %	$(\Delta P/P)_{T-E}$ %	Shaft power kW	Shaft power hp	Fuel flow kg/h	Fuel flow lbm/hr	η_e ratio** erg/gig
2184	.669	1.474	2.097	76.93	-	-	-	-	2.2	2.9	33.2	73.1	-
314	.319	.703	1.495	47.32	-	-	-	-	- 1.6	- 2.1	23.5	51.8	-
177	.458	1.010	1.714	67.94	-	-	-	-	12.1	16.2	32.4	71.5	-
363	.319	.703	1.510	48.54	-	-	-	-	- 0.7	- 1.0	23.6	52.0	-
539	.410	.903	1.708	63.79	-	-	-	-	10.0	13.4	29.3	64.6	-
265	.401	.885	1.722	66.61	-	-	-	-	11.6	15.6	28.7	63.2	-
642	.325	.717	1.678	55.22	-	-	-	-	4.7	6.3	23.7	52.3	-
528	.364	.802	1.786	65.79	-	-	-	-	10.6	14.2	26.0	57.3	-
665	.629	1.387	2.459	69.70	5.17	2.217	81.53	4.37	28.2	37.8	41.5	91.5	.977
752	.402	.886	2.491	68.75	2.35	2.345	75.78	2.87	18.4	24.7	32.1	70.7	.931
807	.217	.479	2.500	65.03	1.10	2.390	73.22	2.98	9.5	12.7	25.9	57.1	.961
856	.090	.199	2.426	60.10	0.57	2.356	70.00	1.72	1.7	2.3	22.2	48.9	.970
905	.256	.564	2.233	51.49	-0.15	2.205	63.22	0.98	- 9.2	-12.4	17.1	37.7	.962
2335	.688	1.517	2.504	69.27	6.35	2.198	83.30	4.96	40.1	53.8	49.0	108.0	1.011
2478	.513	1.130	2.523	67.53	3.54	2.335	79.21	3.46	29.4	39.5	37.9	83.5	.920
2429	.415	.916	2.352	59.21	2.47	2.252	76.63	1.68	15.3	20.5	31.9	70.3	.969
2894	.312	.688	2.092	46.93	1.65	1.961	73.23	3.68	- 6.1	- 8.2	23.6	52.1	.953
2845	.236	.520	1.796	35.12	1.34	1.740	63.43	1.34	-18.3	-24.6	18.5	40.7	.896
1106	.959	2.114	3.257	71.25	7.10	2.759	83.06	7.92	41.7	55.9	53.4	117.8	.972
1155	.792	1.746	3.234	68.93	3.19	2.853	80.48	5.21	27.1	36.4	40.2	88.7	.968
1204	.651	1.436	3.218	64.30	1.71	2.914	74.67	7.43	8.5	11.4		70.6	.959
3276	1.070	2.358	3.182	70.14	8.73	2.594	84.98	9.25	59.5	79.8	32.0	152.1	1.028
3031	1.091	2.405	3.211	70.02	9.08	2.610	82.73	9.25	52.8	70.8	67.0	147.8	.997
2584	.739	1.630	3.129	67.25	5.10	2.726	82.84	6.62	47.3	63.5	51.1	112.7	.977
2645	.533	1.175	2.928	57.61	3.52	2.696	78.60	3.77	23.1	31.0	40.6	89.6	.978
1910	.225	.497	1.953	52.14	0	1.957	60.57	-0.38	- 9.6	-12.9	13.2	29.0	.969
1959	.232	.511	1.886	50.48	0	1.906	48.61	-1.42	-17.4	-23.4	9.7	21.4	.840
2008	.236	.520	1.846	49.12	0	1.910	36.15	-3.80	-26.2	-35.2	7.2	15.8	.707
1488	.462	1.019	1.741	69.91	-	-	-	-	8.2	11.0	27.9	61.6	-
2233	.631	1.392	2.141	68.85	7.73	1.829	82.00	3.33	26.6	35.7	45.0	99.2	1.011
279	.442	.974	2.173	69.89	5.36	1.976	81.23	3.39	23.4	31.4	38.7	85.3	.983
334	.458	1.010	2.153	70.31	5.57	1.946	80.43	3.71	14.2	19.1	33.3	73.5	.968
606	.558	1.231	2.142	70.20	5.61	1.936	81.16	3.68	13.7	18.4	32.8	72.4	.977
384	.574	1.266	2.135	70.79	5.79	1.903	79.14	4.71	- 0.6	- 0.8	26.6	58.6	.968
535	.591	1.302	2.112	70.64	5.69	1.886	78.09	4.65	- 0.7	- 0.9	26.1	57.6	.956
487	.605	1.334	2.136	70.92	5.94	1.904	78.15	4.71	- 0.5	- 0.7	26.4	58.3	.956
433	.623	1.374	2.125	70.28	5.98	1.869	78.15	5.78	-12.4	-16.0	25.8	56.8	.928

TABLE VI. (cont)

Reading No.	$W_a\sqrt{\theta}/\delta$ kg/s	$W_a\sqrt{\theta}/\delta$ lbm/sec	R_c	η_c %	$(\Delta P/P)_{C-T}$ %	R_e	η_T* %	$(\Delta P/P)_{T-E}$ %	Shaft power kW	Shaft power hp	Fuel flow kg/h	Fuel flow lbm/hr	η_T ratio** eng/rig
959	.660	1.455	2.454	70.74	6.04	2.146	80.99	6.13	13.9	18.6	35.7	78.8	.972
1008	.710	1.566	2.458	71.56	7.71	2.079	78.65	7.46	- 8.2	-11.0	27.0	59.6	.960
1057	.719	1.586	2.446	71.64	7.88	2.059	81.03	7.96	-15.0	-20.1	24.9	55.0	.998
3325	.860	1.895	2.604	69.70	-	-	-	-	43.4	58.3	57.7	127.1	-
1253	.979	2.158	3.239	71.31	7.14	2.697	81.48	9.32	16.9	22.7	45.0	99.3	.946
1302	.998	2.201	3.228	71.54	9.09	2.574	79.56	11.27	-24.1	-32.3	33.3	79.4	.912
1351	1.019	2.247	3.207	71.60	9.48	2.453	-	14.48	-56.3	-75.6	27.3	60.1	-
3227	1.138	2.509	3.404	69.18	9.08	2.739	83.07	10.14	62.0	83.2	72.9	150.8	.991
3178	1.153	2.541	3.363	68.57	9.31	2.700	82.09	10.00	38.8	52.0	64.7	142.7	.972
3129	1.165	2.568	3.287	67.37	9.43	2.639	79.44	9.81	3.7	4.9	53.8	118.5	.930
3472	1.245	2.744	3.525	66.01	10.42	2.816	-	9.77	-13.3	-17.8	54.2	119.5	-

*Turbine efficiency calculated from compressor and shaft work mechanical loss, turbine inlet temperature, and turbine expansion ratio.

**Ratio of calculated turbine efficiency to turbine rig efficiency.

On build 3, the engine was operated for 15:22 hr. At the end of this period, high compressor vibration and noise were encountered. Teardown of the engine revealed that the bump stop had rubbed heavily against the mating portion of the turbine rotor shaft. The outside diameter of the compressor impeller had also rubbed on the diffuser housing, and the turbine exducer had rubbed the abradable coating on the turbine shroud. The impeller radial clearance was increased, and provision was made for additional bump stop clearance. The forward engine mounts were also reworked to increase their flexibility in the fore-and-aft direction to prevent a suspected thermal distortion of the engine structure.

Builds 4, 5, 6, and 7 were all terminated by rubbing of the bump stop. Running time on each of these builds was as follows:

BU 4	8 hr, 55 min
BU 5	6 hr, 34 min
BU 6	7 hr, 25 min
BU 7	1 min

After the failures on builds 4, 5, and 6, the bump stops were replaced without removing the engine from the test cell in order to expedite testing. On teardown 6 it was noted that the total runout at the rear end of the turbine rotor shaft was 0.2 mm (0.007 in.). An attempt was made to operate the engine with a new bump stop on build 7; however, excessive vibration was encountered at rotor speeds above 20,000 rpm. For this reason running was terminated after 1 min.

A high oil consumption problem was encountered on build 4. It was determined that the oil drain line, which returned oil from the turbine bearing to the sump, was too small, causing oil to back up through the turbine labyrinth seal. The drain line size was increased, and no further problems in this area were encountered.

Inspection of the engine on teardown 7 showed that the turbine inner seal assembly had rubbed against the turbine wheel. The seal assembly was machined to the same thickness as the backplate, and no further rubbing occurred during subsequent running. Also, on this teardown, seven diffuser vanes and five turbine vanes were replaced because of slight bending noted at the axis of rotation. In addition, several of the ceramic bushings around the turbine vane shafts were replaced because of chipping and cracking.

It was at this time, as noted previously, that a decision was made to increase the oil flow and pressure to the bump stop by use of a parallel, external oil supply. In conjunction with this change, the compressor labyrinth seal clearance was increased, and the labyrinth seal airflow was also increased to ensure sealing with the increased oil supply. During subsequent testing no measurable wear or excessive vibration was noted in the bump stop area.

The engine was operated for 31 min on build 8, at which time testing was terminated by a fatigue failure of the turbine rotor shaft adjacent to the compressor locknut threads. It was determined that this failure initiated at a small, localized fatigue crack, which was propagated when the shaft was bent to alleviate a runout condition incurred on the previous failure.

Because no additional Mar-M246 turbine rotors were available, the original Inco 713LC rotor was installed on build 9.

On this buildup, the engine was operated for a total of 8:59 hr. At this time a major failure was experienced in the turbine area. Teardown revealed that the primary cause was a turbine blade fatigue failure. Three blades exhibited evidence of fatigue, which appears to be induced by coincidence of a high frequency blade bending mode with a stator vane engine order near the engine maximum operating speed. Figures 29 and 30 show the turbine wheel failure. Secondary damage resulting from the blade failure included:

- o Damage to all remaining turbine blades
- o Spalling of the turbine bearing race
- o Breakage of four turbine vanes and damage to the remaining 16
- o Severe abrasion of the coating on the turbine shroud
- o Damage to four turbine spacer shields
- o Torsional failure of the turbine shaft adjacent to its output drive spline

Since the major objectives of the program had been satisfied, testing was terminated at this point.

COMBUSTOR PERFORMANCE

The only problem with the combustor was some carbon formation around the variable geometry and radial swirl exits. The combustor geometry was set so that the engine fluctuations in speed and temperature were minimal. Most of the operation was between 30 and 40% open. Starting and operating performance was quite satisfactory during all running.

TEST RESULTS AND DISCUSSION OF RESULTS

INTRODUCTION

The engine was tested in two phases to characterize its performance: IGV mapping and DV/TV mapping. These data were analyzed and compared to an existing (i.e., "original") computer performance model.

Test data confirmed that part power fuel consumption can be improved by adjusting the variable geometry to low-flow settings. DDA concluded that certain of the test points were operated at TV settings different than originally scheduled. That correlation between test data and the original computer model could be improved by making six relatively minor adjustments to the model was also found. Operating the adjusted model at geometry settings actually tested improved the model vs test correlation.

A summary of the testing and analysis is first outlined. Detailed discussions of each item summarized is then presented.

PERFORMANCE SUMMARY

IGV Mapping

Testing of the AGT-2 engine at 66 and 76% $N/\sqrt{\theta}$ nominal speeds over the full range of IGV travel showed the following results.

$N/\sqrt{\theta}$, %	DV, %*	TV, %*	IGV (deg) at max SHP	Maximum shaft power change over full range of IGV travel	
				kW	shp
66	33.5	33.5	3.6	1.5	2.0
66	100	118	22.2	1.3	1.8
76	100	118	13.0	0.7	1.0

These data indicate the variable IGV's have a minimal effect on the engine performance; however, a schedule of closed IGV with closed DV and open IGV with open DV as shown below appears to be optimum.

IGV, deg*	DV, %
1.5	31.5
1.5	63.5
14.4	92.5
21.6	100.0

*NOTE: See Figures 23, 25, and 27 for definition of IGV, DV, and TV travel.

DV and TV Mapping

Testing of a matrix of DV and TV settings at 59 and 70% nominal speeds was used to determine an optimum DV to TV schedule for minimum fuel consumption. These data show that at any DV setting the optimum TV setting is the most closed while still maintaining adequate compressor surge margin. The result is a closed TV and closed DV at low power levels, while high power levels required open TV and DV. Optimum settings follow:

DV, %	TV, %
31.5	53.5
41.0	60
52.5	70
72.5	90
100.0	120

Data vs Engine Model

Engine test points were simulated using a computer model of the engine. Input to the model consisted of the following test parameters corrected to standard ambient conditions of sea level and 15.6°C (60°F):

- o Rotor speed ($N/\sqrt{\theta}$)
- o Compressor diffuser vane setting (DV)
- o Turbine vane setting (TV)
- o Turbine inlet temperature (TIT/θ)
- o Burner variable geometry (BVG)

In addition to this data, the model used test rig compressor and turbine performance and theoretical values for pressure, leakage, mechanical, and radiation losses to calculate the thermodynamic cycle performance for each data point. During the calculation, the model used an iterative technique for flow and energy conservation.

Simulated performance parameters using this model showed a wide scatter when compared with test data (Figures 61 through 69). Analysis of the test data showed possible error in engine airflow measurement resulting from leakage downstream of the measuring station and error in TV settings resulting from vane and linkage damage, which is discussed under "Mechanical Problems." Similarly, the airflow measurement error was present during compressor rig testing, which resulted in the engine model airflow being in error.

The original engine model did not properly account for radiation loss, which by experience from similar test programs is approximately 2.0% of fuel input energy; therefore, the model combustion efficiency was decreased from 99.7% to 97.9%. Also, the model did not account for the additional mechanical loss associated with the addition of the bump stop to the engine for rotor vibration control. This loss was determined to be 2.8 kW (3.8 hp) at 100% N and is proportional to the square of rotor speed.

Using the updated radiation and mechanical loss estimates, the model was revised to accept as input:

- Rotor speed ($N/\sqrt{\theta}$)
- Compressor diffuser vane setting (DV)
- Turbine inlet temperature (TIT/θ)
- Fuel flow ($W_f/\delta\sqrt{\theta}$)
- Compressor pressure ratio (R_c)
- Compressor efficiency (ηc)
- Turbine expansion ratio (R_e)
- Turbine efficiency (ηT)

The model output consisted of:

- Required engine airflow
- Required combustor pressure loss
- Required turbine vane setting
- Compressor rig-to-engine airflow adjustment
- Compressor rig-to-engine efficiency adjustment
- Turbine rig-to-engine efficiency adjustment in addition to the cycle thermodynamic performance

Each test data point was run through this model, and the results were used to produce generalized adjustments, which when applied to the original model resulted in an adjusted model that closely approximated actual engine performance. These adjustments follow:

- Decrease combustor efficiency from 99.7 to 97.7%
- Add bump stop power loss of 2.8 kW (3.8 hp) at 100% N and proportional to the square of rotor speed
- Adjust compressor rig airflow (Figure 75)
- Adjust compressor rig efficiency (Figure 76)
- Set combustor pressure loss (Figure 77)
- Scale turbine rig efficiency by 0.98 (Table VI)

Using the adjusted model, engine performance was simulated at the same conditions as, and compared with, the original model predicted performance. The results are shown on Figures 87 through 90 and in Table VII. On an overall performance basis of fuel consumption and shaft power, the engine performance was slightly poorer than the original model predictions with the greatest difference being at low speed and low power in the variable geometry mode. Fixed geometry to variable geometry performance improvements ranged from approximately 28% fuel reduction at 14.9 kW (20 hp) and 70% speed to 25% reduction at 59.6 kW (80 hp) and 100% speed.

Engine-to-Rig Component Correlation

Generally good correlation was achieved between the engine compressor performance and compressor rig performance. Compressor pressure ratio correlation was good at all speeds and geometry settings. Engine compressor efficiency was better than rig efficiency at the maximum flow geometry settings and high speeds, being 3.5% better at 90% speed and 100% DV.

Correlation of engine turbine performance with turbine rig performance showed engine turbine efficiency to be approximately 2.0 points less than the rig efficiency. Because of errors in turbine geometry settings, a comparison of engine and rig flow capacities could not be made.

TABLE VII. - COMPARISON OF ORIGINAL (UNADJUSTED) MODEL PREDICTED PERFORMANCE WITH ADJUSTED MODEL SIMULATED ENGINE PERFORMANCE

Rotor speed, %	70	80	90	100
Shaft power, kW (hp)	14.9 (20)	29.8 (40)	44.7 (60)	59.6 (80)
Unadjusted model (predicted performance)				
Fixed geometry fuel flow, kg/h (lbm/hr)	34.7 (76.5)	46.8 (103.2)	57.9 (127.7)	67.8 (149.5)
Variable geometry fuel flow, kg/h (lbm/hr)	24.8 (54.7)	34.7 (76.5)	43.8 (96.6)	51.0 (112.5)
Fixed geometry to variable geometry fuel reduction, %	28.5	25.9	24.4	24.7
Adjusted model (simulated engine performance)				
Fixed geometry fuel flow, kg/hr (lbm/hr)	35.7 (78.7)	47.7 (105.1)	58.4 (128.7)	67.8 (149.5)
Variable geometry fuel flow, kg/hr (lbm/hr)	25.9 (57.0)	35.0 (77.2)	43.8 (96.6)	50.8 (112.0)
Fixed geometry to variable geometry fuel reduction, %	27.6	26.5	25.0	25.1
Unadjusted model/adjusted model				
Fixed geometry fuel ratio	0.972	0.982	0.991	1.000
Variable geometry fuel ratio	0.960	0.991	1.000	1.004

PERFORMANCE MAPPING

Effect of IGV Settings

Initial testing of the AGT-2 engine determined the effects of compressor variable inlet guide vanes on engine performance and established a schedule of IGV to compressor variable diffuser vanes for further engine testing. These data are shown on Figure 31 as corrected power and fuel flow vs IGV at constant speed, TIT, DV, and TV. Although the data (Figure 31) shows a minimal effect of IGV on engine performance, an optimum schedule was selected for further engine testing. This test schedule is compared with the composite compressor rig map schedule on Figure 32. Because of IGV actuator and linkage limitations the IGV travel for the engine test was limited to a range from 1.5 to 22.3 deg rather than the 0- to 27.3-deg range for the compressor rig test. Because of the minimal performance effect of the IGV's, the small differences between the test and compressor map schedules did not present a problem for analysis of engine test data. As discussed previously, the minimal effects of the IGV were expected based on previous rig test results. These showed the variable DV to be superior to the variable IGV for extending the compressor flow range of stable operation. Also, inlet flow distortions may have reduced the effectiveness of the IGV.

Effect of DV and TV Settings--Original Engine Model

The second phase of the test program characterized the engine performance effects of variable diffuser vane and turbine vane. Figures 33 through 43 show predicted engine performance using a computer model of the AGT-2 engine with rig performance maps for the variable geometry compressor and turbine. Compressor and turbine rig performance maps are shown on Figures 44 through 56, and Figure 57 shows estimated turbine diffuser pressure loss as a function of diffuser inlet flow and turbine corrected speed. The turbine diffuser loss was based on turbine rotor exit swirl and Mach number. Table VIII shows maximum power parameters for the predicted AGT-2 nonrecuperative maximum power performance.

TABLE VIII. - PREDICTED AGT-2 NONRECUPERATIVE MAX POWER PERFORMANCE PARAMETERS

Ambient total pressure, kPa abs (psia)	101.325 (14.696)
Ambient temperature, °C (°F)	15.6 (60)
Inlet pressure loss, %	1.0
Inlet air flow, kg/s (lbm/sec)	1.283 (2.828)
Compressor pressure ratio	4.278
Compressor efficiency, %	72.8
Compressor discharge bleed	
Cooling to turbine inlet, %	0.53
Cooling to turbine exit, %	0.21
Overboard leakage, %	3.5
Compressor inlet guide vane setting	(composite with compressor diffuser vane)
Compressor diffuser vane setting, % throat	100
Compressor to burner duct pressure loss, %	2.0
Fuel lower heating value, MJ/kg (Btu/lbm)	43.424 (18,400)
Fuel hydrogen to carbon mass ratio	0.1667
Fuel density, kg/L (lbm/gal)	82 (6.8)
Combustion efficiency, %	99.7
Combustor inlet Mach number	0.15
Combustor pressure loss, %	5.84
Turbine inlet temperature	
Scroll inlet, °C (°F)	037.8 (1900)
Rotor inlet, °C (°F)	1033.9 (1893)
Rotor shaft speed, rpm	53,000 (100%)
Turbine expansion ratio	
(scroll inlet to rotor exit)	3.372
Turbine adiabatic efficiency, %	83.2
Turbine efficiency ratio (N_R effect)	0.9879
Turbine vane setting, % throat	120
Turbine diffuser pressure loss, %	1.3
Exhaust duct pressure loss, %	12.6
Output shaft speed, rpm	4 000 (100%)
Engine accessory load, kW (hp)	5.97 (8.0)
Rotor bearing and windage, kW (hp)	2.61 (3.5)
Reduction gear box loss, %	1.0
Output shaft power, kW (hp)	143.9 (193.1)
Fuel flow, kg/h (lbm/hr)	101.7 (224.1)
Specific fuel consumption, mg/W·h (lbm/hp-hr)	705.6 (1.160)

Figures 33 through 36 show the effects of DV and TV on engine performance parameters of fuel flow and shaft power at constant rotor speeds (N) of 70, 80, 90, and 100% and maximum continuous turbine inlet temperature of 926.7°C (1700°F). These data show that at constant rotor speed, reduced fuel consumption can be achieved at constant shaft power by optimizing the DV and TV settings. It should be noted that reduced TV settings at constant DV setting result in decreased compressor surge margin as the operating point approaches the surge line of the compressor resulting in reduced flow capacity of the turbine. Figure 37 shows TV setting vs compressor surge margin at constant DV setting, N, and TIT. Selecting a minimum surge margin of 8% steady state will allow surge-free operation during engine transients and non-standard day operation. Figure 38 is a cross plot of Figure 37 showing DV vs TV setting for 8% surge margin at constant N and TIT. Because the DV to TV schedules for 8% minimum surge margin are very similar for all speeds and to simplify the engine control, a single schedule was selected as shown on Figure 39. This schedule between 40 and 91% TV setting will meet the 8% minimum surge margin at all engine speeds. Above 91% TV setting and above 96.3% rotor speed the selected schedule will result in reduced surge margin to a minimum of 2.5% at 100% speed.

Figures 40 through 43 show predicted engine performance at constant engine speeds for the variable geometry engine using the variable geometry schedule of Figure 39 compared with the predicted performance of a fixed geometry engine with variable TIT at constant 100% DV and 120% TV. Maximum power is achieved in both cases at 1037.8°C (1900°F) TIT with 100% DV and 120% TV.

The performance of a true fixed geometry engine would be better than the predicted performance shown on Figures 40 through 43 because the vane end-wall clearance required for vane actuation in the variable geometry engine would not be present in a fixed geometry engine. The clearance required in the variable geometry engine results in end-wall leakage and reduced component efficiency.

AGT-2 engine testing for performance effects of variable DV and TV consisted of:

1. Testing a matrix of DV and TV settings at rotor speeds of 59 and 70% $N/\sqrt{\theta}$ nominal and constant turbine inlet temperature of 788°C (1450°F) TIT/θ nominal to establish an optimum DV vs TV schedule
2. Using the DV vs TV schedule established in (1) above for testing at 70, 77, and 90% $N/\sqrt{\theta}$ near maximum continuous turbine inlet temperature, 926.7°C (1700°F) TIT/θ, to determine variable geometry effects
3. Simulating a fixed geometry engine by testing at 70, 77, 90, 95, and 100% $N/\sqrt{\theta}$ with 100% DV and 120% TV from near 926.7°C (1700°F) TIT/θ to low TIT

Figures 58 and 59 show test results of fuel flow vs shaft power for the matrix of DV and TV at 59 and 70% $N/\sqrt{\theta}$ nominal. Because of the similarity of test results (Figure 59) and predicted performance (Figure 33 at 70% $N/\sqrt{\theta}$ in terms of trends) and because predicted performance shows a single DV vs TV schedule may be used at all speeds, a schedule of DV vs TV was established from Figure 59 for use in further testing. This test schedule is shown on Figure 60

compared with the predicted schedule from Figure 39. To minimize the risk of compressor surge and possible engine damage, the test schedule called for TV throat areas greater than that predicted at the same DV throat area.

DATA ANALYSIS PROCEDURE

The following outline briefly describes the procedure used for analysis of the engine test data. More detailed explanations are presented later.

- o Run original engine model to test conditions and compare results with test data
- o Determine model adjustments required to match test data (i.e., overall and component performance) at specific data points
- o Generalize required model adjustments to best fit the test data
- o Simulate engine performance using adjusted model and compare results with original predicted performance

ORIGINAL MODEL SIMULATION

Further engine testing consisted of operation over a range of TIT and DV and TV settings (per Figure 60) at constant engine speeds. These data were then modeled using the computer model with component rig performance maps at the test conditions of N, TIT, DV, TV, and BVG. The results of the modeling are compared with test data on Figures 61 through 69 as follows:

Model vs test	Figure
Shaft power	61
Fuel flow	62
Compressor inlet air flow	63
Compressor pressure ratio	64
Compressor efficiency	65
Turbine expansion ratio	66
Compressor exit to turbine pressure loss	67
Turbine exit to ambient pressure loss	68
Turbine efficiency	69

The following off design assumptions were made in the model:

- o Combustion efficiency is constant 99.7%
- o Rotor bearing and windage loss is given by:
  $HP_{B\&W} = 5.0\ (\text{rotor speed}/63{,}000)^2$
- o Accessory drive loss is given by
  $HP_{Acc} = 8.0\ (\text{rotor speed}/53{,}000)^2$
- o Reduction gearbox loss is 1.0% of input power
- o Burner ΔP was scaled as a function of test BVG (Figure 70)
- o Rig turbine efficiency was scaled by 0.9879 to account for estimated rig to engine Reynolds number effect

All engine parameters (Figures 61 through 69) show considerable deviation of the model data from the actual test data.

REQUIRED MODEL ADJUSTMENTS

Analysis of the engine test and modeling techniques indicated the model required adjustment to match the test results more closely. Based on previous test experience, the engine radiation heat loss to ambient through the engine skin is approximately 2% of fuel flow; therefore, model burner efficiency was decreased from 99.7 to 97.7%.

Analysis indicated a need for an additional mechanical power loss of 2.8 kW (3.8 hp) at 100% N as a result of the addition of the bump stop to minimize rotor shaft vibration. This loss was assumed proportional to the square of rotor speed (typical bearing loss).

The following model parameters were then adjusted to achieve a match of certain test parameters for each data point.

Model parameter	Test parameter
Compressor rig airflow	Fuel flow
TV	Compressor pressure ratio
Compressor rig efficiency	Engine compressor efficiency
Turbine rig efficiency	Turbine efficiency (calculated)
ΔP-compressor to turbine	Turbine expansion ratio

Because the airflow-measuring station for both the engine test and the compressor rig test was upstream of a leak source at the compressor variable geometry linkage opening, it was decided to use the measured fuel flow and burner temperture rise to compute the required airflow. Also it was noted from the unadjusted model airflow vs measured airflow (Figure 63) that there are two distinct sets of data characterized by different airflow orifice diameters. Four orifice sizes were used during the engine testing--101.6 mm (4.0 in.) dia, 139.7 mm (5.5 in.) dia, 171.5 mm (6.75 in.) dia, 203.2 mm (8.0 in.) dia--because of the extreme flow range of the engine. Airflow data taken with the largest orifice--203.2 mm (8.0 in.) dia--are not consistent with the three small orifice sizes or with model airflow indicating inaccuracy in the large orifice airflow data.

Teardown inspections of the engine showed damage to the TV's, i.e., bent tips and twisted shafts, indicating that the positioning of the vanes was probably not consistent with actuator positioning. On this probability and the scattering of unadjusted model pressure ratio vs test pressure ratio (Figure 64), it was decided to adjust model TV to match the test pressure ratios.

Model compressor efficiency was adjusted to match engine test efficiency for all data points.

The unadjusted model varied combustor pressure loss as a function of combustor position based on estimates from the combustor design group (Figure 70). This loss is included in the model compressor-to-turbine pressure loss versus the engine test value (Figure 67). Because of the poor matching of the model and test data at the closed combustor positions, it appears there is a probable error in the reported test combustor position. Based on this and the error of

generally less than 1.5 points between the model exhaust pressure loss and the engine test value (Figure 68), DDA decided to adjust the combustor pressure loss to match test turbine expansion ratio.

Test turbine efficiency was calculated based on compressor work, shaft power, mechanical power loss, turbine inlet temperature and turbine expansion ratio. The model turbine efficiency was then adjusted to match the calculated test efficiency.

The results are shown on Figures 71 through 74 as DV vs adjusted TV, model shaft power, airflow, and compressor to turbine pressure loss versus test values. The adjusted variable geometry schedule (Figure 71) shows two sets of data, which are characterized by engine build, thus indicating a turbine geometry calibration change between BU 2 through BU 8 and BU 9. This is in all probability a result of the damaged turbine vane mentioned earlier and thermal expansion.

Thus when the measured values of fuel flow, compressor efficiency, compressor pressure ratio, turbine inlet temperature, turbine expansion ratio, calculated turbine efficiency, compressor diffuser vane setting, and rotor RPM are put into the model, horsepower, airflow, and compressor-to-turbine pressure loss are calculated results as shown on Figures 72 through 74.

Calculated horsepower (Figure 72) agrees very well with the measured value from test.

Figure 73 shows model airflow versus test with results similar to the unadjusted model (Figure 63). Again the data taken with the large orifice is distinctly different from data obtained with the smaller orifice plates.

The matching of model compressor to turbine pressure loss to test data (Figure 74) is improved over the unadjusted model (Figure 67).

GENERALIZED MODEL ADJUSTMENTS

Based on the resulting adjustments to the model to match each data point, generalized adjustments, which when applied to the model will result in model performance that is representative of and in good agreement with engine test data, were developed. Figure 75 shows the incremental change of airflow vs compressor rig flow that must be added to rig flow to match engine flow. The increment varies from 0.08 kg/s (0.17 lbm/sec) at 0.18 kg/s (0.4 lbm/sec) rig flow to -0.07 kg/s (-0.15 lbm/sec) at 1.36 kg/s (3.0 lbm/sec) rig flow. Figure 76 shows the ratio of engine compressor efficiency to rig efficiency as a function of rig flow. This correction factor varies from 1.0 at 0.15 kg/s (0.34 lbm/sec) rig flow to 1.057 at 1.36 kg/s (3.0 lbm/sec) rig flow. Figure 77 shows the burner pressure loss as a function of burner inlet flow to achieve a match on turbine expansion ratio. This compares with the unadjusted model (Figure 70), which also varied with burner variable geometry position. In addition to these corrections, the turbine rig efficiency must be scaled by a factor of 0.98 to match the calculated turbine efficiency. This compares with a 0.9879 factor used in the unadjusted model for the effect of Reynolds number from cold rig to hot engine. Table VI shows the engine-to-rig turbine efficiency ratio required to match the calculated turbine efficiency.

To verify these generalized adjustments, the model was rerun to test conditions of N, TIT, DV, and the specific TV setting points per Figure 71. Figures 78 through 86 show the model results versus engine test results. For most parameters, substantial improvements were made in matching model results to test results as shown in Table IX.

TABLE IX. - PERCENTAGE OF MODEL DATA POINTS WITHIN SPECIFIED TOLERANCE BAND OF ENGINE DATA POINTS

Parameter	Tolerance	Unadjusted model, %	Adjusted model, %	Points improvements
Shaft power	± 3.7 kW (± 5.0 hp)	42	65	23
Fuel flow	± 2.3 kg/h (± 5.0 lbm/hr)	66	94	28
Compressor pressure ratio	± 0.1	58	90	32
Compressor efficiency	± 5.0 points	72	90	18
Turbine expansion ratio	± 0.1	52	90	38
Turbine efficiency	± 5.0 points	87.5	69	-18.5
Compressor-turbine pressure loss	± 1.0 points	36	75	39
Exhaust pressure loss	± 1.0 points	58	63	5

ADJUSTED MODEL PERFORMANCE

Table VI and Figures 78 through 86 indicate the generalized adjustments that result in an adjusted model performance, which is representative of engine performance. Using the adjusted model, engine performance was simulated at constant engine speeds for the variable geometry engine using the predicted variable geometry schedule of Figure 39 and for a fixed geometry engine with variable TIT at constant 100% DV and 120% TV. The engine test performance as represented by the adjusted model is compared with the predicted engine performance on Figures 87 through 90 at rotor speeds of 70, 80, 90, and 100% $N/\sqrt{\theta}$.

Table X shows the correlation of simulated engine performance using the adjusted model to predicted performance using the unadjusted model. The maximum shaft power deviation is 3.7%, and the maximum fuel flow deviation is 4.6%.

Table XI shows the fuel flow reduction from fixed to variable geometry using simulated engine performance. Maximum fuel flow reductions occur at low power settings, being near 30% reduction at zero output power. At 14.9 kW (20 shp), the reduction ranges from 27.4% at 70% speed to 29.8% at 100% speed.

Although model adjustments were required to obtain model versus test agreement for all performance parameters, the original (i.e., unadjusted) model agreed well with test data on an overall horsepower versus fuel flow basis (ref Figures 87 through 90).

TABLE X. - SHAFT POWER AND FUEL FLOW CHANGE FROM PREDICTED PERFORMANCE TO SIMULATED ENGINE PERFORMANCE AT VARIOUS ENGINE CONDITIONS

Condition	Predicted performance	Adjusted model simulation	Percent change--predicted to simulated
100% N, 1 037.8°C (1900°F)			
SHP	143.8 kW (193 hp)	148.3 kW (199 hp)	3.1
W_f	101.6 kg/h (224 lbm/hr)	103.4 kg/h (228 lbm/hr)	1.8
100% N, 926.7°C (1700°F)			
SHP	113.3 kW (152 hp)	115.5 kW (155 hp)	2.0
W_f	88.5 kg/h (195 lbm/hr)	89.4 kg/h (197 lbm/hr)	1.0
100% N, 59.6 kW (80 hp), fixed geometry			
W_f	67.8 kg/h (149.5 lbm/hr)	67.8 kg/h (149.5 lbm/hr)	0.0
100% N, 59.6 kW (80 hp), variable geometry			
W_f	51.0 kg/h (112.5 lbm/hr)	50.8 kg/h (112 lbm/hr)	-0.4
90% N, 1 037.8°C (1900°F)			
SHP	89.8 kW (120.5 hp)	92.4 kW (124 hp)	2.9
W_f	78.2 kg/h (172.5 lbm/hr)	80.5 kg/h (177.5 lbm/hr)	2.9
90% N, 926.7°C (1700°F)			
SHP	70.8 kW (95 hp)	73.4 kW (98.5 hp)	3.7
W_f	69.2 kg/h (152.5 lbm/hr)	71.0 kg/h (156.5 lbm/hr)	2.6
90% N, 44.7 kW (60 hp), fixed geometry			
W_f	57.8 kg/h (127.5 lbm/hr)	58.5 kg/h (129 lbm/hr)	1.2
90% N, 44.7 kW (60 hp), variable geometry			
W_f	43.8 kg/h (96.5 lbm/hr)	43.8 kg/h (96.5 lbm/hr)	0.9
80% N, 1 037.8°C (1900°F)			
SHP	62.2 kW (83.5 hp)	63.3 kW (85 hp)	1.8
W_f	65.3 kg/h (144 lbm/hr)	67.1 kg/h (148 lbm/hr)	2.8
80% N, 926.7°C (1700°F)			
SHP	49.9 kW (67 hp)	50.7 kW (68 hp)	1.5
W_f	57.8 kg/h (127.5 lbm/hr)	59.2 kg/h (130.5 lbm/hr)	2.4
80% N, 29.8 kW (40 hp), fixed geometry			
W_f	46.7 kg/h (103 lbm/hr)	47.6 kg/h (105 lbm/hr)	1.9
80% N, 29.8 kW (40 hp), variable geometry			
W_f	34.7 kg/h (76.5 lbm/hr)	35.2 kg/h (77.5 lbm/hr)	1.3
70% N, 1 037.8°C (1900°F)			
SHP	44.0 kW (59 hp)	44.3 kW (59.5 hp)	0.8
W_f	53.5 kg/h (118 lbm/hr)	55.3 kg/h (122 lbm/hr)	3.4
70% N, 926.7°C (1700°F)			
SHP	33.9 kW (45.5 hp)	34.3 kW (46 hp)	1.1
W_f	47.6 kg/h (105 lbm/hr)	49.2 kg/h (108.5 lbm/hr)	3.3
70% N, 14.9 kW (20 hp), fixed geometry			
W_f	34.7 kg/h (76.5 lbm/hr)	35.6 kg/h (78.5 lbm/hr)	2.6
70% N, 14.9 kW (20 hp), variable geometry			
W_f	24.7 kg/h (54.5 lbm/hr)	25.9 kg/h (57 lbm/hr)	4.6

TABLE XI. - PERCENT REDUCTION OF FUEL FLOW USING VARIABLE GEOMETRY

Shaft power, kW (hp)	Rotor speed, %			
	70	80	90	100
0 (0)	28.9	31.3	32.4	32.4
14.9 (20)	27.4	28.8	28.7	29.8
29.8 (40)	19.0	26.7	28.7	29.4
44.7 (60)	---	19.1	25.2	30.4
59.6 (80)	---	---	17.1	25.3
74.5 (100)	---	---	---	19.8
104.3 (140)	---	---	---	8.6

RECUPERATIVE PERFORMANCE

Figure 91 shows the performance of the AGT-2 as a recuperative engine using the engine model as compared to predicted performance of the original recuperative engine design with predicted component maps.

Specific fuel consumption vs shaft horsepower at 70% $N/\sqrt{\theta}$ and open geometry position for the nonrecuperative engine is also shown in this figure. The solid line is based upon the computer simulation using component rig maps, while the circles represent engine data from current testing.

Again, both sets of data show good correlation between predicted performance and actual performance.

CONCLUSIONS

The AGT-2 engine was designed as a recuperative, single-shaft automotive gas turbine of 167.8 kW (225 shp) rating with wide-range, variable geometry compressor and turbine and a low emission, variable geometry burner. The engine in the original design configuration underwent very limited testing in 1974.

The existing AGT-2 engine was rebuilt in a nonrecuperative configuration and was performance tested between June and December 1978. This testing was to characterize the performance of a single-shaft engine incorporating wide-range, variable geometry components. Additionally, the test results were to be used to verify engine modeling techniques using a digital computer program with component rig test performance maps.

Results of this testing supported the following conclusions:

- o Significant engine performance improvements are available by using compressor variable diffuser vanes and variable turbine vanes. These improvements are particularly significant at part-power conditions. A variable geometry to fixed geometry performance comparison showed, as an example at 14.9 kW (20 shp), a reduction in fuel flow from 27.4% at 70% engine speed to 29.8% at 100% engine speed using the adjusted model simulation at 926.7°C (1700°F) TIT and 8% surge margin DV to TV schedule.
- o Compressor variable inlet guide vanes have minimal effect on the AGT-2 engine performance, although this was expected based on compressor rig test results. Inlet distortion may have reduced IGV effectiveness on the AGT-2 engine.
- o There is an optimum schedule of compressor variable diffuser vanes to turbine variable vanes to achieve best performance while maintaining adequate compressor surge margin.
- o Current engine modeling techniques using component rig test performance maps are sufficiently accurate to predict the overall performance of a gas turbine engine having wide range variable geometry components and a single-shaft configuration.
- o Adjustments to the engine model to simulate test data indicated engine airflow to be 0.08 kg/s (0.17 lbm/sec) higher than rig flow at 0.18-kg/s (0.4-lbm/sec) rig flow and decreasing to 0.07 kg/s (0.15 lbm/sec) lower than rig flow at 1.36-kg/s (3.0-lbm/sec) rig flow. The ratio of engine compressor efficiency to rig efficiency ranged from 1.0 at 0.15-kg/s (0.34-lbm/sec) rig flow to 1.057 at 1.36-kg/s (3.0-lbm/sec) rig flow. The ratio of engine turbine efficiency to rig efficiency was 0.98 at all turbine conditions. Because of errors in reported turbine geometry settings, engine turbine flow capacity was assumed equal to the rig values.

APPENDIX A

List of Symbols and Abbreviations

BHP	Brake horsepower
BU	Build
BVG	Burner variable geometry
DDA	Detroit Diesel Allison
DOE	Department of Energy
DV	Compressor diffuser vane setting
ele	Elements
GM	General Motors
IGV	Compressor inlet guide vane setting
N	Engine speed
N_R	Reynolds number
NASA	National Aeronautics and Space Administration
R_c	Compressor pressure ratio
R_e	Turbine expansion ratio
RPM	Revolutions per minute
SEL	Systems Engineering Laboratory
SFC	Specific fuel consumption
SHP	Shaft horsepower
T/C	Thermocouple
TIT	Turbine inlet temperature
TV	Turbine vane setting
V_{CR}	Velocity at conditions corresponding to Mach number of 1
W	Gas flow
W_a	Airflow
W_f	Fuel flow
γ	Ratio of specific heats
γ^*	Ratio of specific heats at U.S. standard sea level conditions of 1.013×10^2 kPa and 288.2 K
ϵ	Specific heat ratio correction, $\frac{\gamma^* (2/(\gamma^*-1))^{\gamma^*/(\gamma^*-1)}}{\gamma (2/(\gamma-1))^{\gamma/(\gamma-1)}}$
η_C	Compressor efficiency
η_T	Turbine efficiency
ρ	Ratio of absolute pressure to standard absolute pressure at U.S. standard sea level conditions of 1.013×10^2 kPa and 288.2 K
θ	Ratio of absolute temperature to standard absolute temperature at U.S. standard sea level conditions of 1.013×10^2 kPa and 288.2 K
θ_{CR}	Squared ratio of critical velocity at inlet to critical velocity at U.S. standard sea level conditions of 1.013×10^2 kPa and 288.2 K
Btu/lbm	British thermal units per pound mass
^oC	Degrees Celcius
^oF	Degrees Farenheit
ft/sec	Feet per second
hp	Horsepower
in.	Inches
kg	Kilograms
kg/L	Kilograms per liter

$kg \cdot m^2$	Kilogram meters squared
kg/s	Kilograms per second
kPa	Kilopascals
kPa abs	Kilopascals absolute
kW	Kilowatts
lbm	Pounds mass
lbm/gal	Pounds mass per gallon
lbm/hp-hr	Pounds mass per horsepower hour
$lbm\text{-}in.^2$	Pounds mass inches squared
lbm/sec	Pounds mass per second
MJ/kg	Megajoules per kilogram
mg/W•h	Milligrams per watt hour
mm	Millimeters
m/sec	Meters per second
psia	Pounds per square inch absolute
psig	Pounds per square inch gage

APPENDIX B

Figures 1 through 91

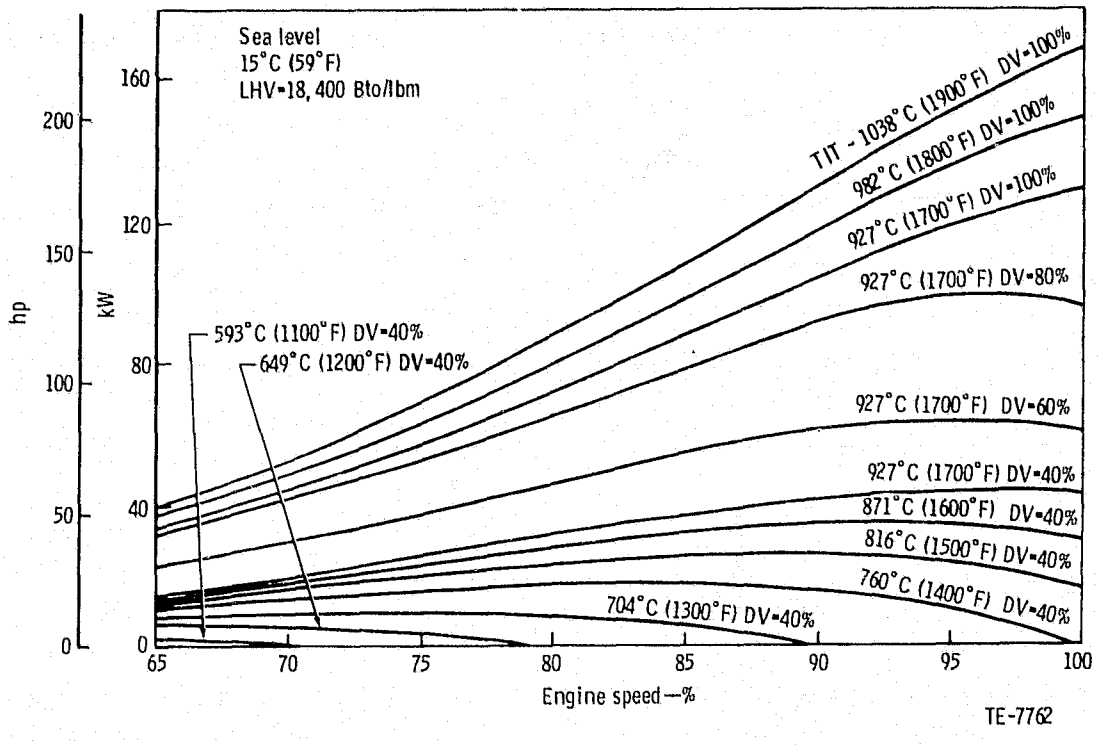

Figure 1. - AGT-2 Variable Geometry Performance.

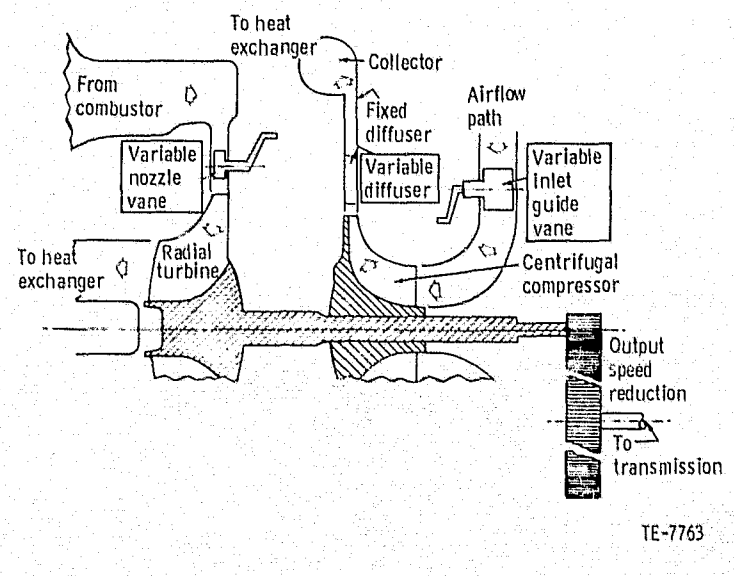

Figure 2. - AGT-2 Automotive Gas Turbine Schematic.

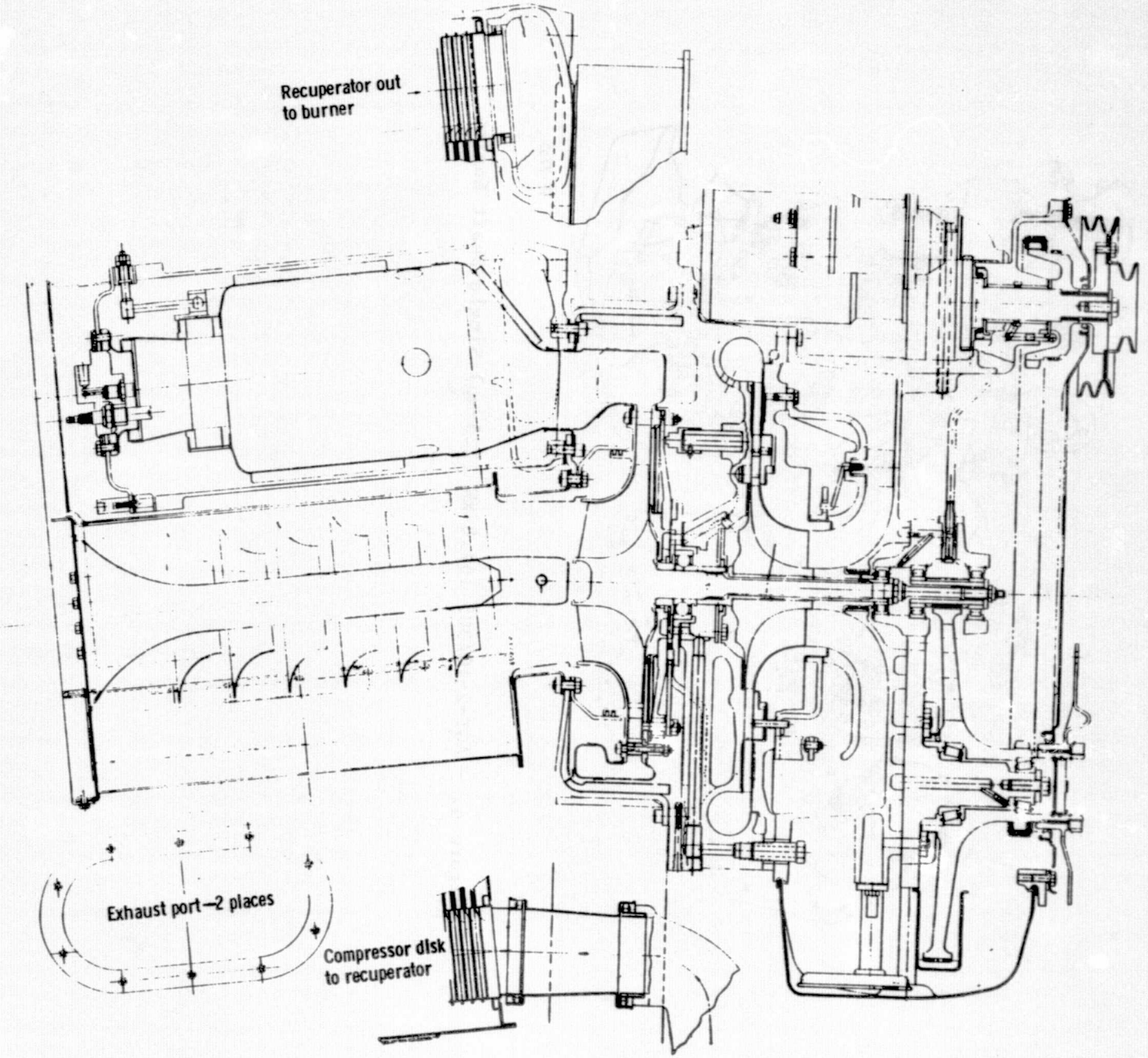

E-7764

Figure 3. - AGT-2 Automotive Gas Turbine Cross Section.

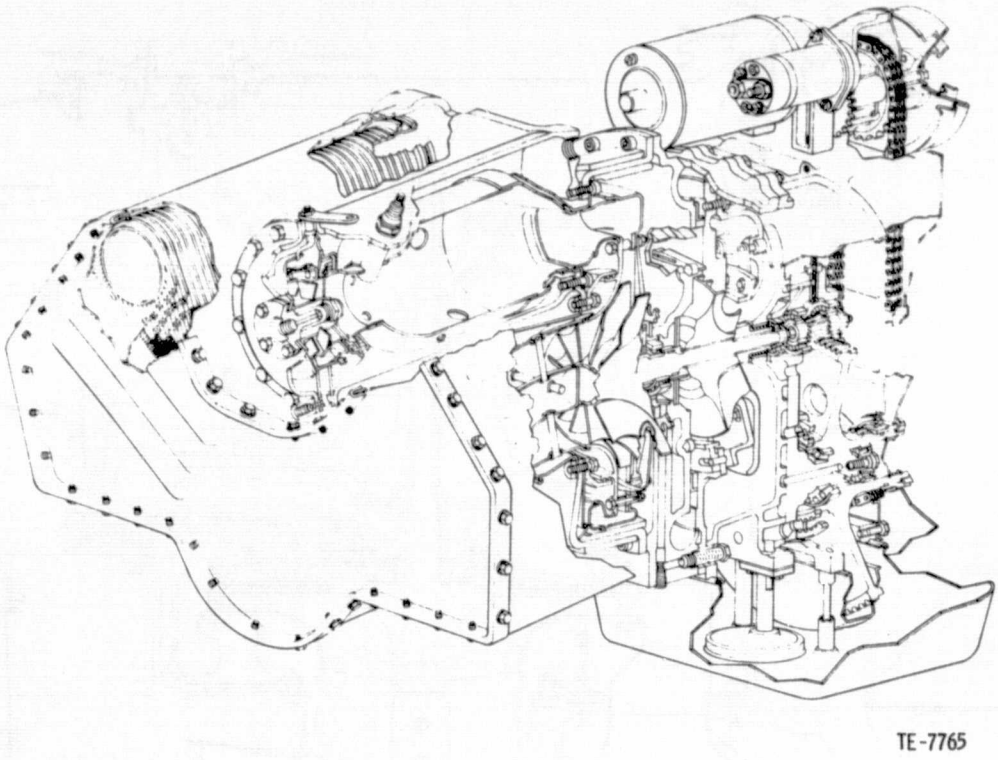

Figure 4. - AGT-2-1C/305 167.8-kW (225-hp) Single-Shaft Engine.

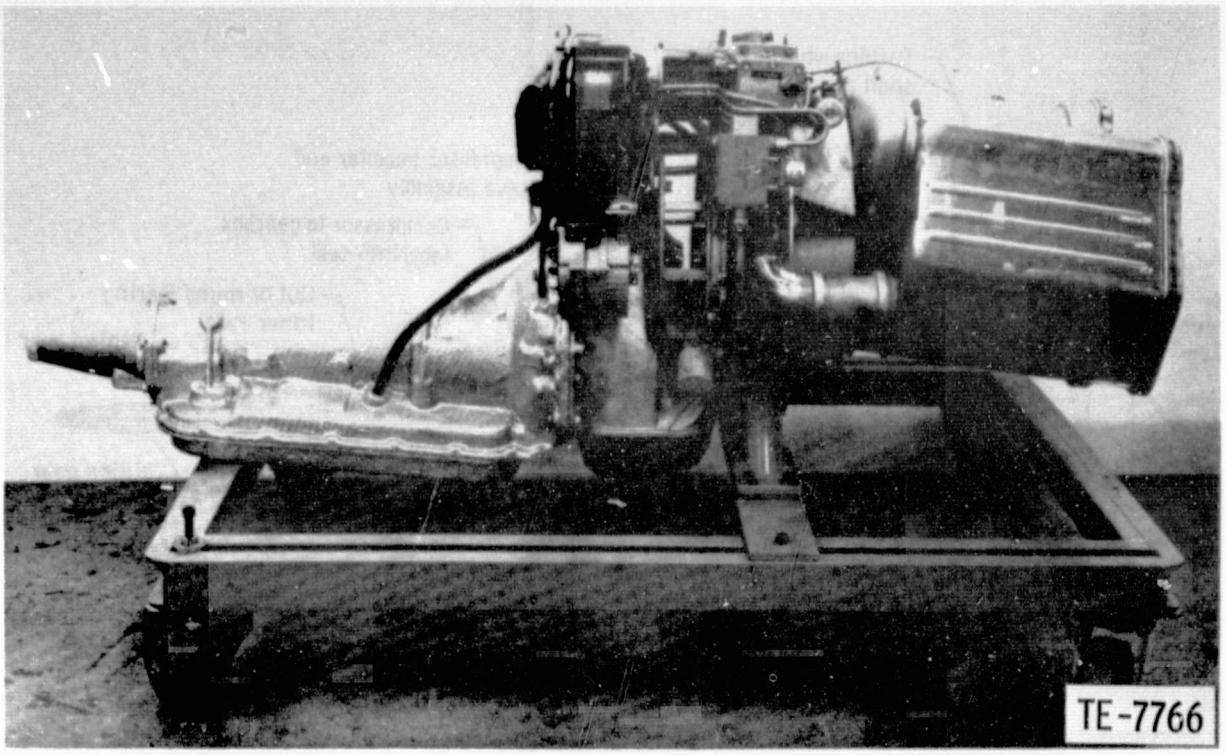

Figure 5. - Mock-Up of AGT-2 Automotive Gas Turbine.

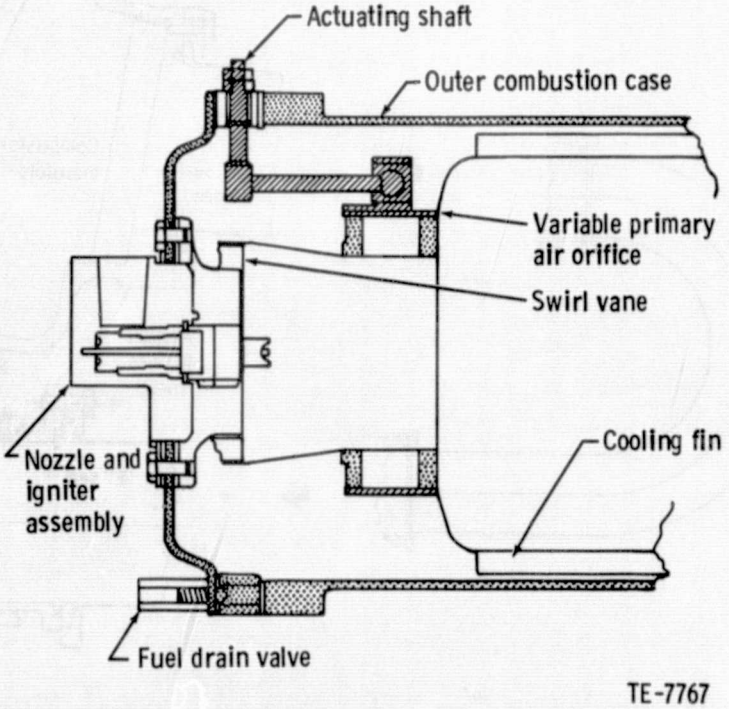

Figure 6. - AGT-2-1C/305 Low Pressure-Drop Combustor.

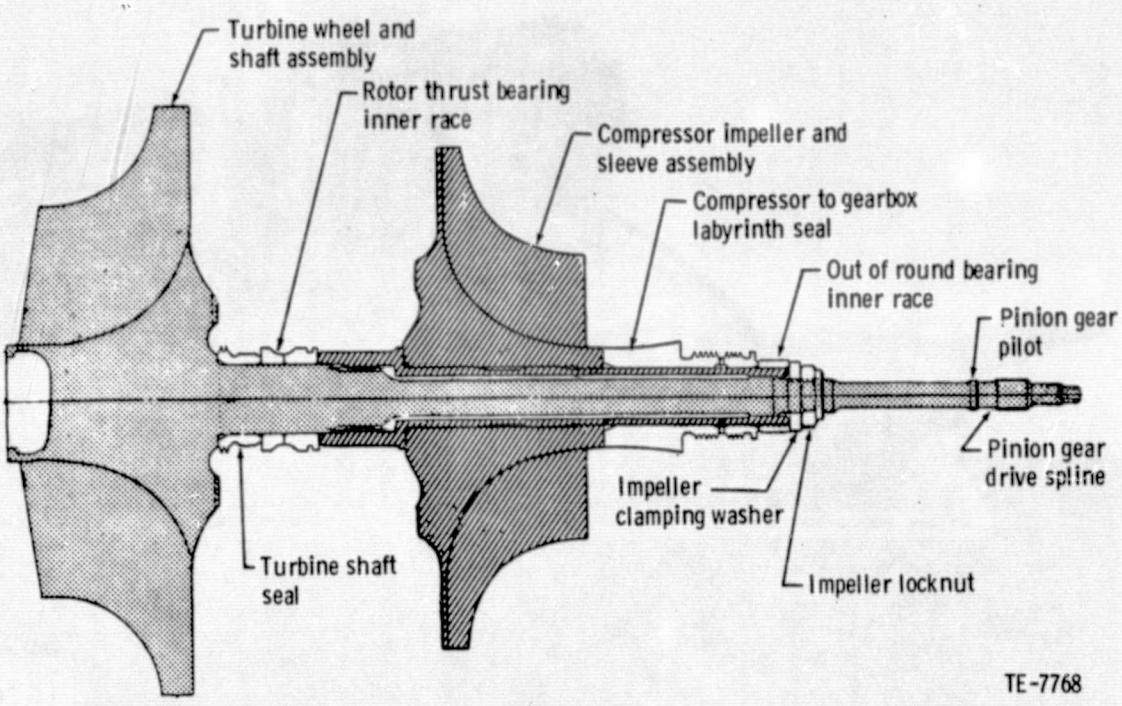

Figure 7. - AGT-2-1C/305 Rotor.

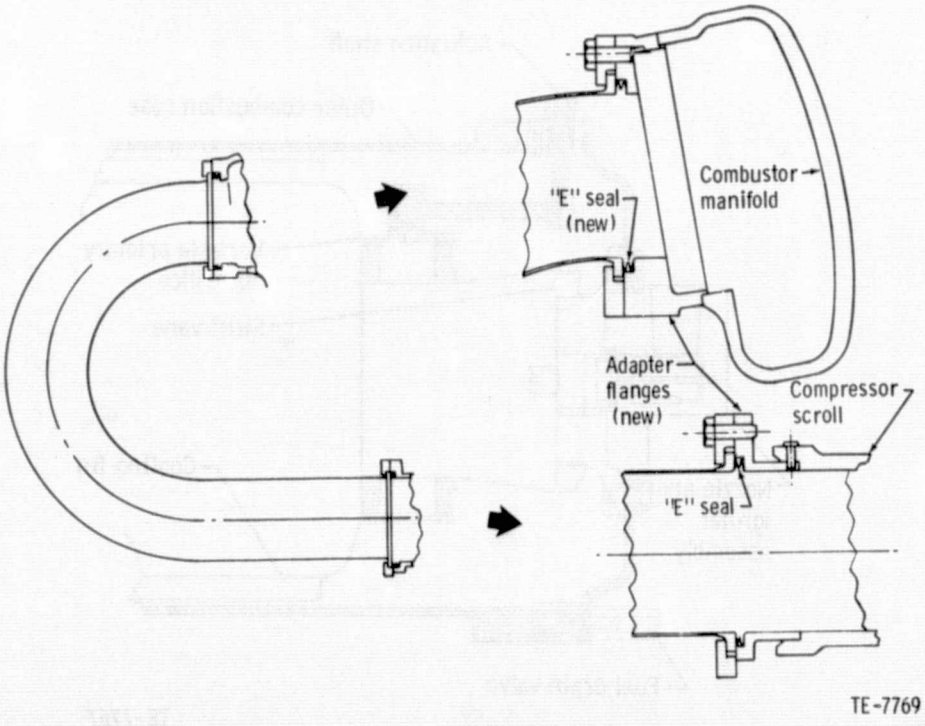

Figure 8. - Transfer Tube Arrangement.

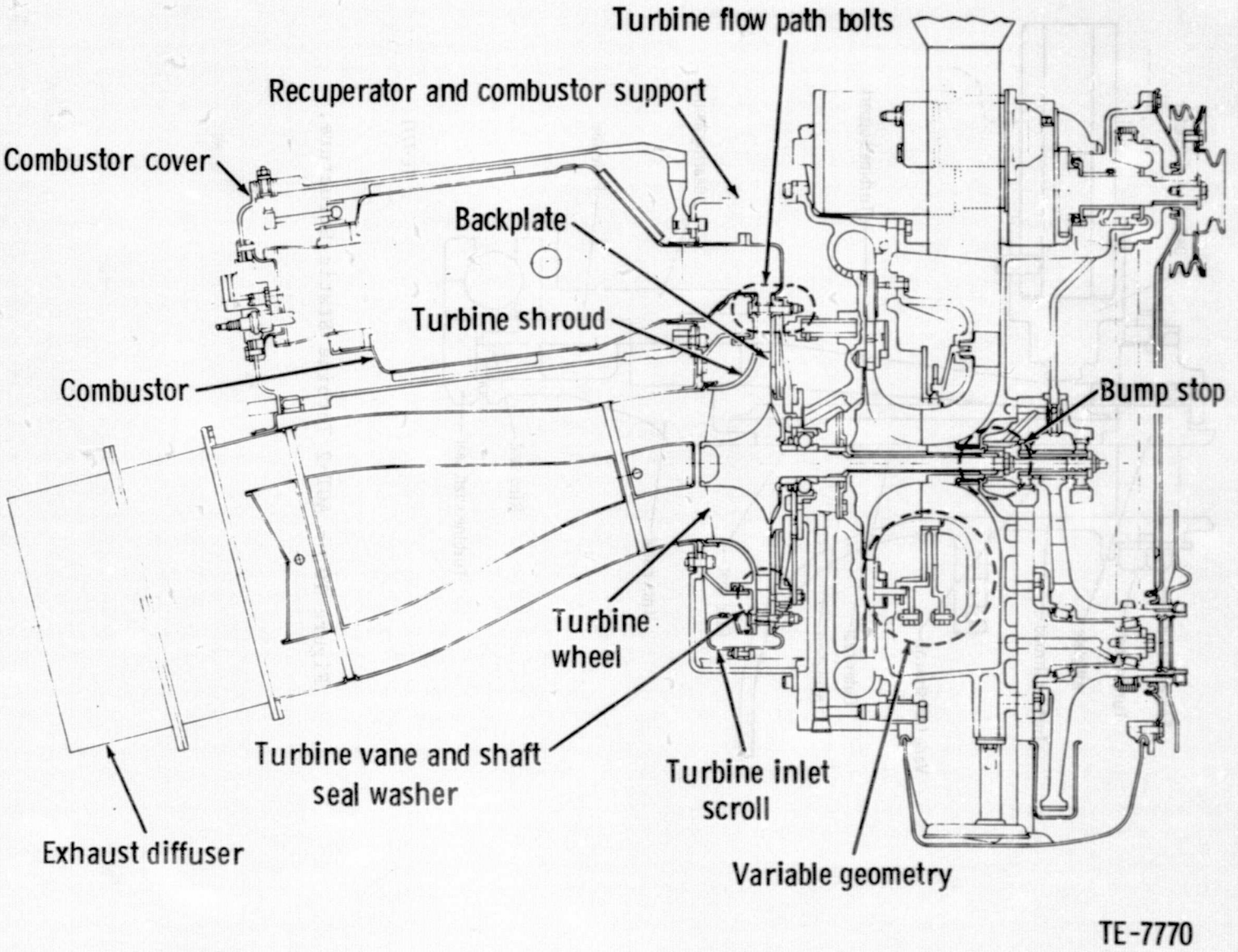

Figure 9. - Modified AGT-2 Engine for NASA/DOE Test.

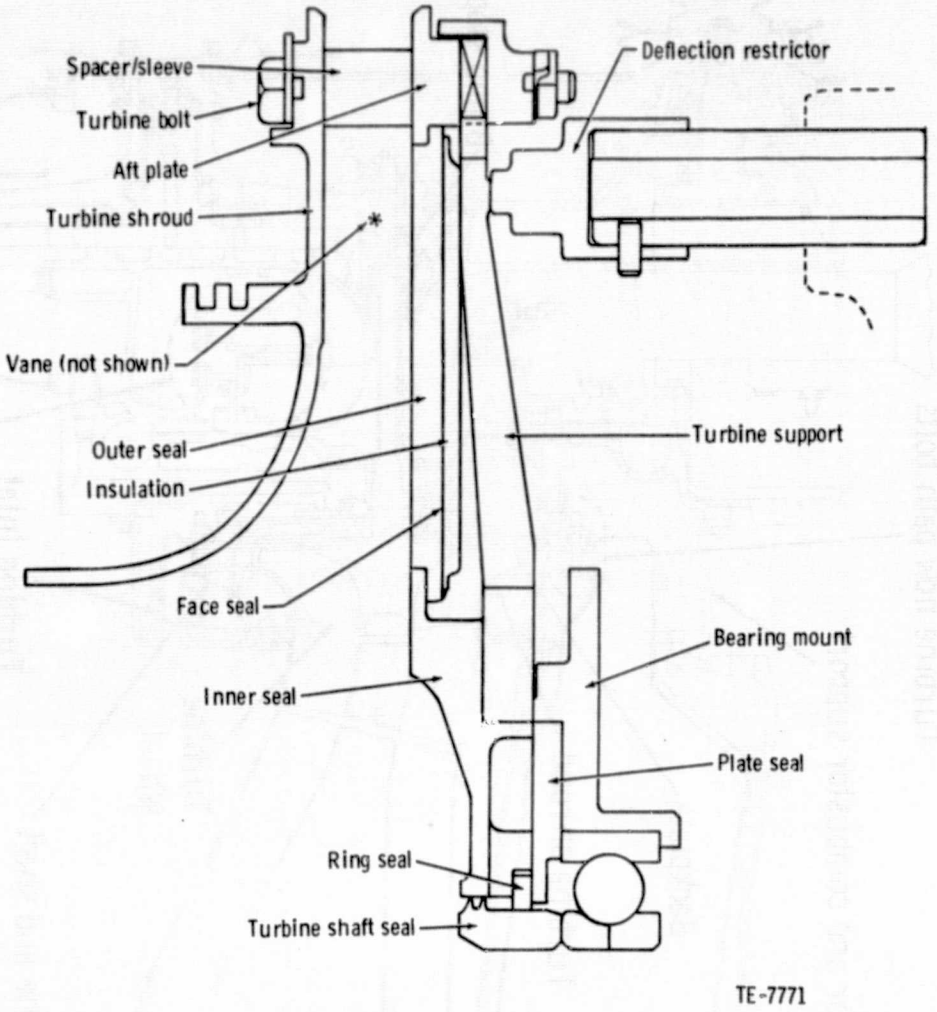

Figure 10. - AGT-2 Turbine Static Structure.

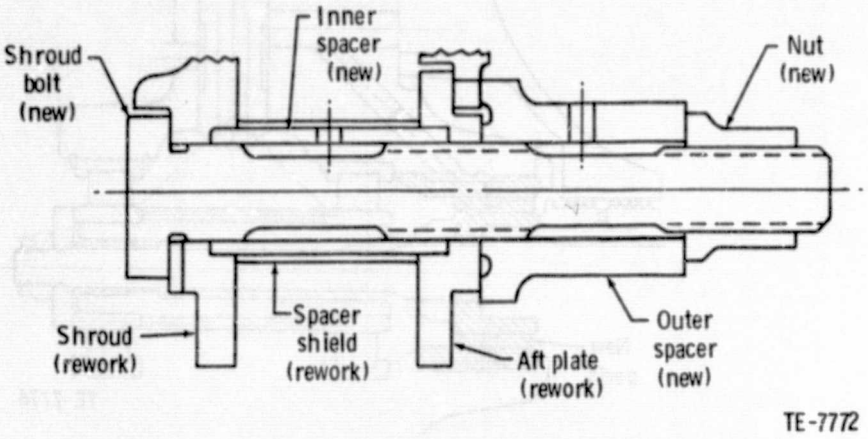

Figure 11. - Turbine Shroud Bolt Arrangement.

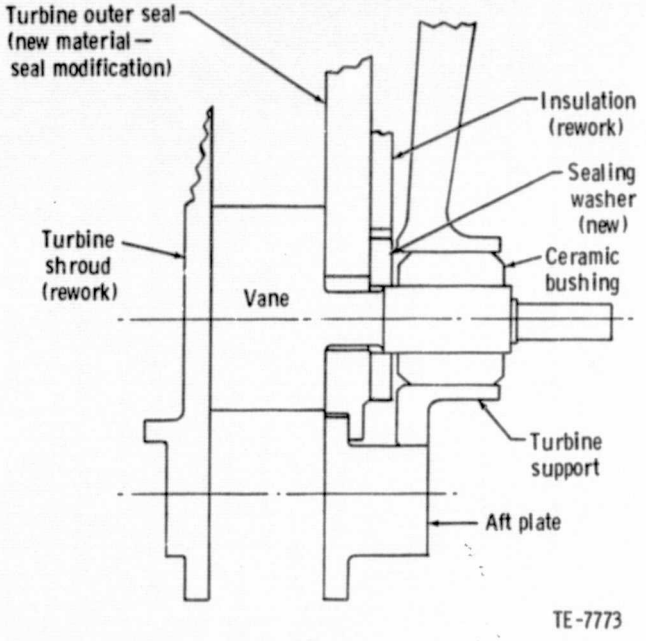

Figure 12. - AGT-2 Turbine Sealing Modifications.

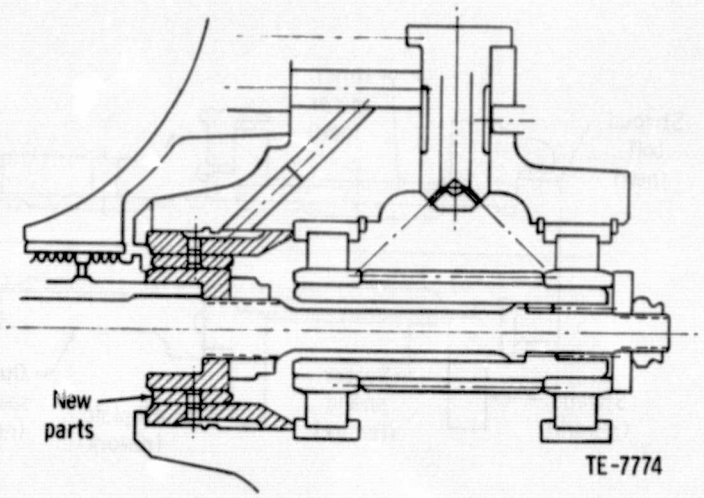

Figure 13. - Bump Stop Arrangement.

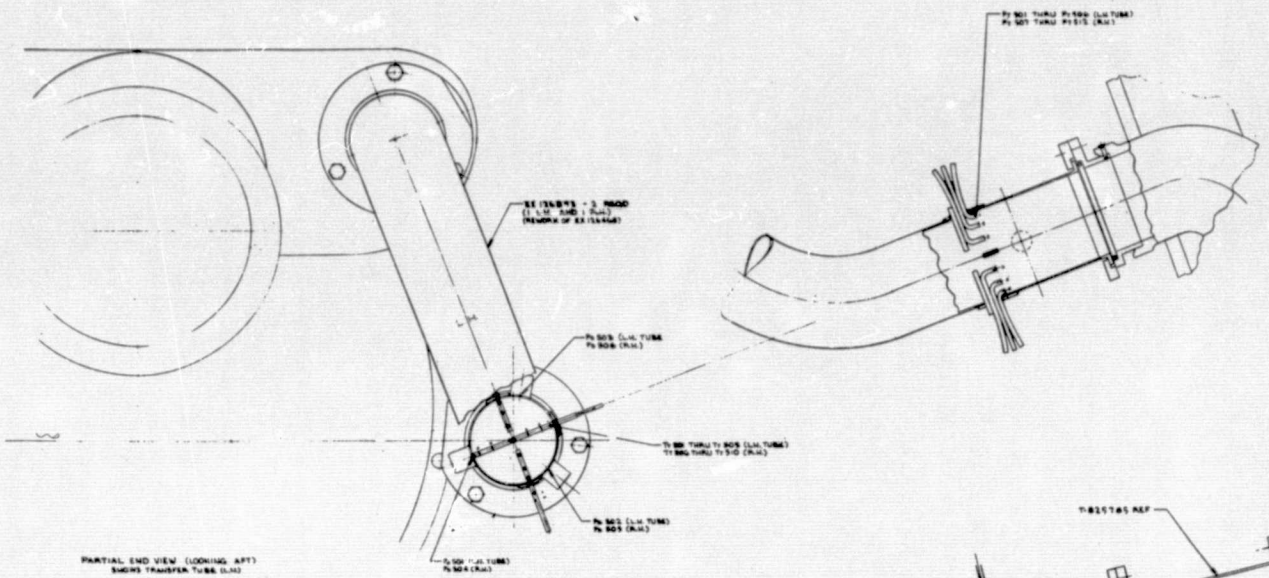

PARTIAL END VIEW (LOOKING AFT)
SHOWS TRANSFER TUBE (LH)

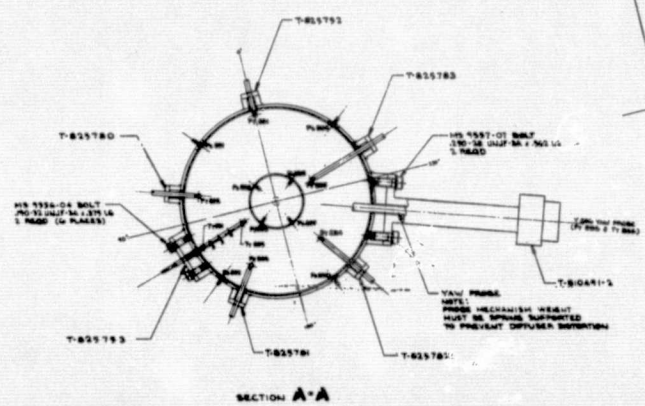

SECTION A-A

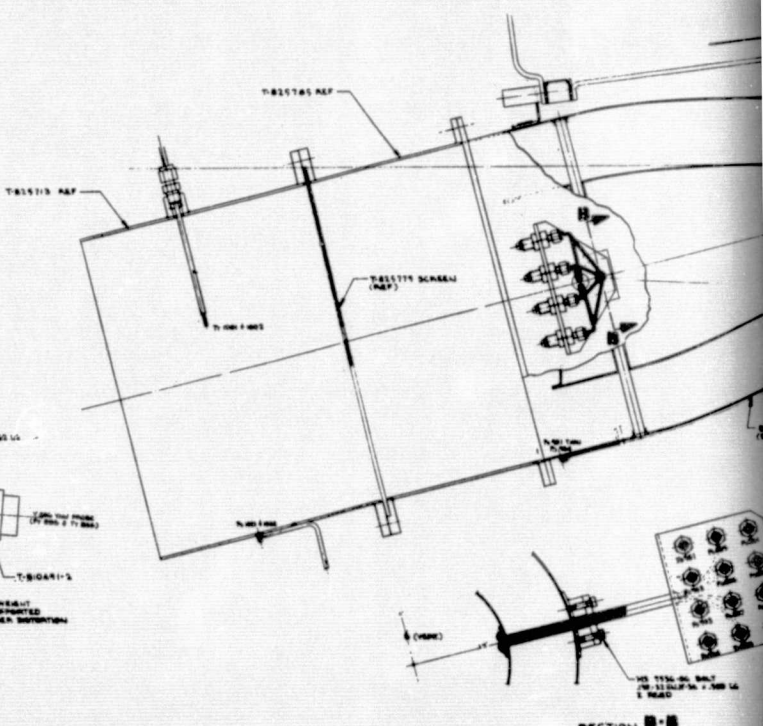

SECTION B-B

Figure

FOLDOUT FRAME

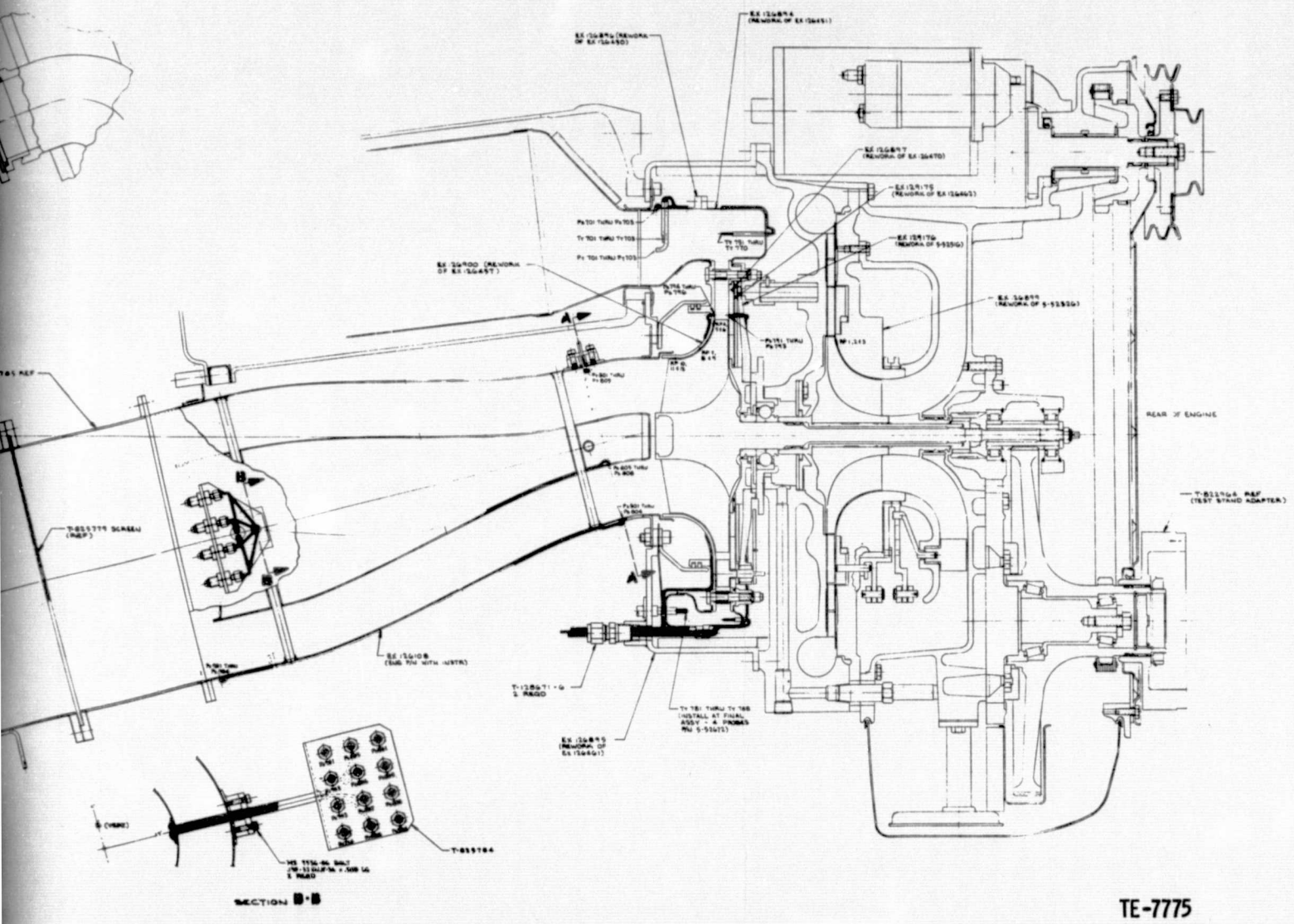

Figure 14. - Layout and Assembly of AGT-2 BU 2 Instrumentation.

2 WITHOUT FRAME

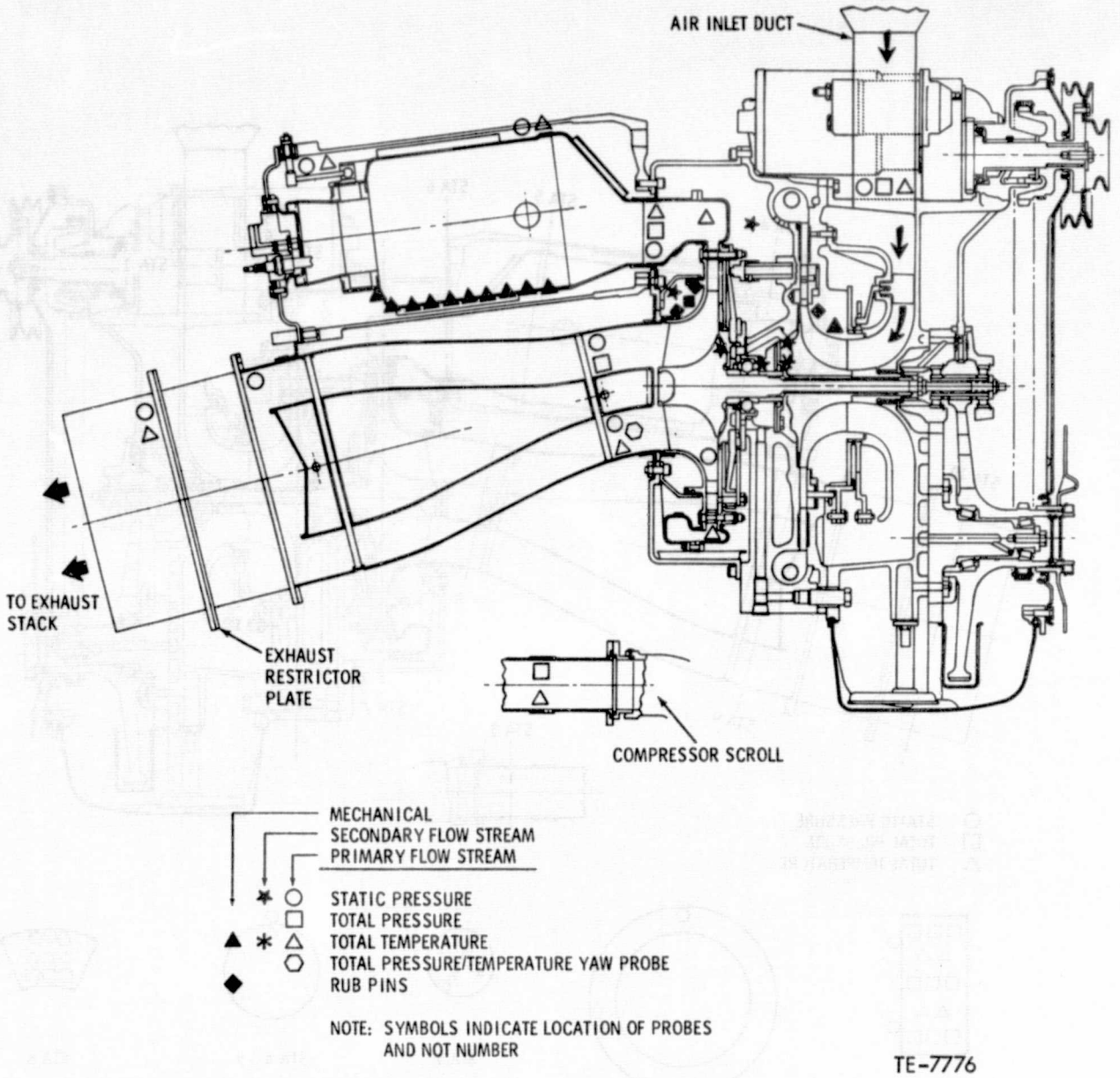

Figure 15. - AGT-2 Instrumentation.

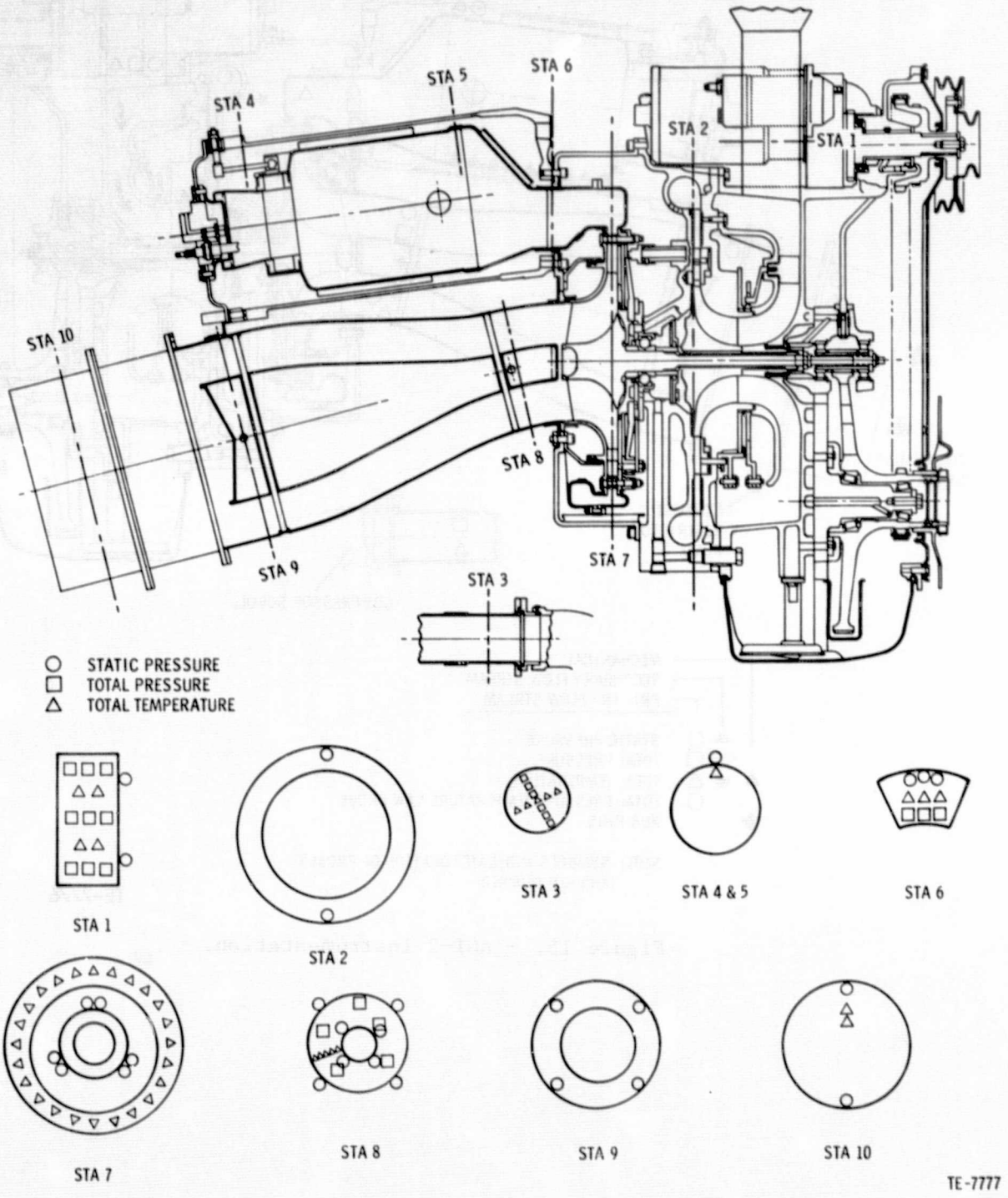

Figure 16. - AGT-2 Instrumentation--Primary Flow Stream.

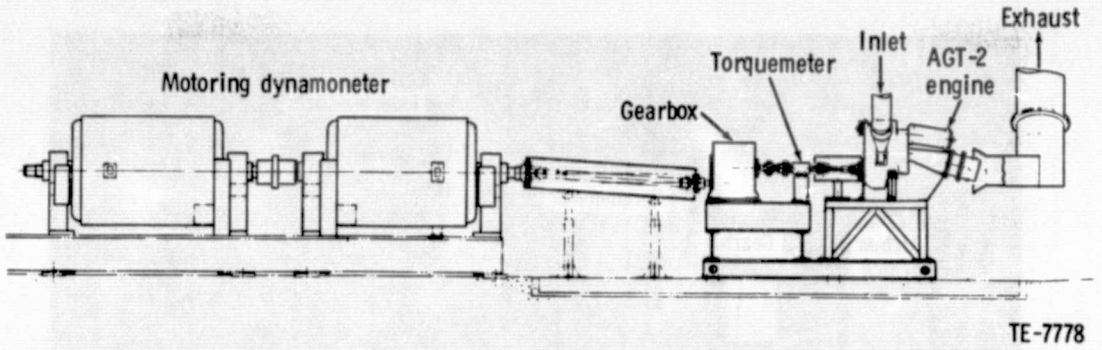

Figure 17. - AGT-2 Test Cell Arrangement.

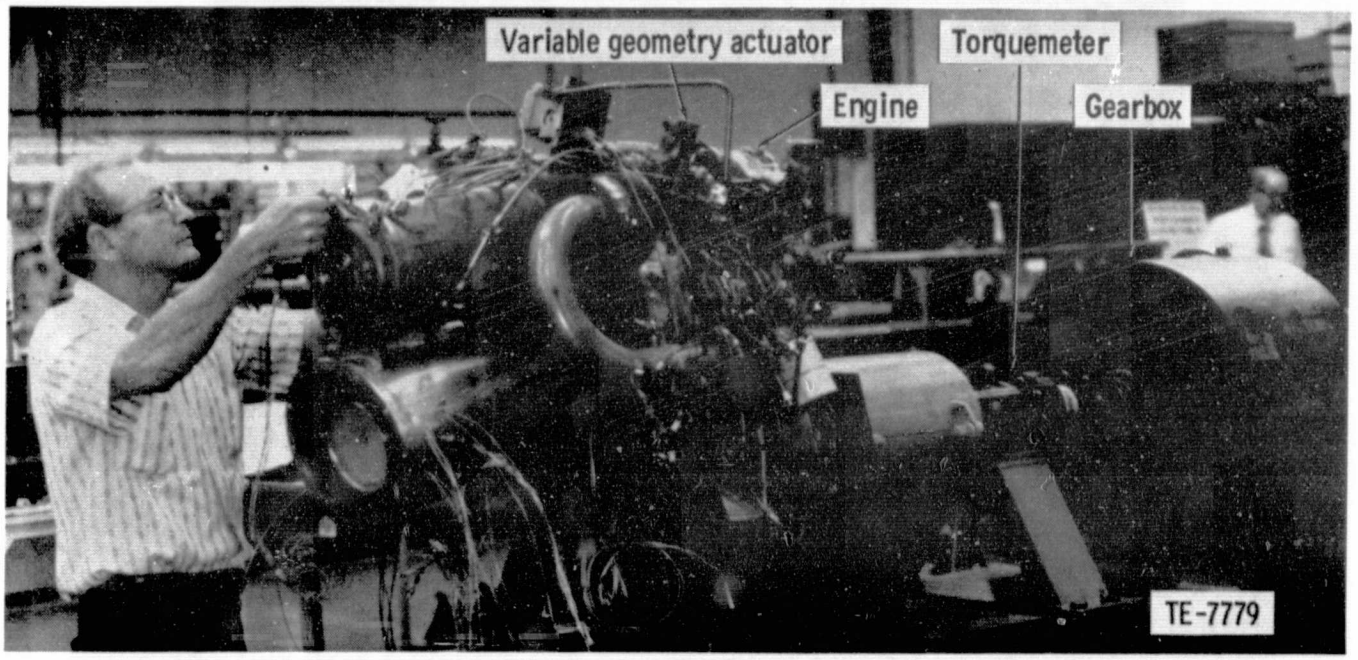

Figure 18. - AGT-2 Engine, Torquemeter, and Gearbox on Base.

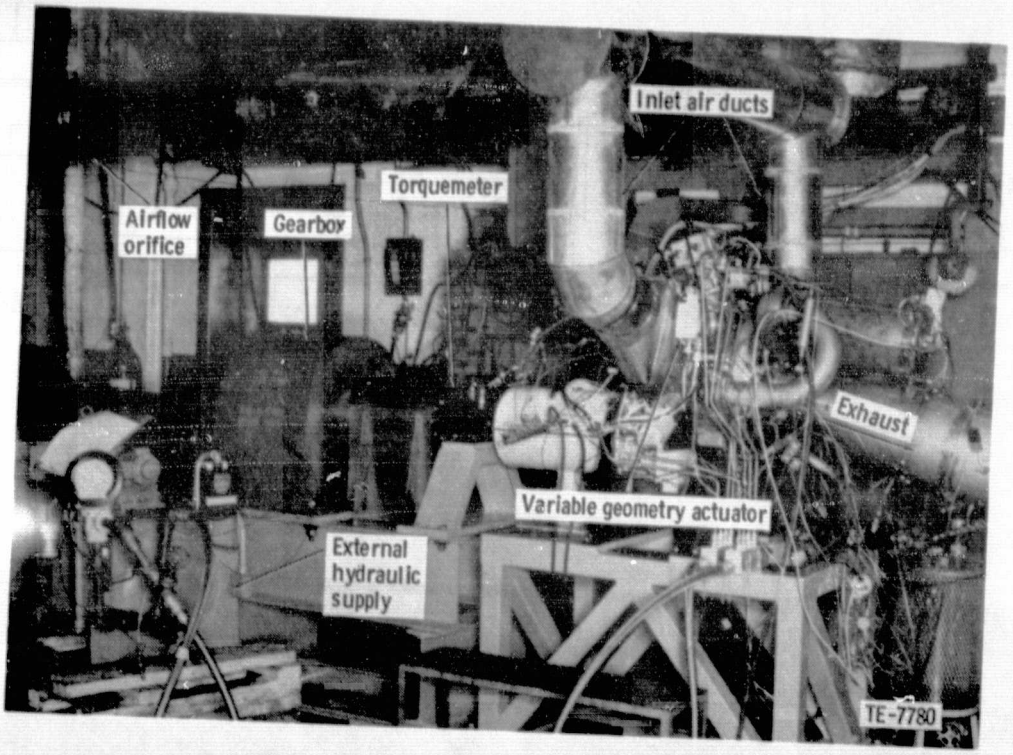

Figure 19. - AGT-2 Test Cell Installation.

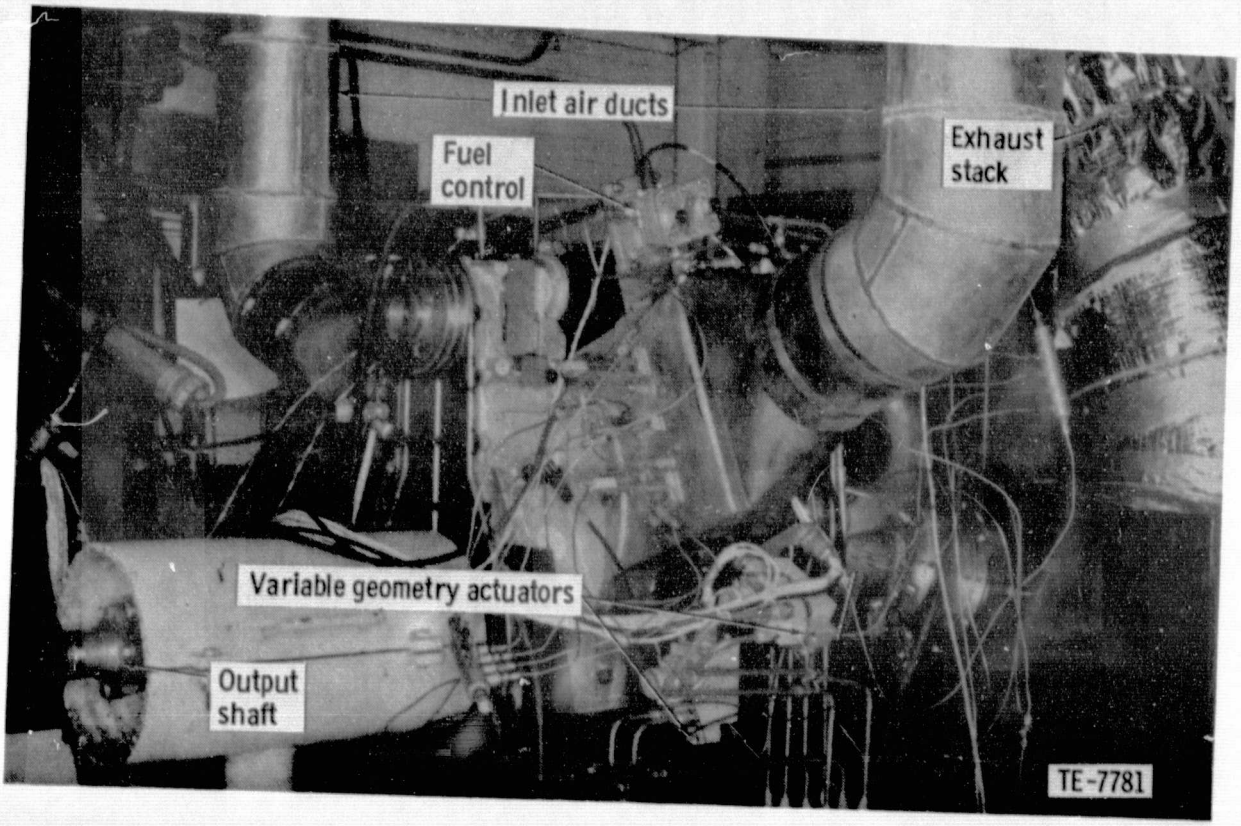

Figure 20. - AGT-2 Test Cell Installation.

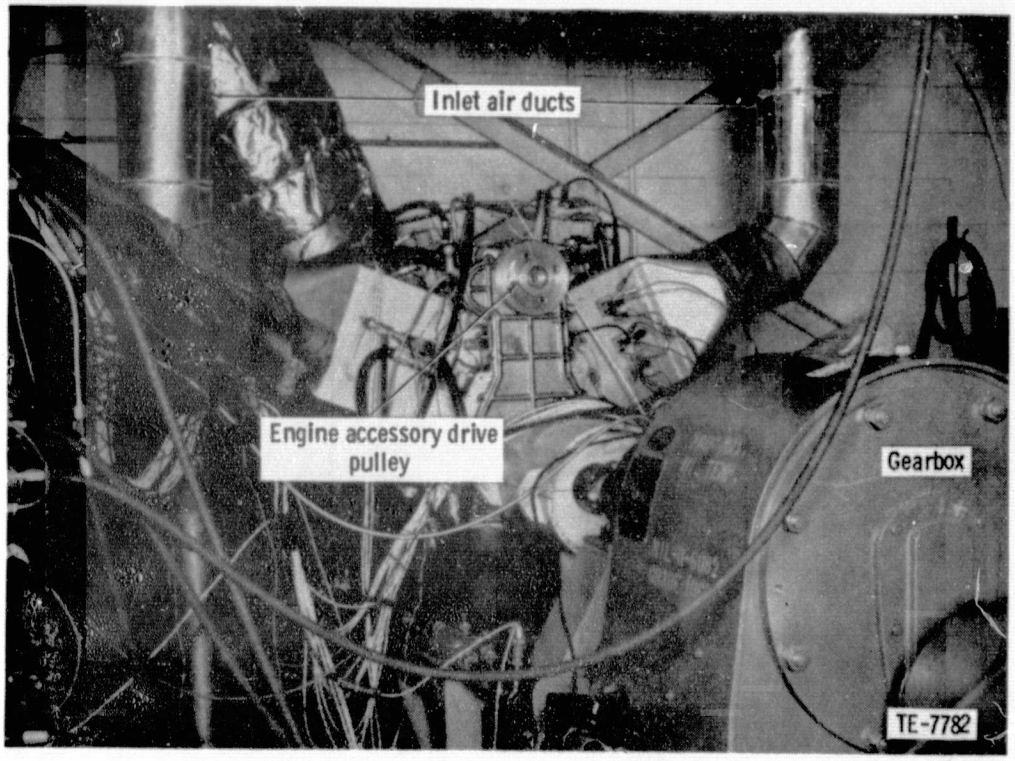

Figure 21. - AGT-2 Test Cell Installation.

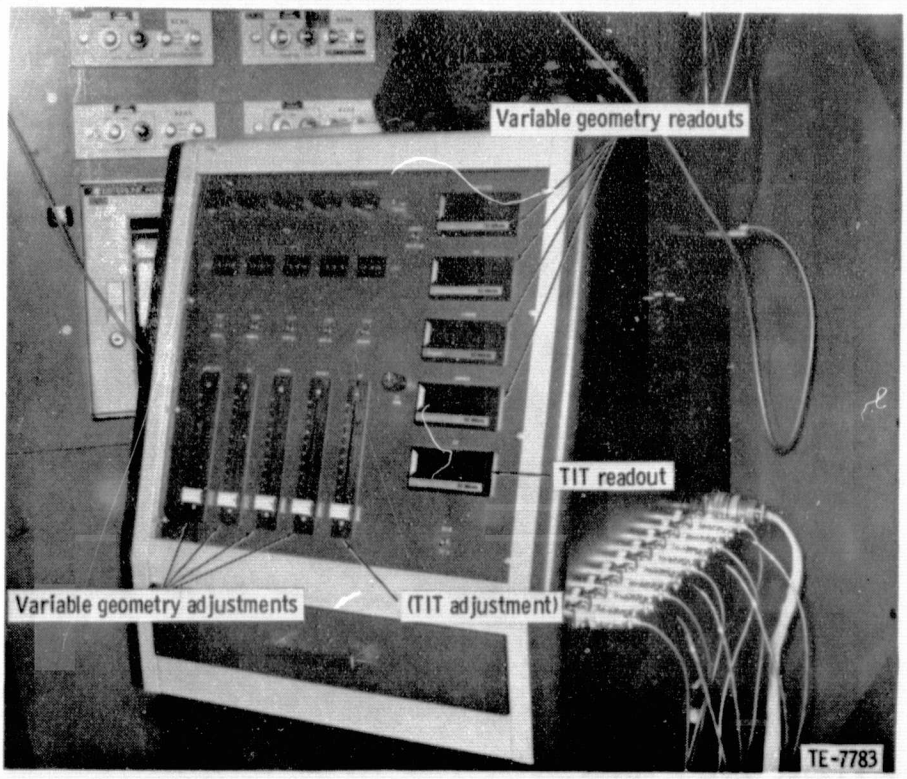

Figure 22. - AGT-2 Test Control Console.

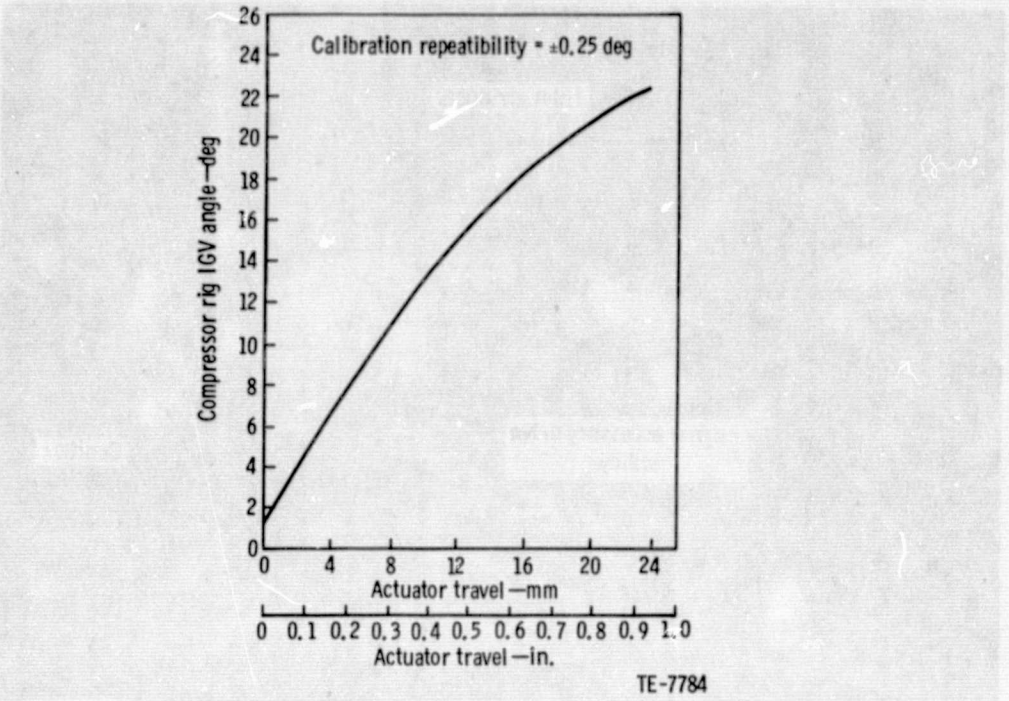

Figure 23. - AGT-2 Engine Inlet Guide Vane Calibration.

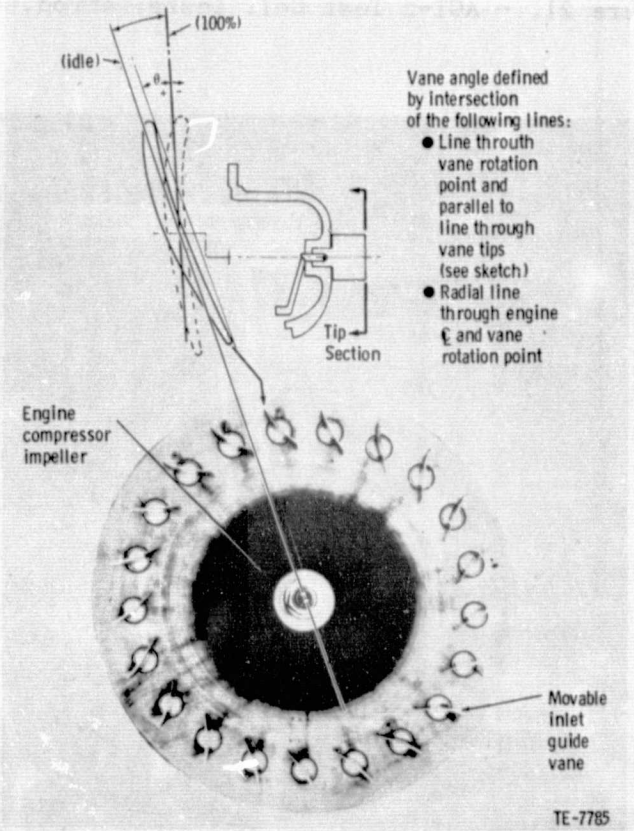

Figure 24. - Inlet Guide Vane Variable Geometry.

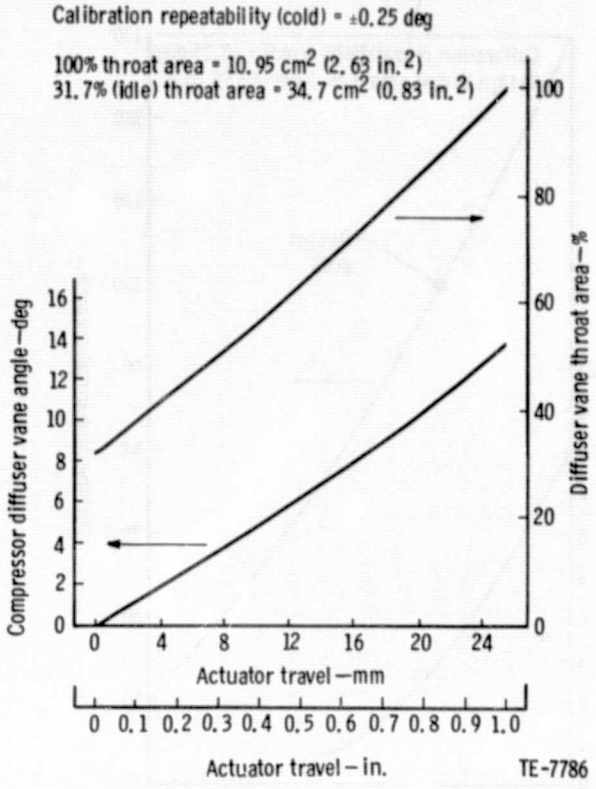

Figure 25. - AGT-2 Engine Compressor Diffuser Vane Calibration.

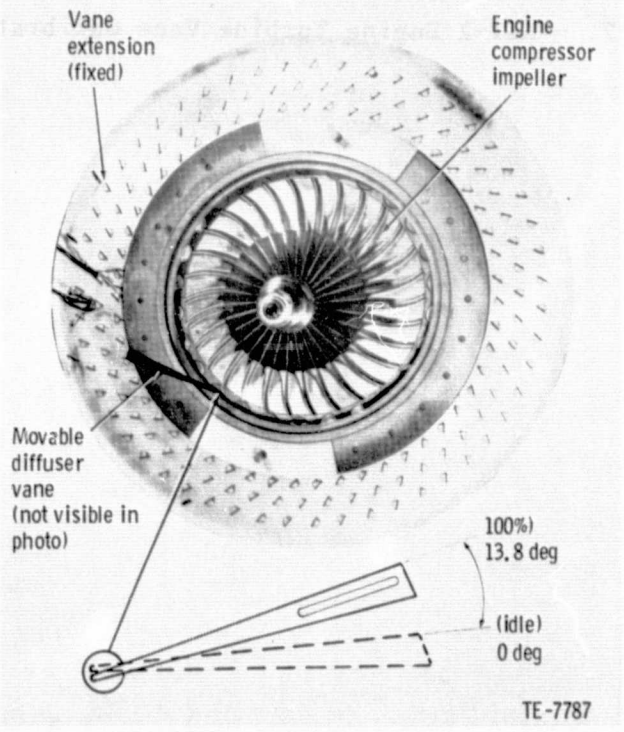

Figure 26. - Diffuser Vane Variable Geometry.

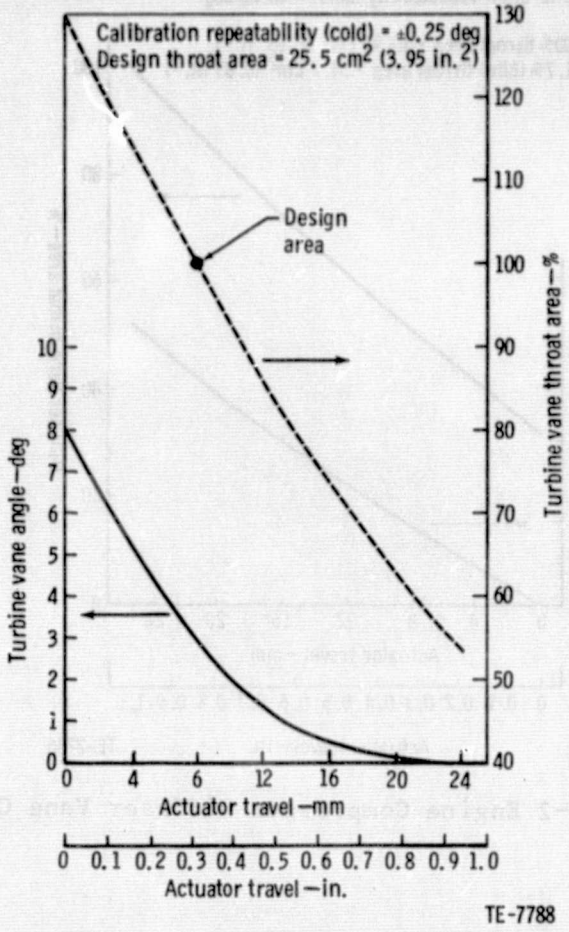

Figure 27. - AGT-2 Engine Turbine Vane Calibration.

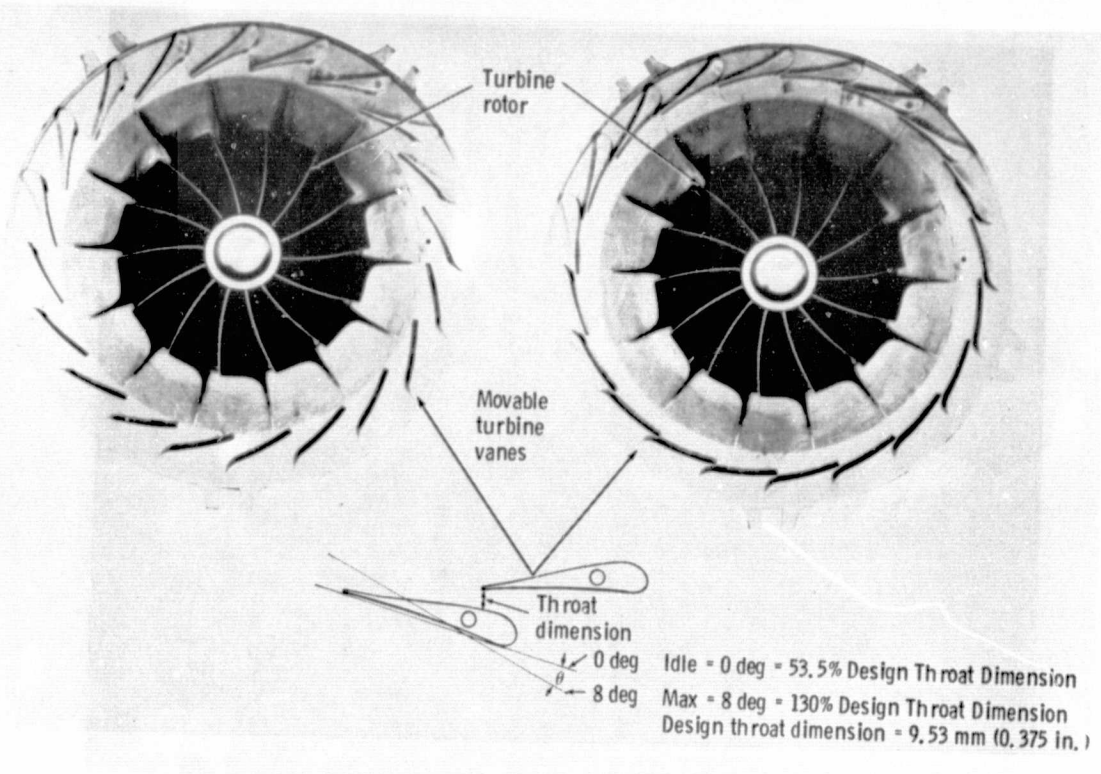

Figure 28. - Turbine Vane Variable Geometry.

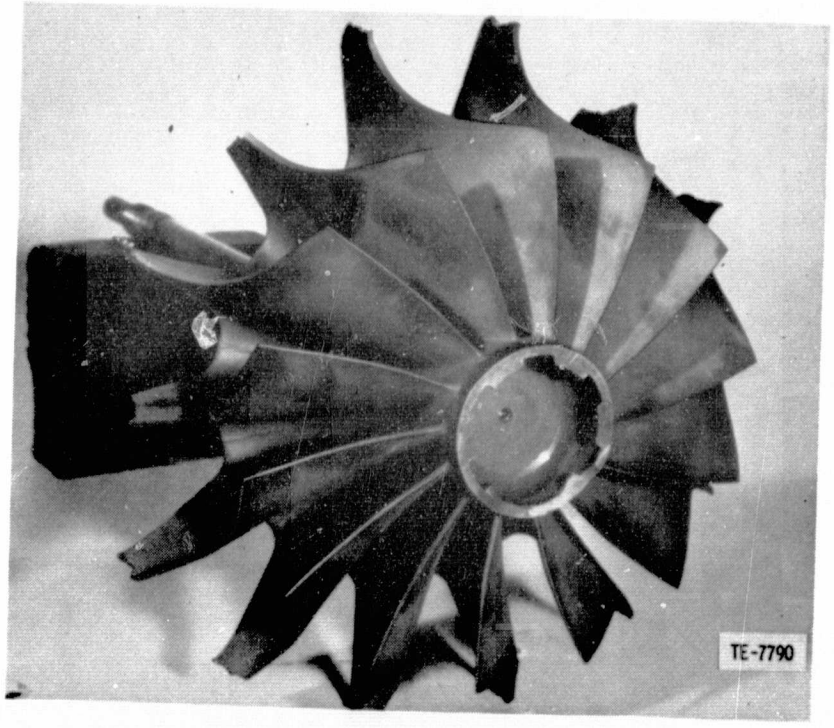

Figure 29. - AGT-2 Turbine Wheel--TD 9.

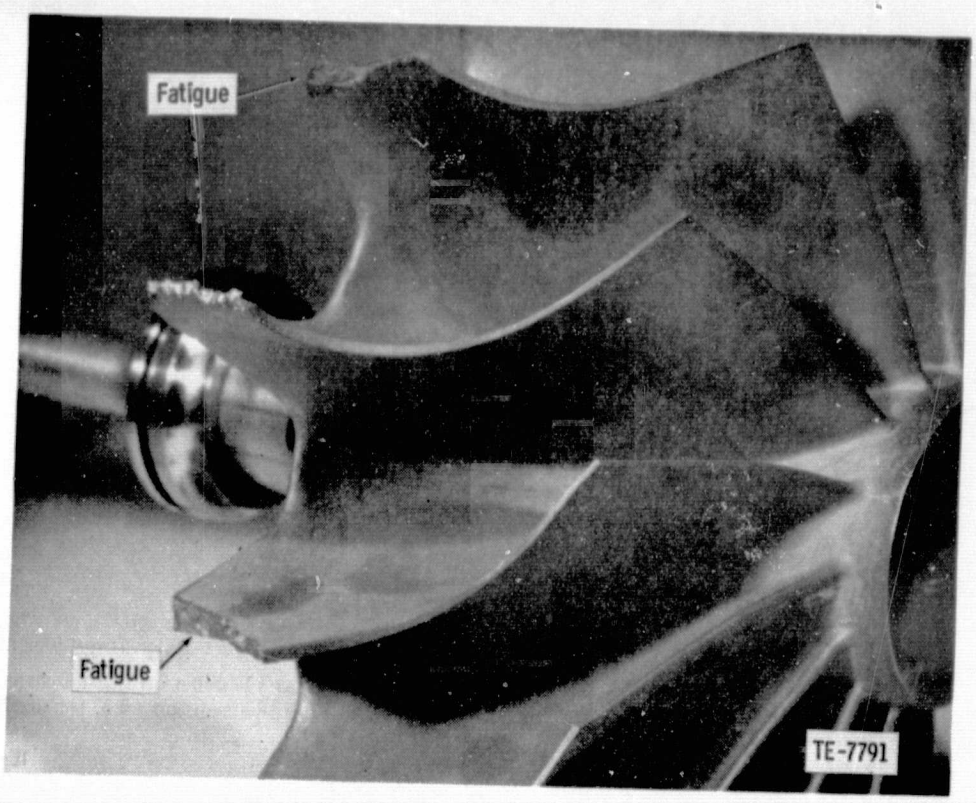

Figure 30. - AGT-2 Turbine Wheel--TD 9.

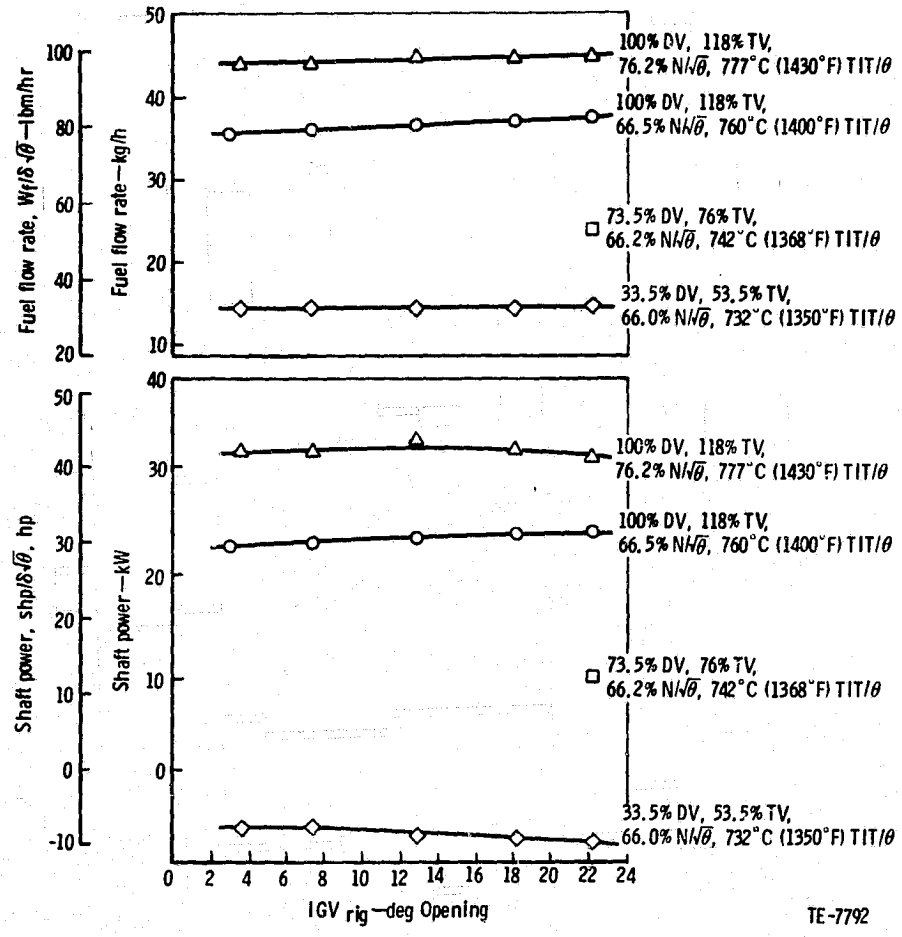

Figure 31. - AGT-2 Test IGV Mapping.

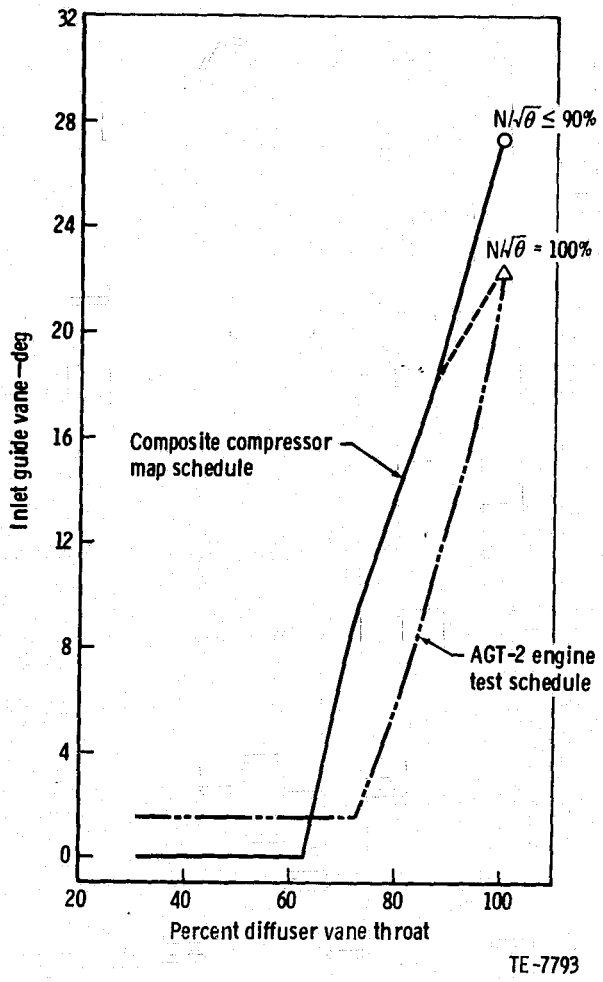

Figure 32. - AGT-2 Composite Compressor Map IGV/DV Schedule.

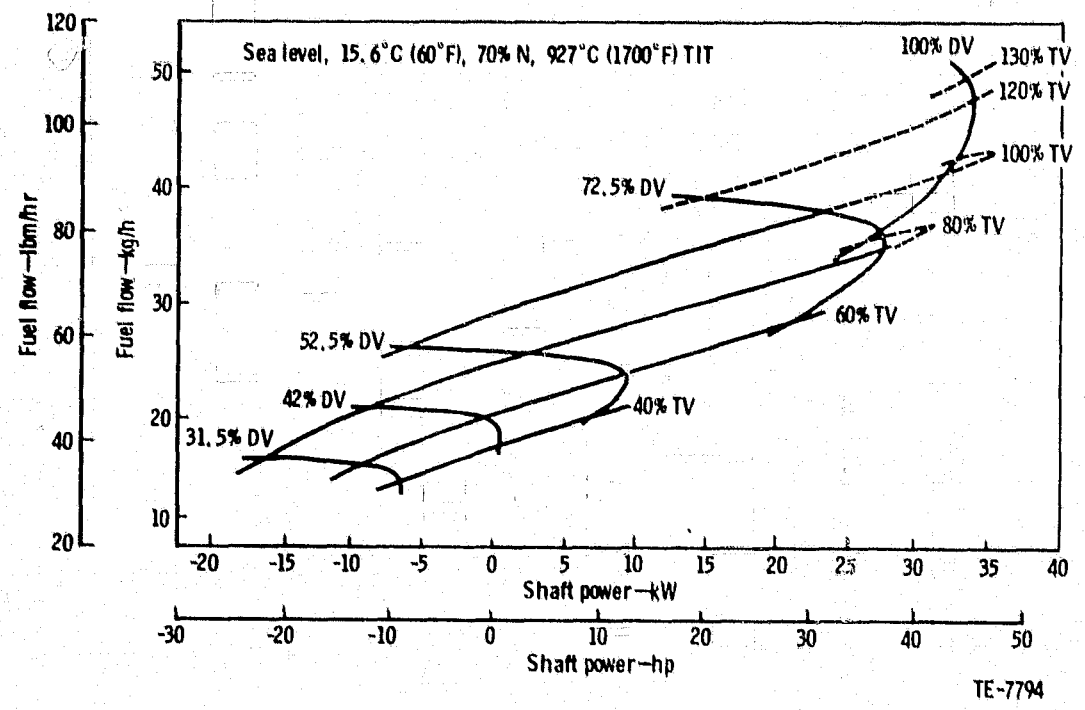

Figure 33. - AGT-2 Predicted Performance.

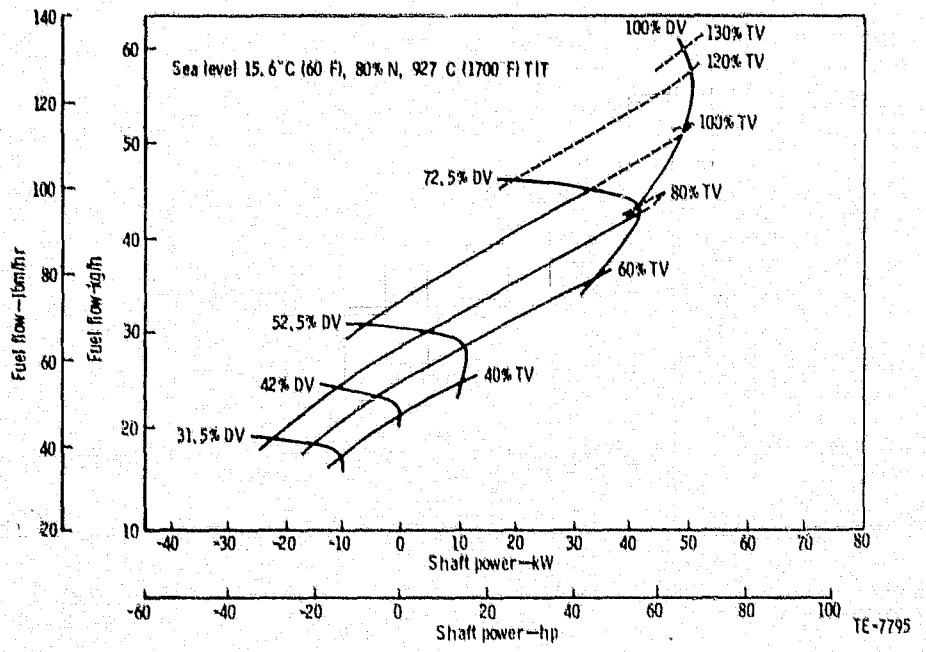

Figure 34. - AGT-2 Predicted Performance.

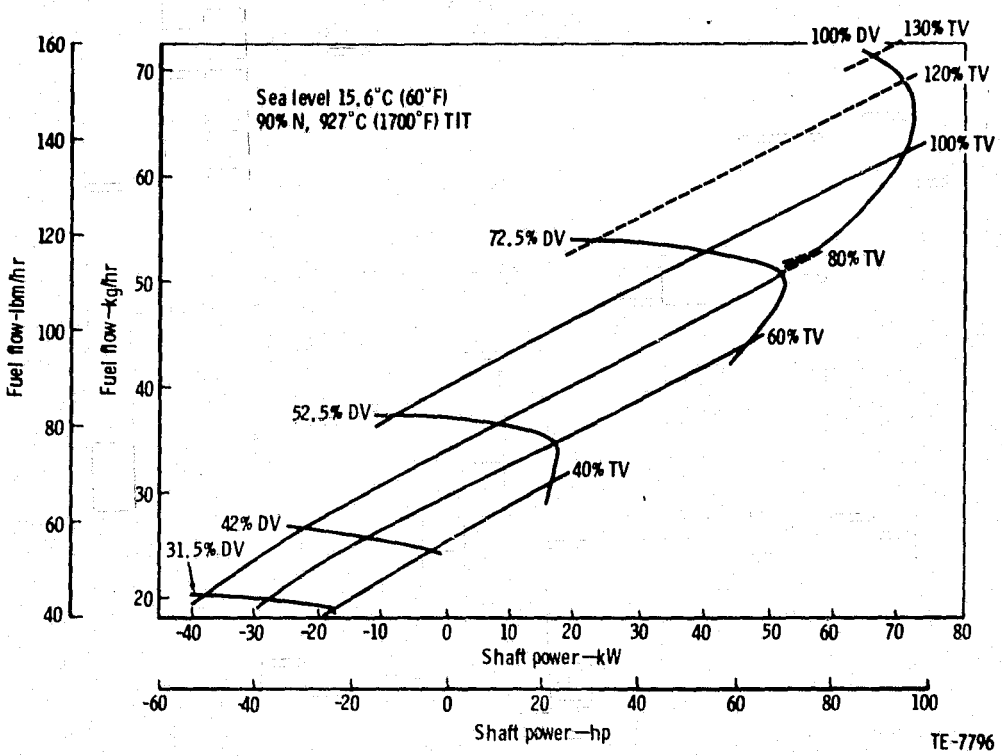

Figure 35. - AGT-2 Predicted Performance.

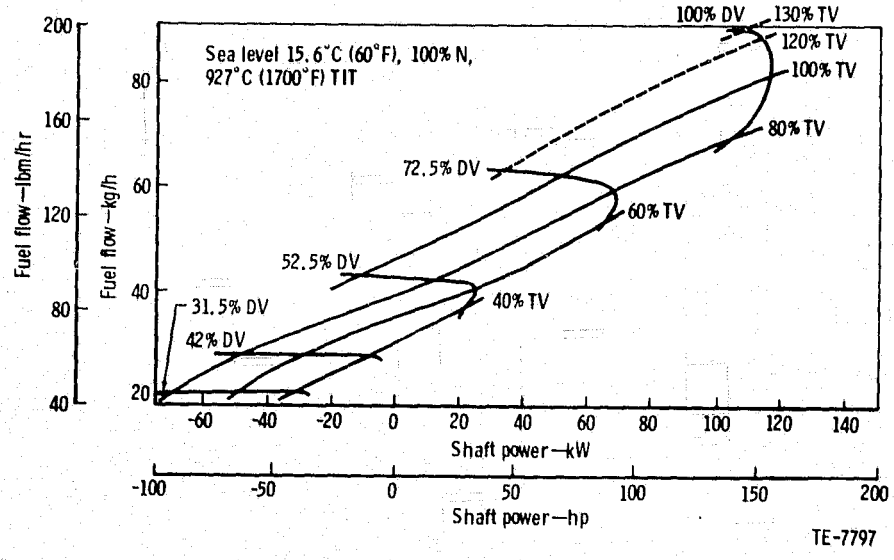

Figure 36. - AGT-2 Predicted Performance.

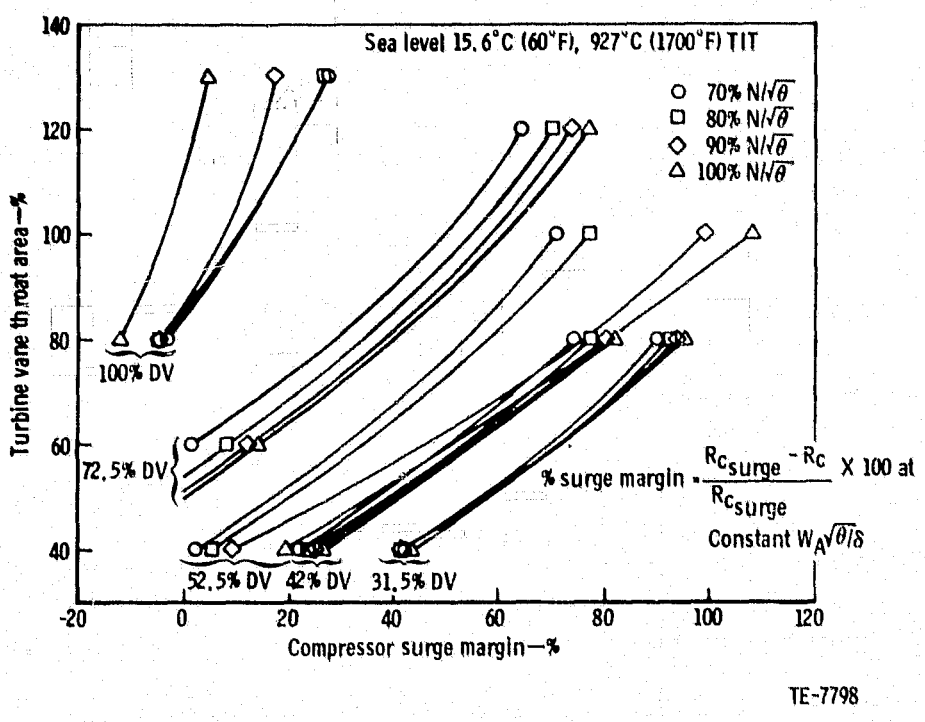

Figure 37. - AGT-2 Predicted Performance.

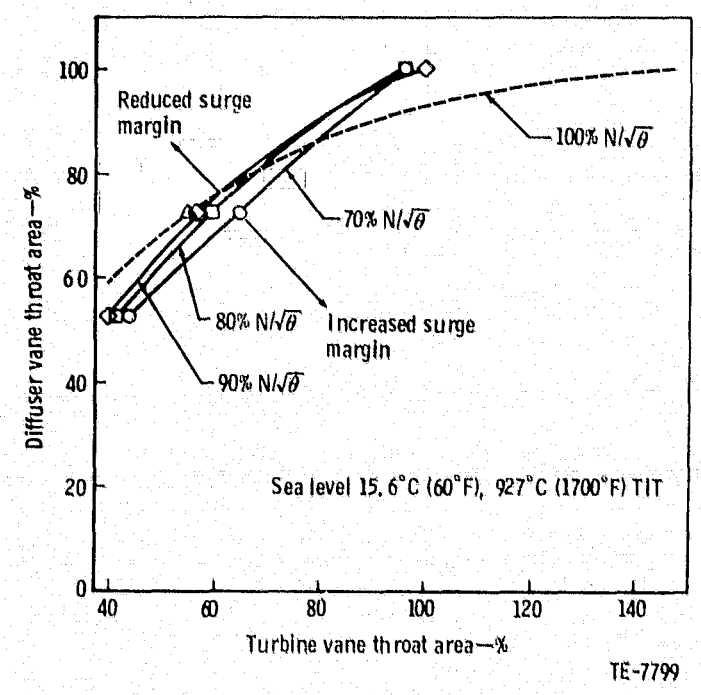

Figure 38. - AGT-2 Predicted Performance--DV vs TV for 8% Compressor Surge Margin.

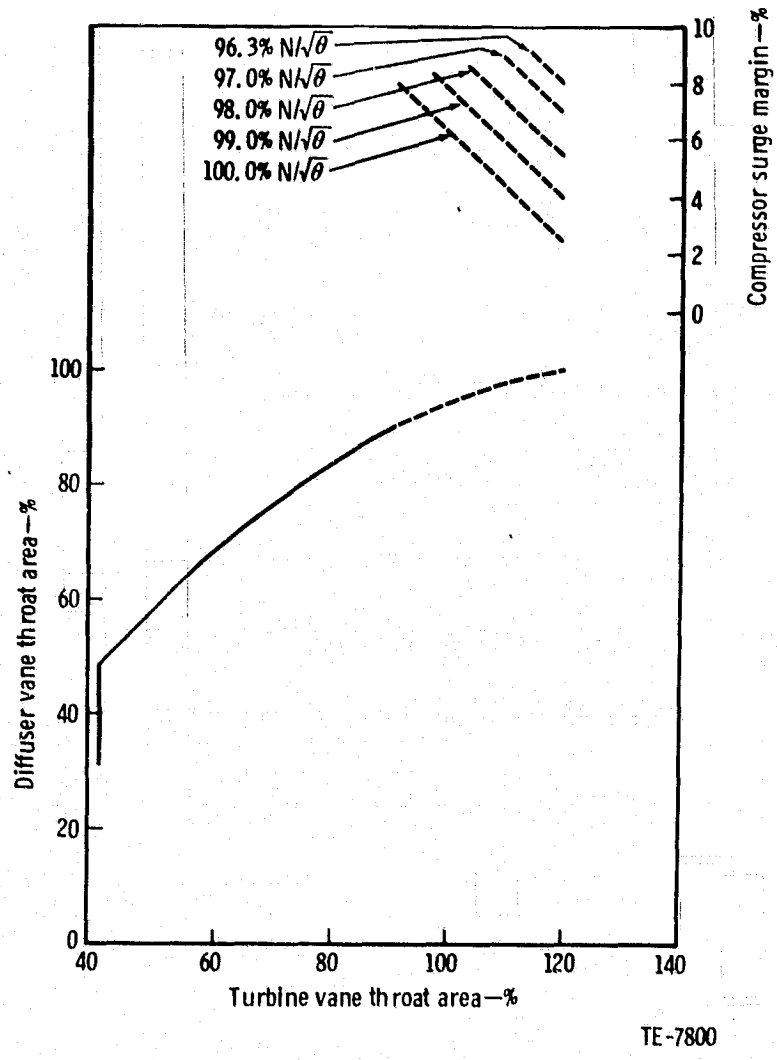

Figure 39. - Predicted Variable Geometry Schedule at 8.0%.

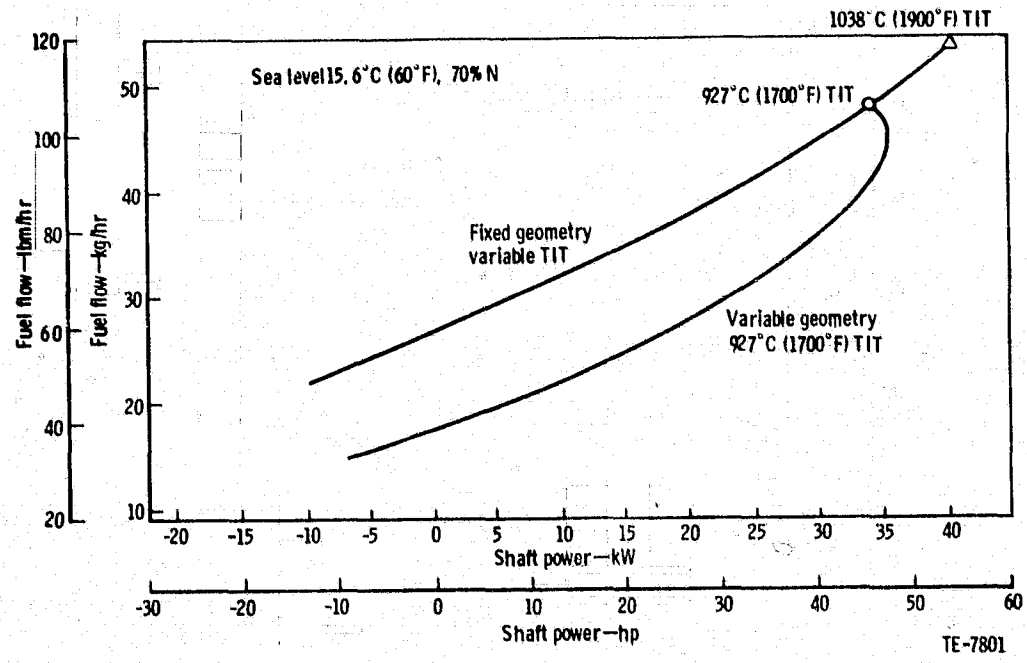

Figure 40. - AGT-2 Predicted Performance.

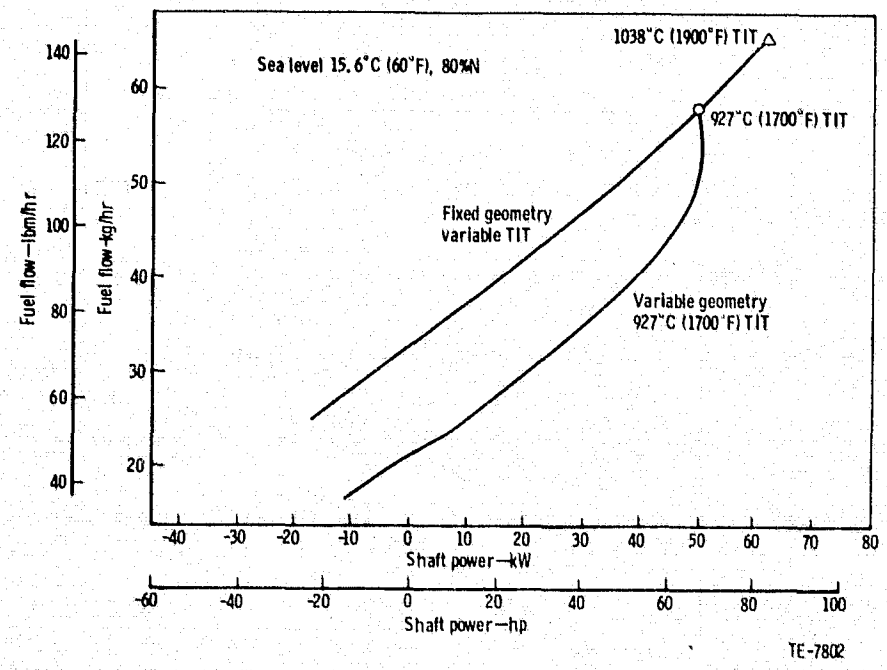

Figure 41. - AGT-2 Predicted Performance.

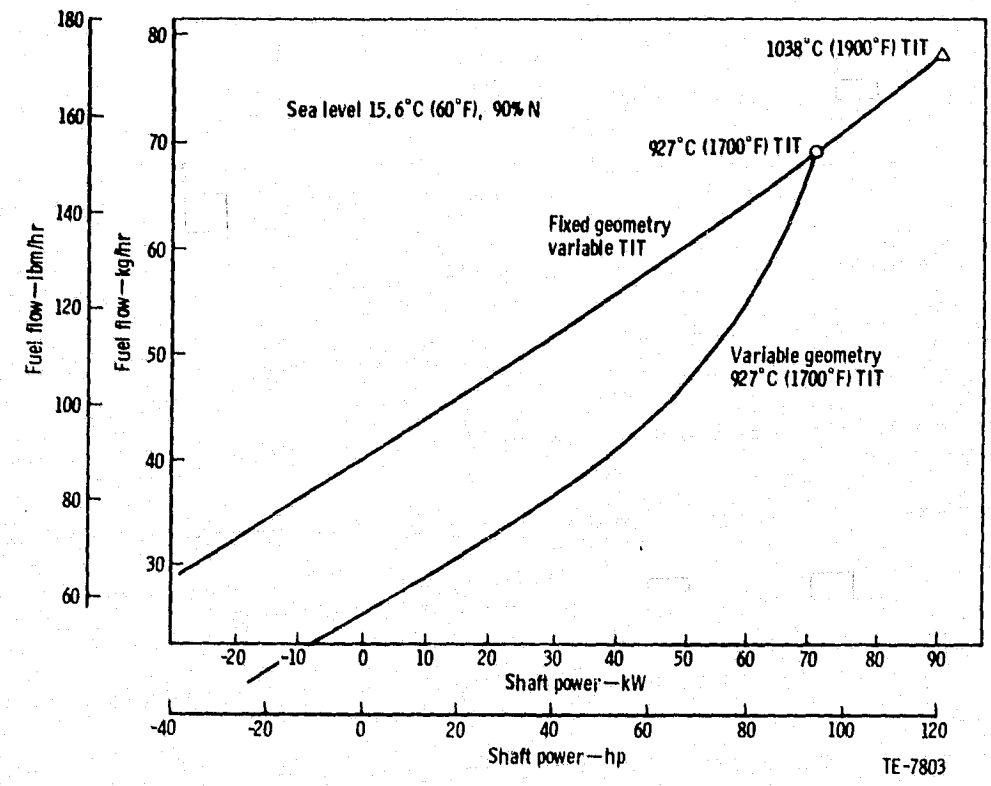

Figure 42. - AGT-2 Predicted Performance.

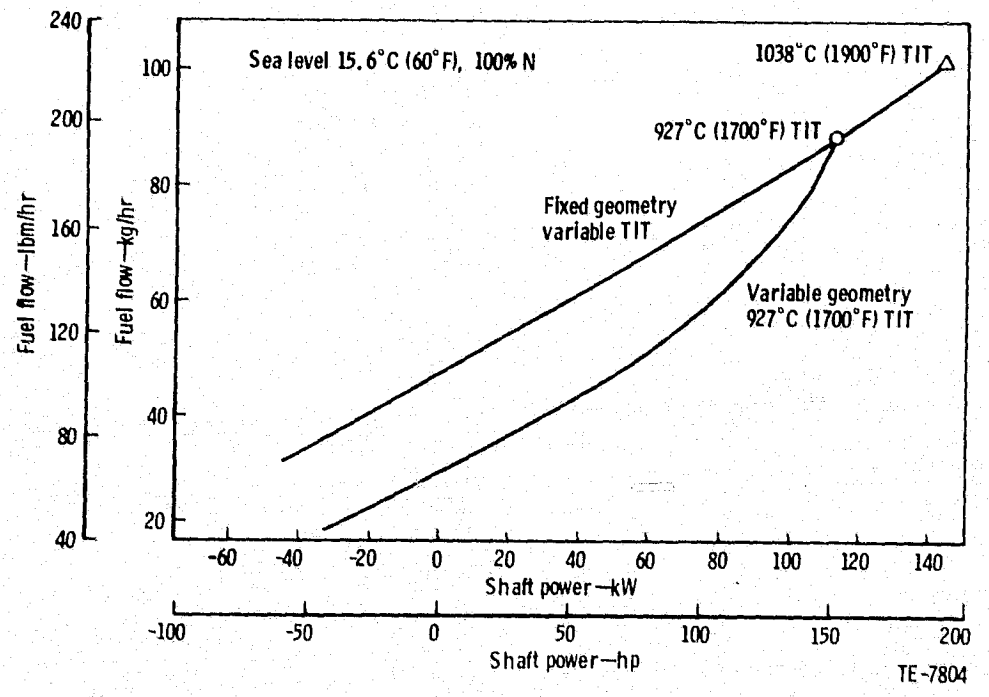

Figure 43. - AGT-2 Predicted Performance.

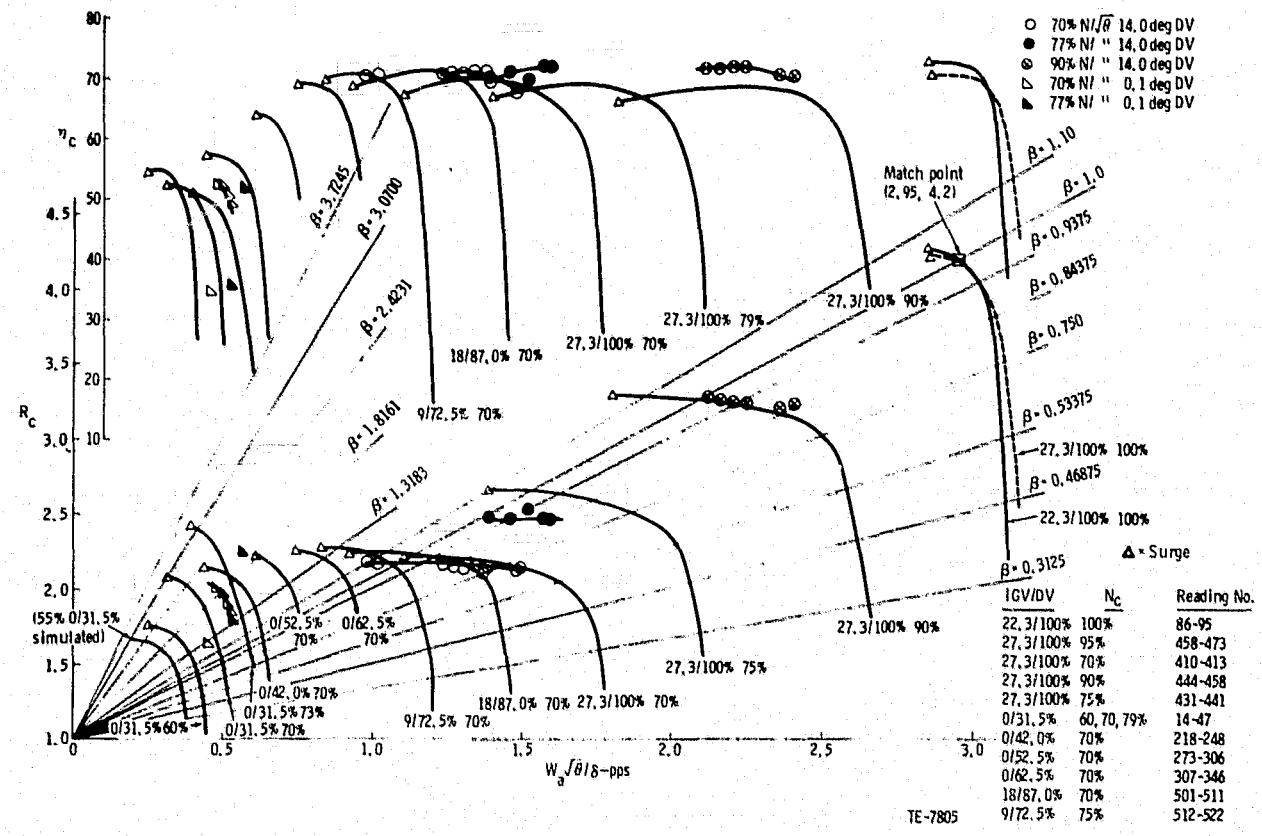

Figure 44. - AGT-2 Compressor Rig Test--31.5 and 100% Diffuser Vane.

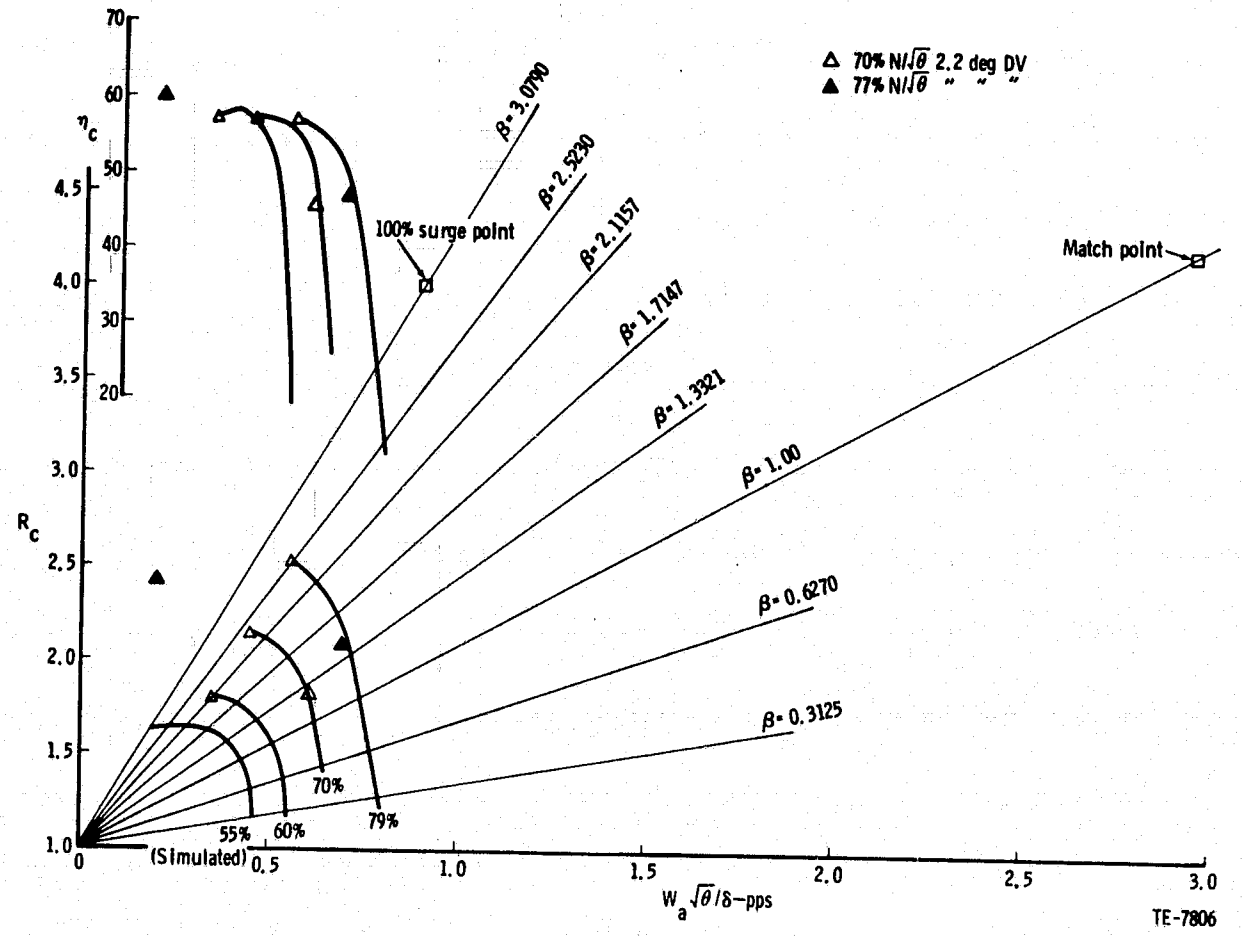

Figure 45. - AGT-2 Compressor Rig Test--0-deg IGV--42% Diffuser Vane.

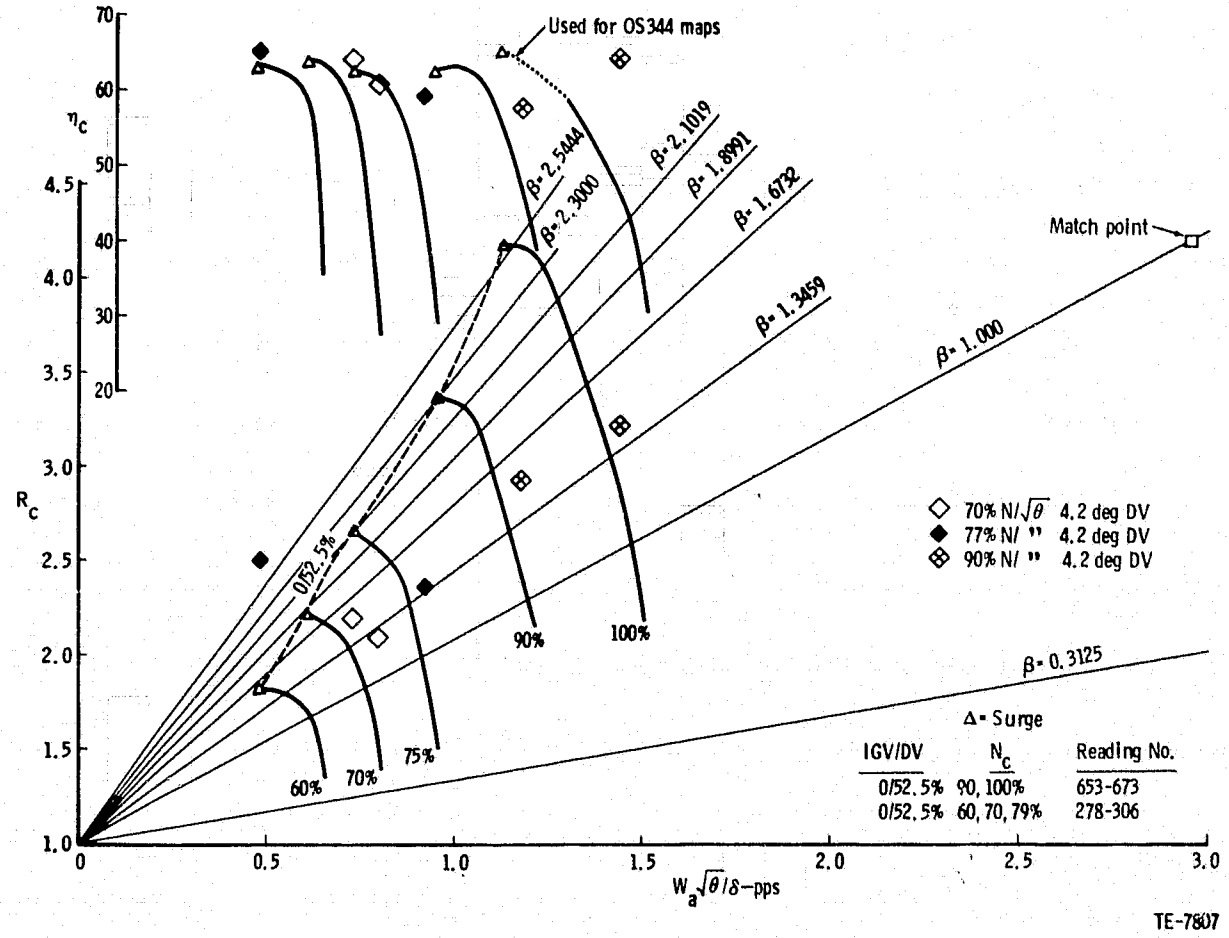

Figure 46. - AGT-2 Compressor Rig Test--0-deg IGV--52.5% Diffuser Vane.

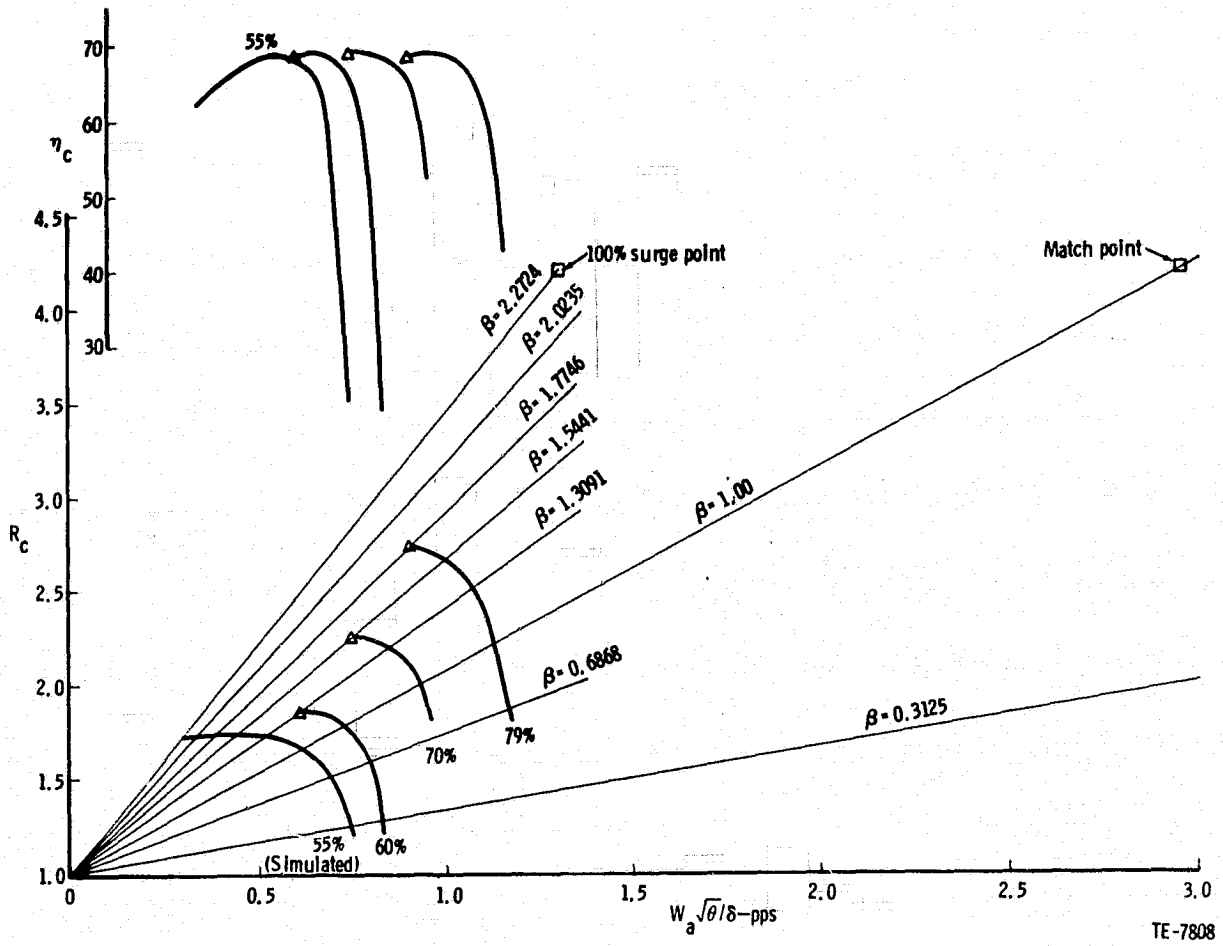

Figure 47. - AGT-2 Compressor Rig Test--0-deg IGV--62.5% Diffuser Vane.

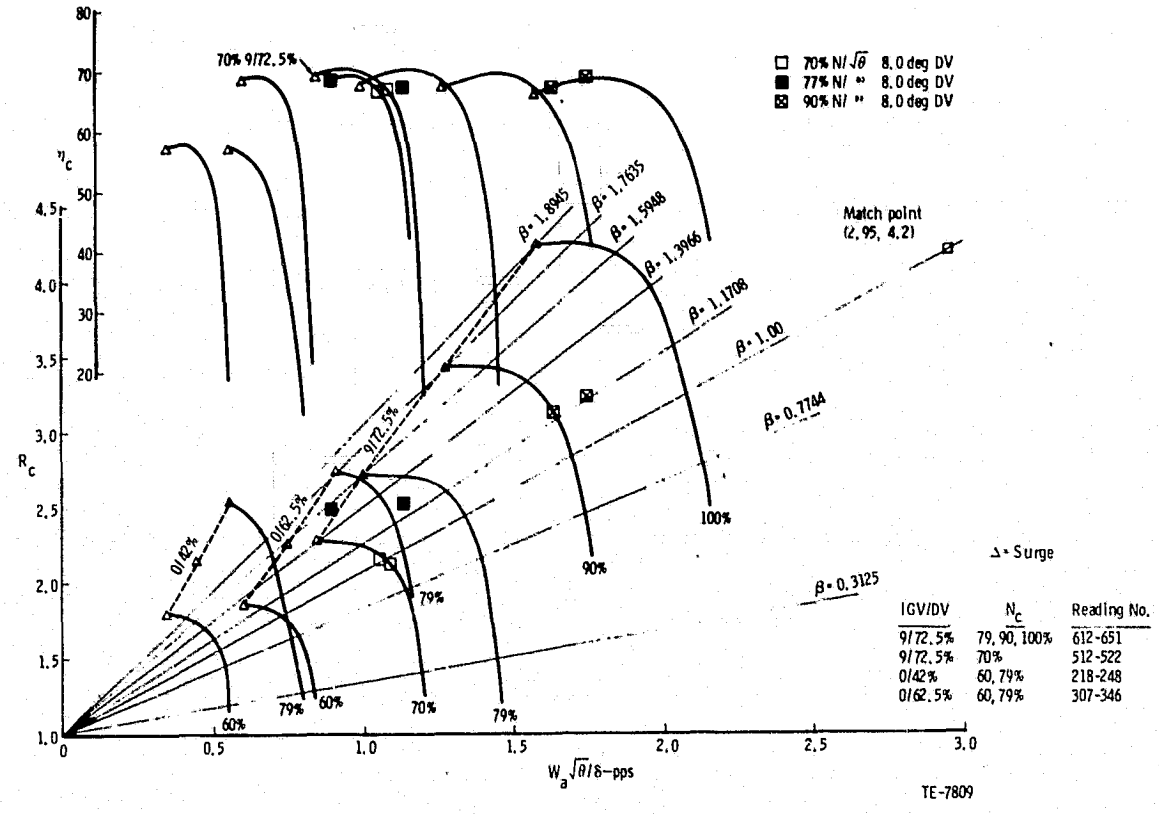

Figure 48. - AGT-2 Compressor Rig Test--9-deg IGV--72.5% Diffuser Vane.

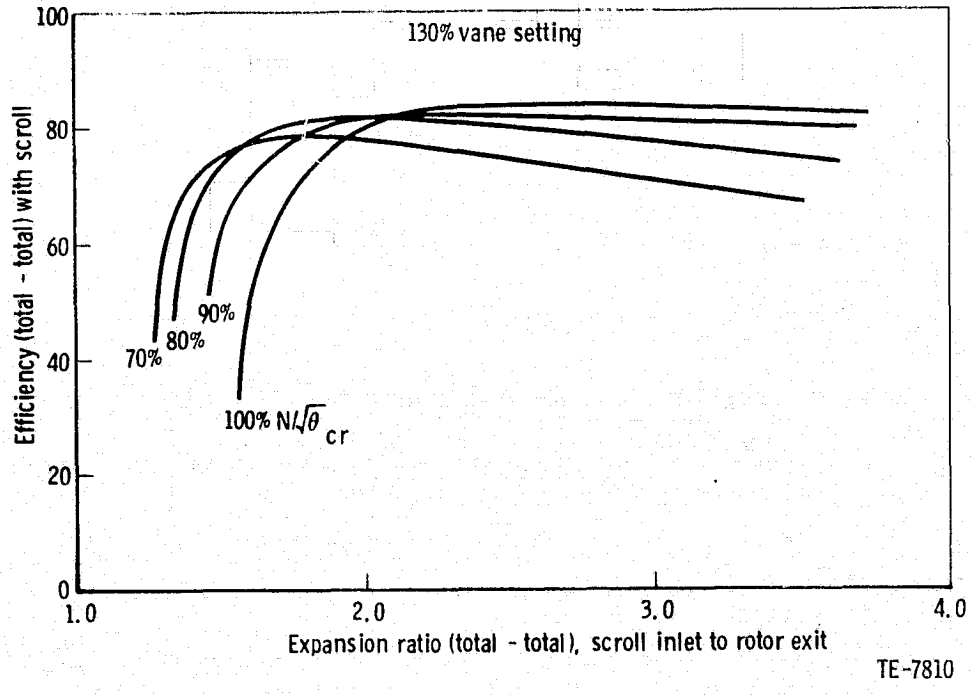

Figure 49. - AGT-2 Turbine Rig Test--BU 3 (corrected).

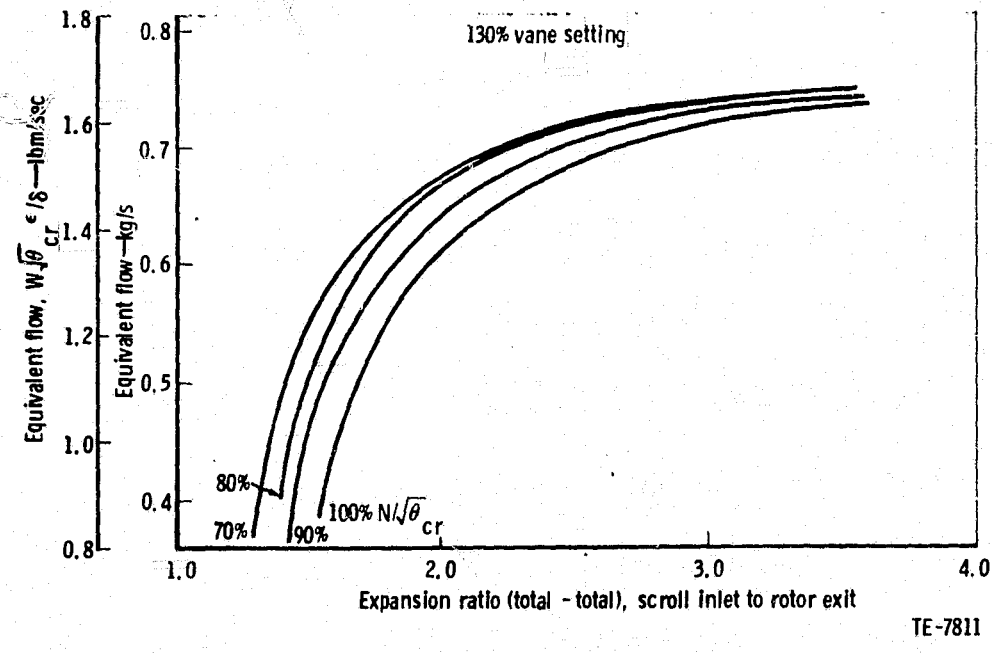

Figure 50. - AGT-2 Turbine Rig Test--BU 3 (corrected).

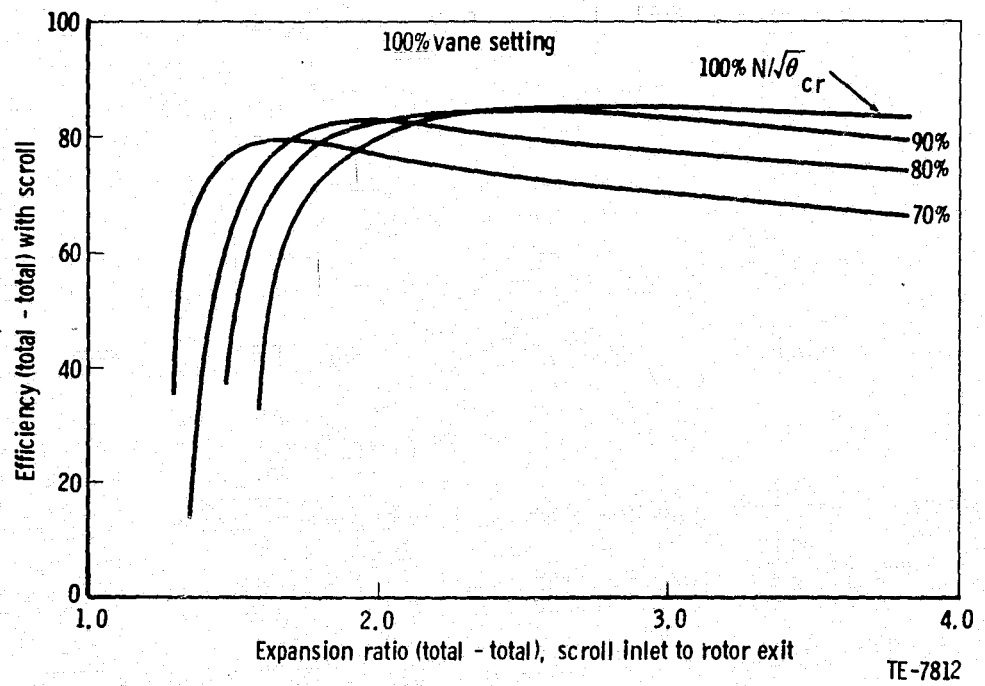

Figure 51. - AGT-2 Turbine Rig Test--BU 3 (corrected).

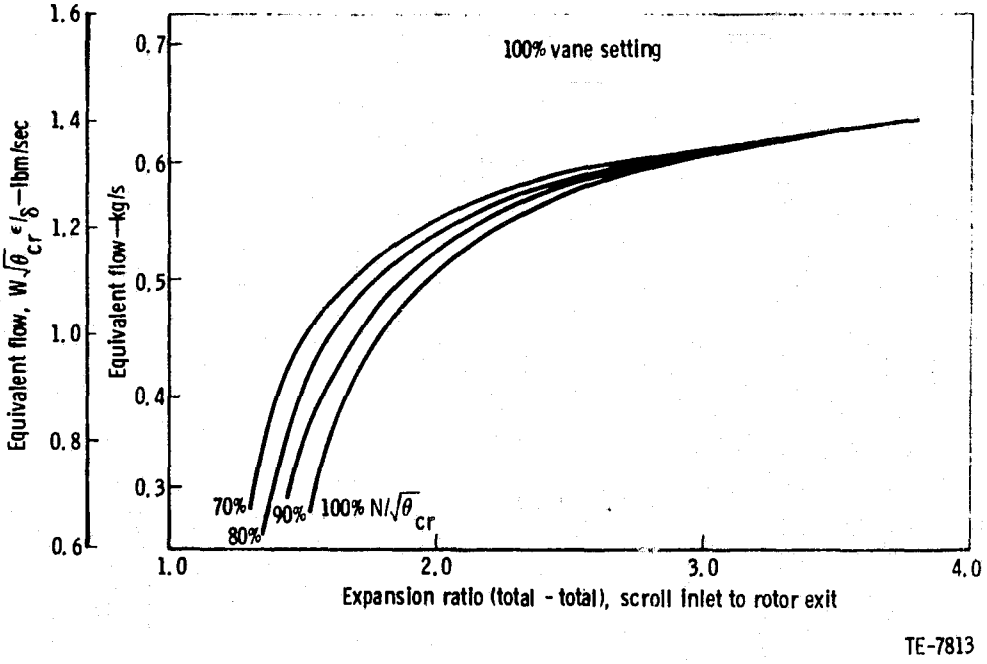

Figure 52. - AGT-2 Turbine Rig Test--BU 3 (corrected).

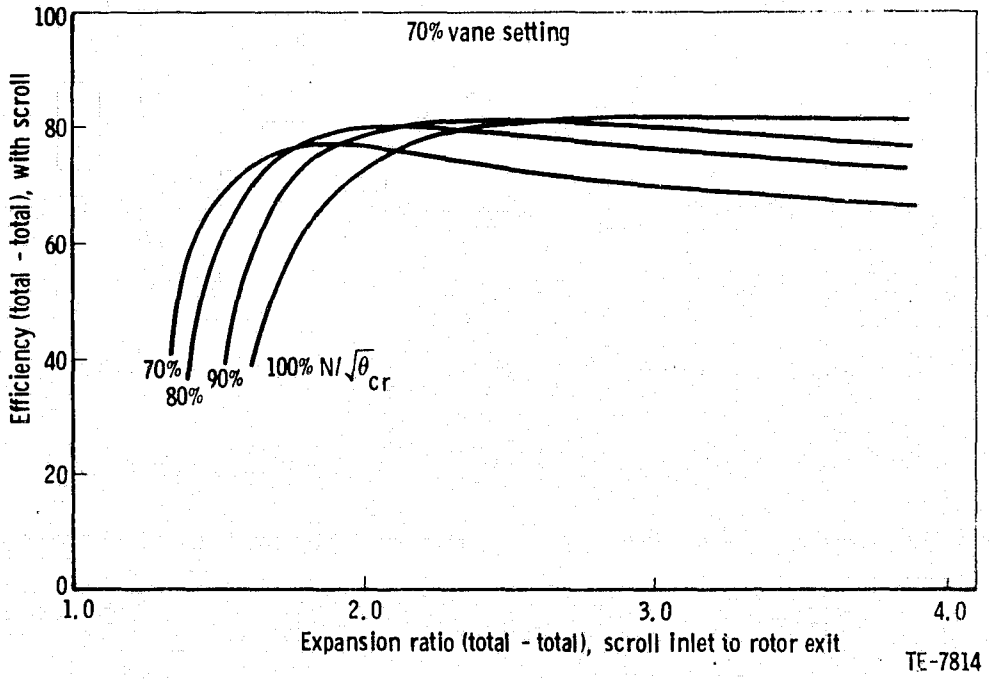

Figure 53. - AGT-2 Turbine Rig Test--BU 3 (corrected).

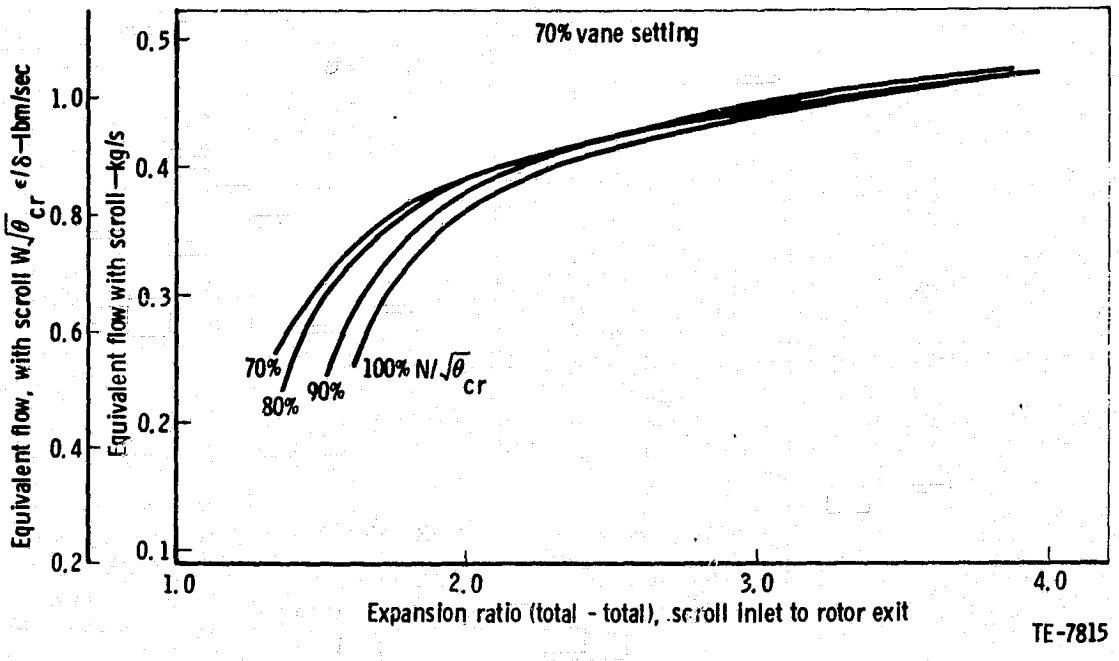

Figure 54. - AGT-2 Turbine Rig Test—BU 3 (corrected).

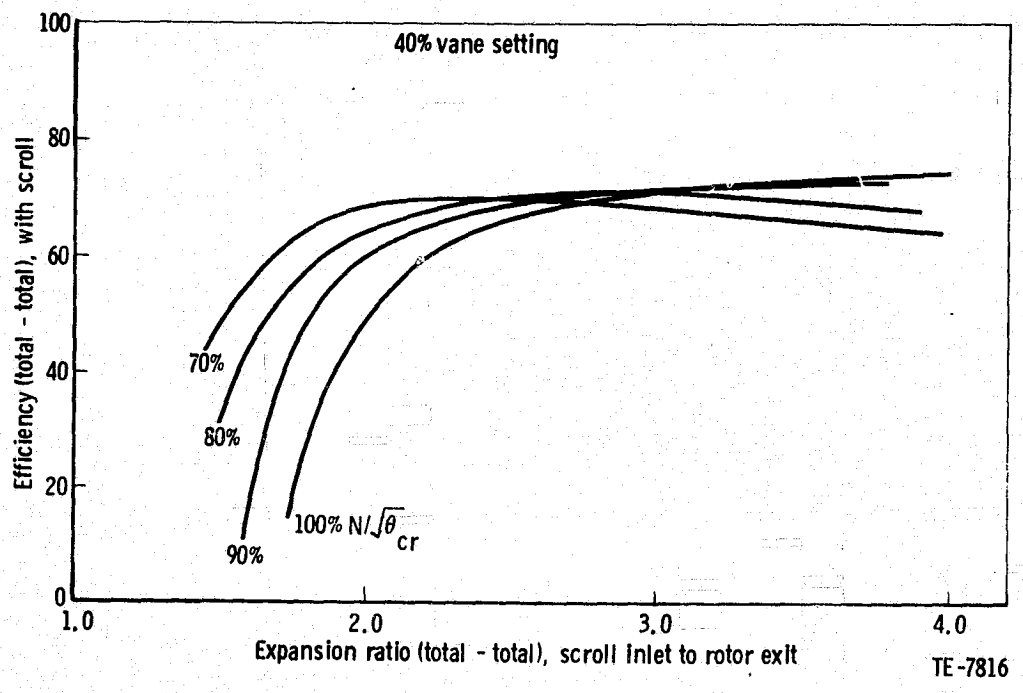

Figure 55. - AGT-2 Turbine Rig Test--BU 3 (corrected).

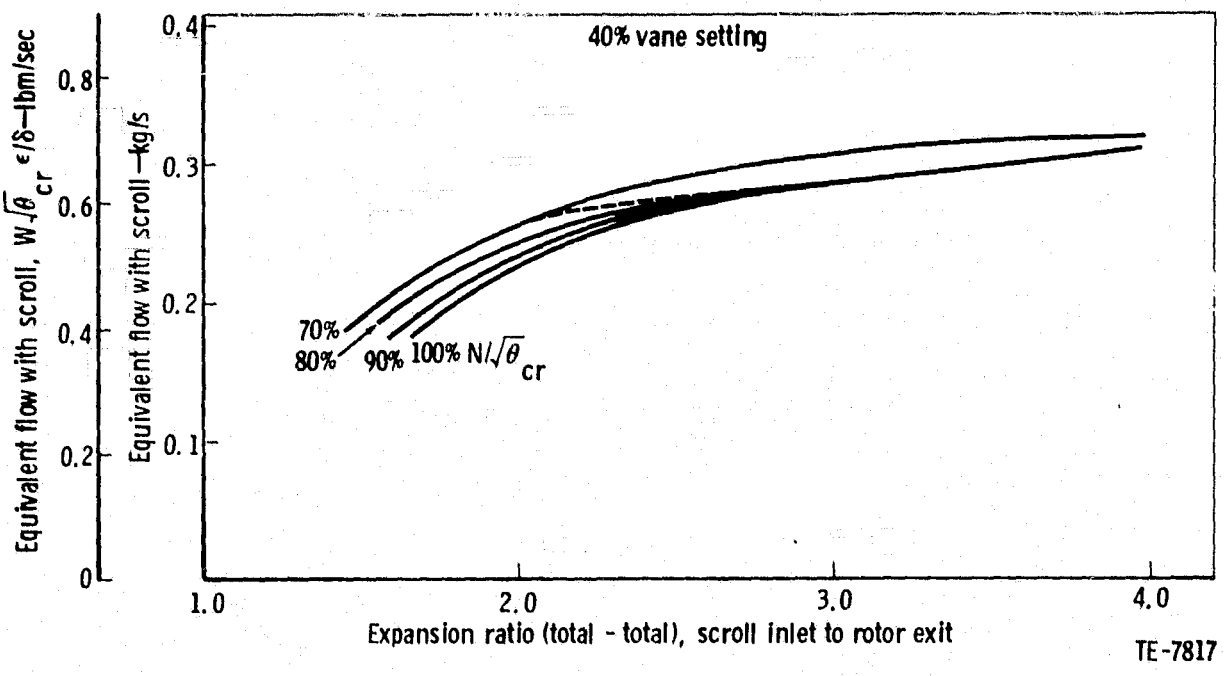

Figure 56. - AGT-2 Turbine Rig Test--BU 3 (corrected).

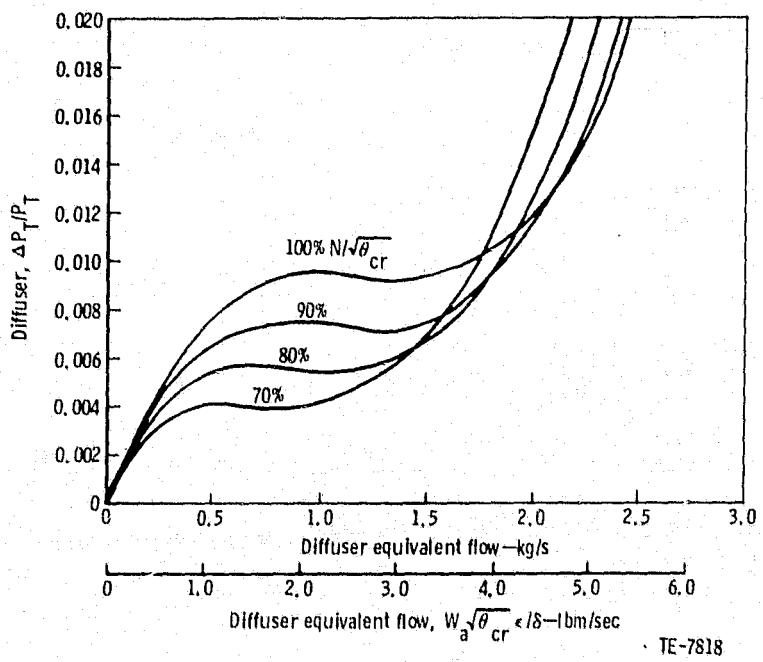

Figure 57. - AGT-2 Turbine Exhaust Diffuser at All Vane Settings.

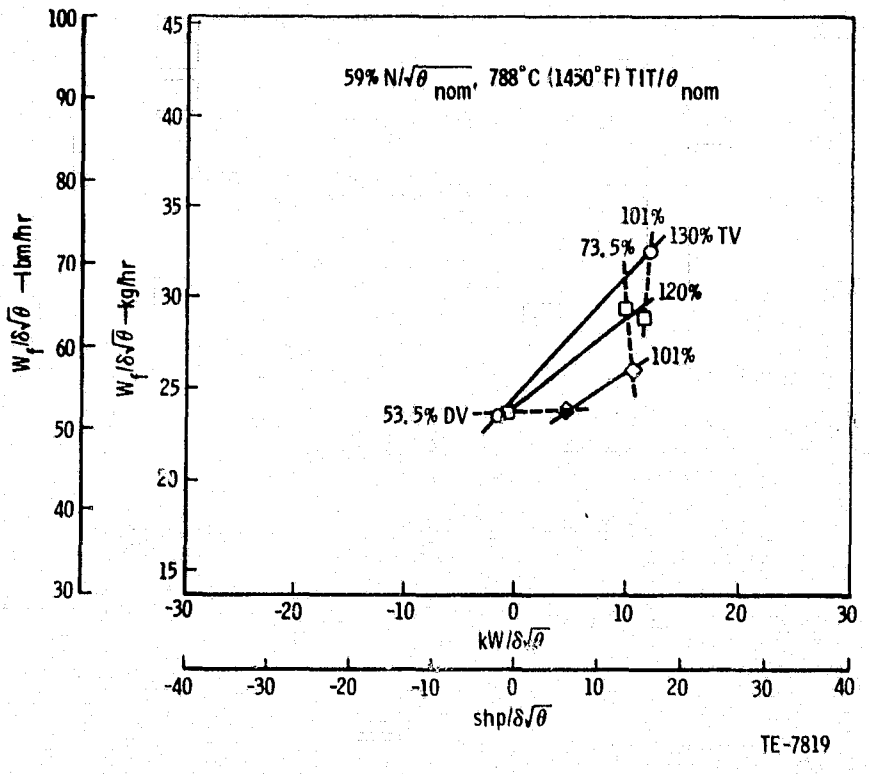

Figure 58. - AGT-2 Test.

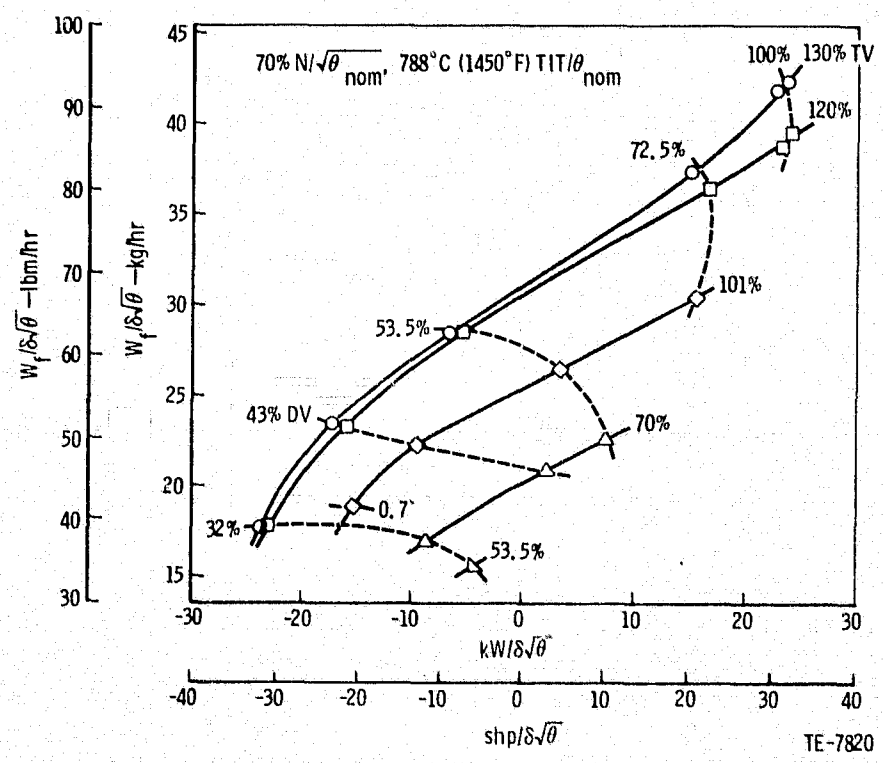

Figure 59. - AGT-2 Test.

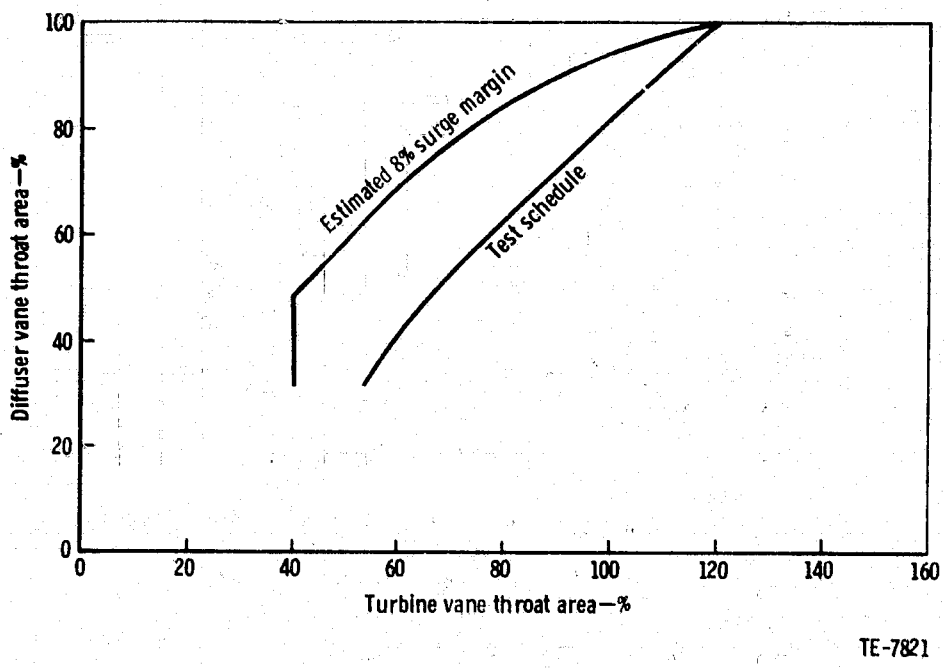

Figure 60. - AGT-2 Compressor-Turbine Variable Geometry Schedule.

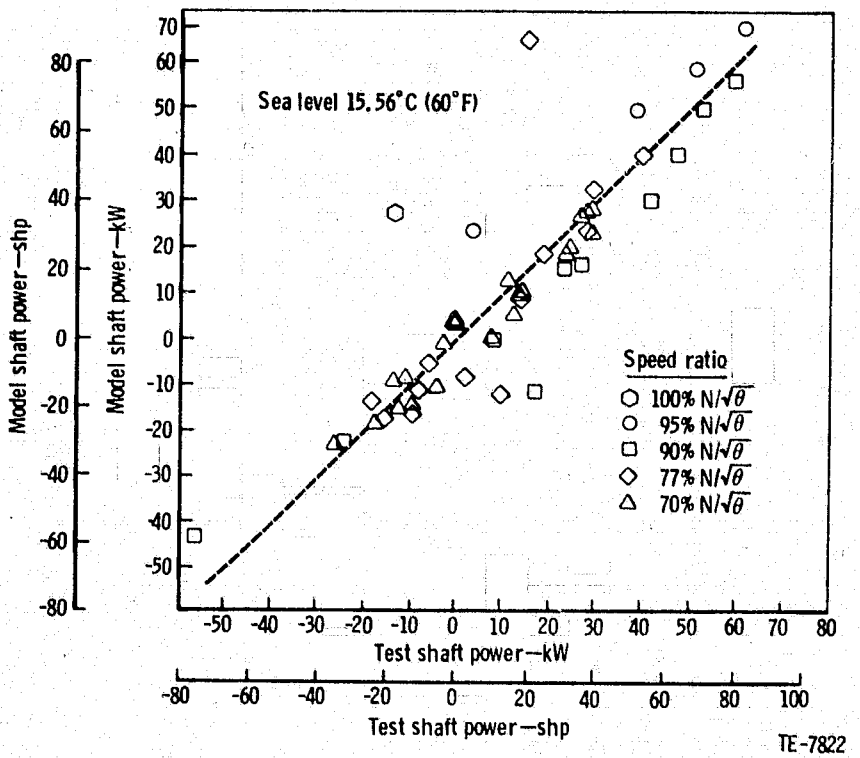

Figure 61. - Unadjusted Model Simulation vs Test Data.

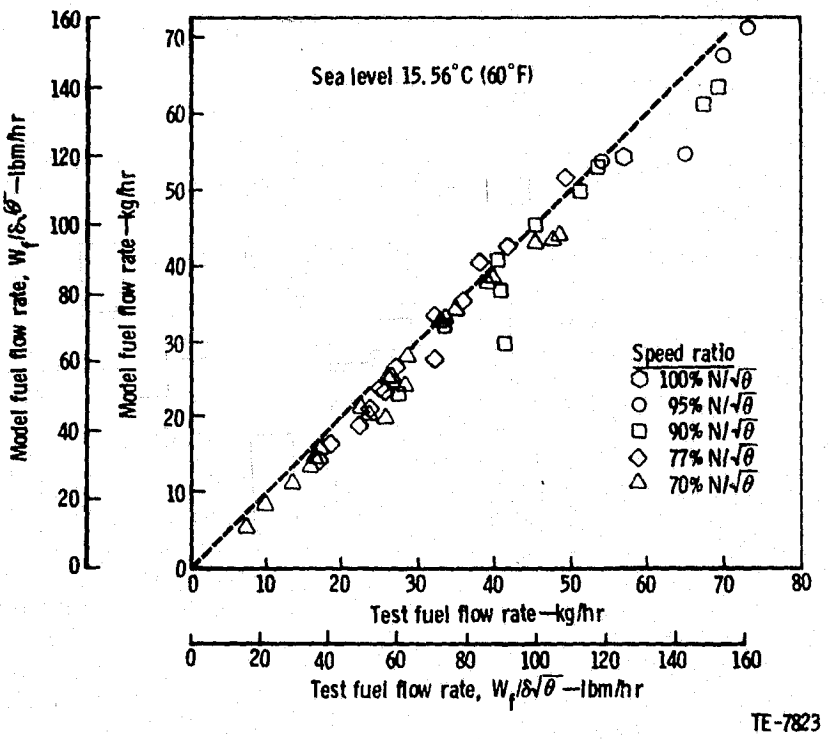

Figure 62. - Unadjusted Model Simulation vs Test Data.

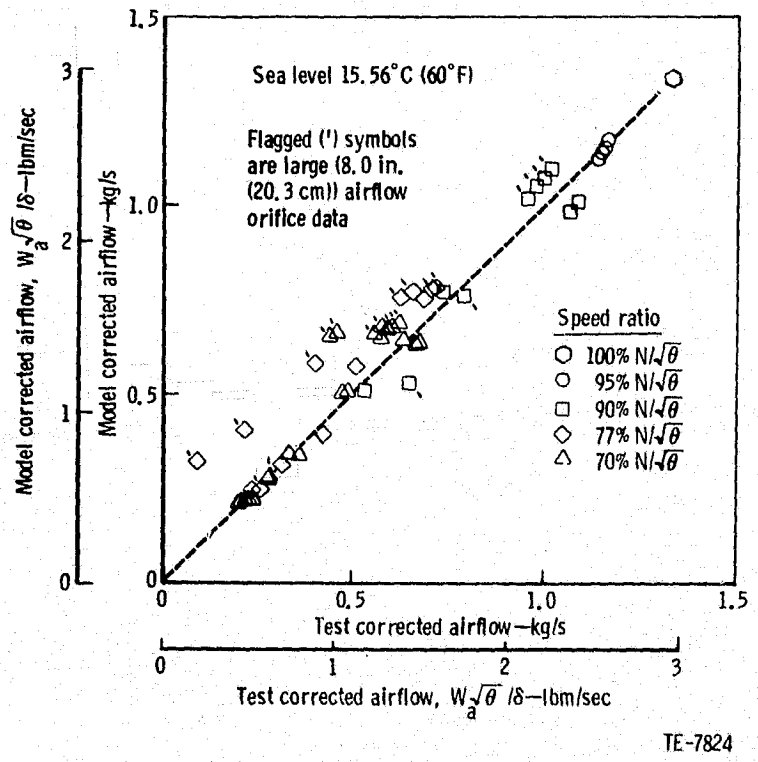

Figure 63. - Unadjusted Model Simulation vs Test Data.

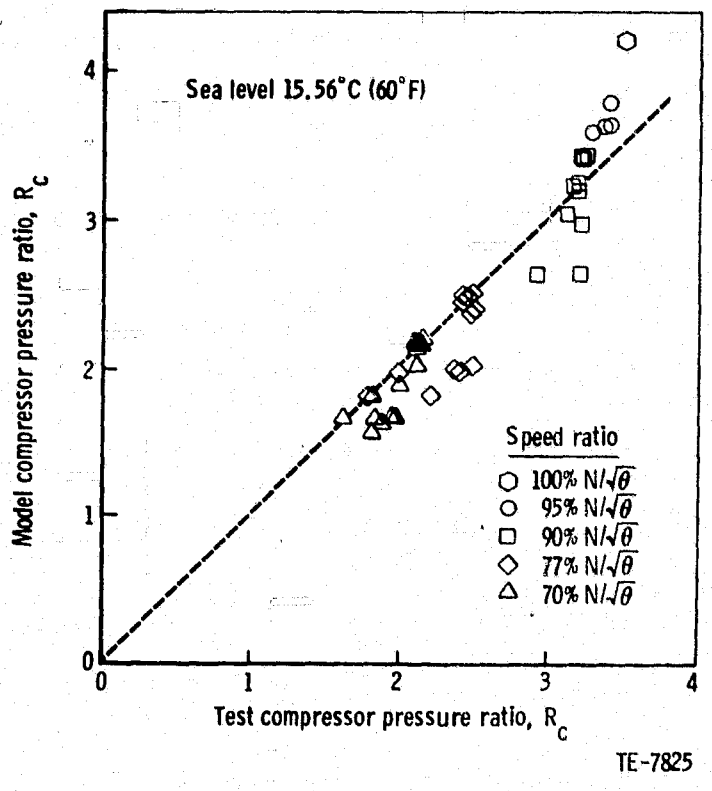

Figure 64. - Unadjusted Model Simulation vs Test Data.

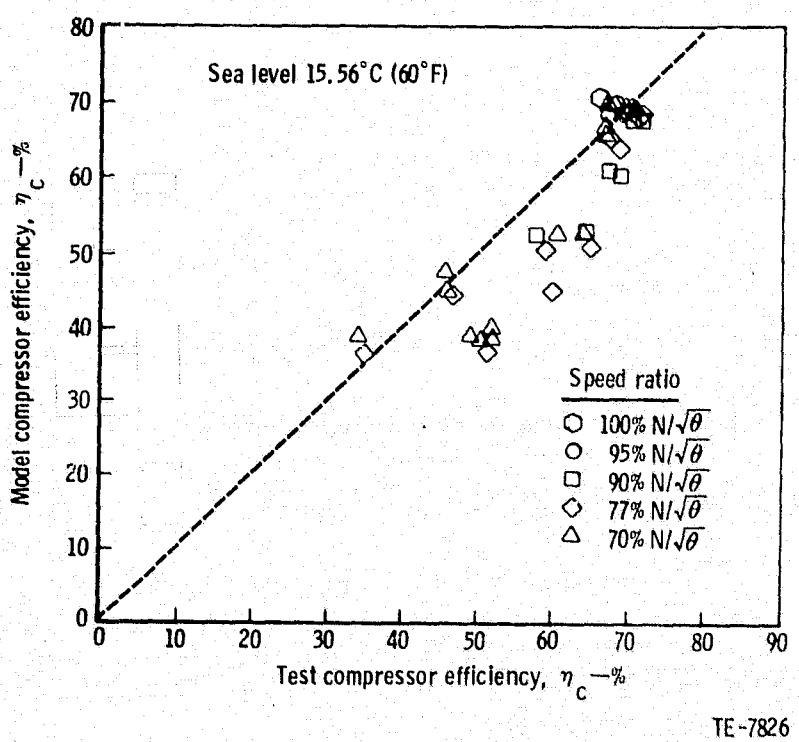

Figure 65. - Unadjusted Model Simulation vs Test Data.

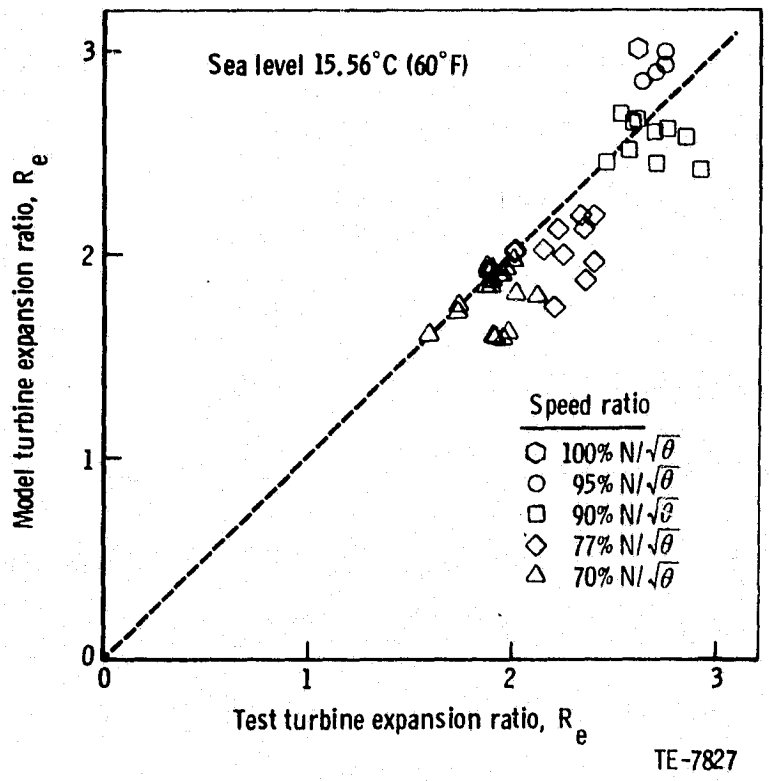

Figure 66. - Unadjusted Model Simulation vs Test Data.

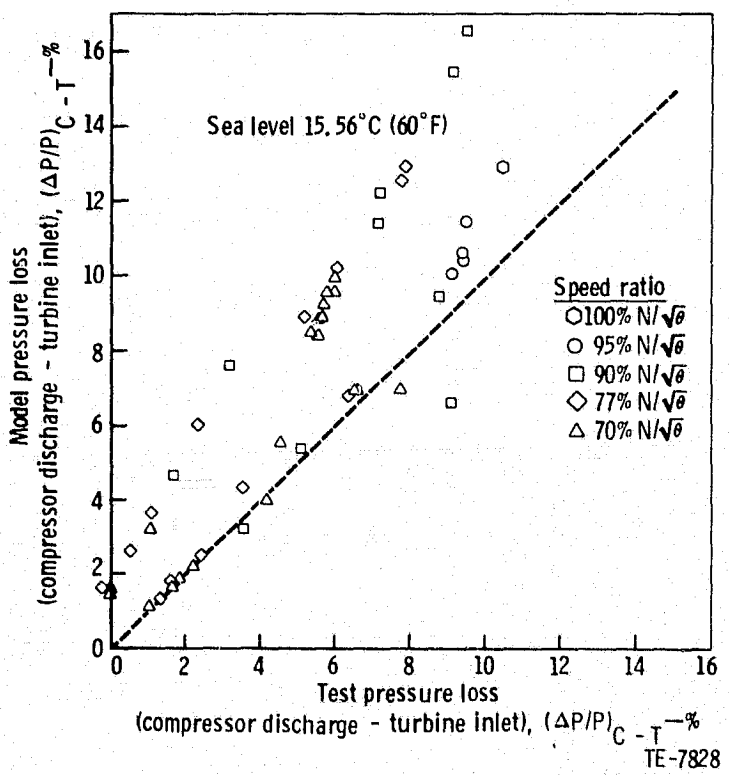

Figure 67. - Unadjusted Model Simulation vs Test Data.

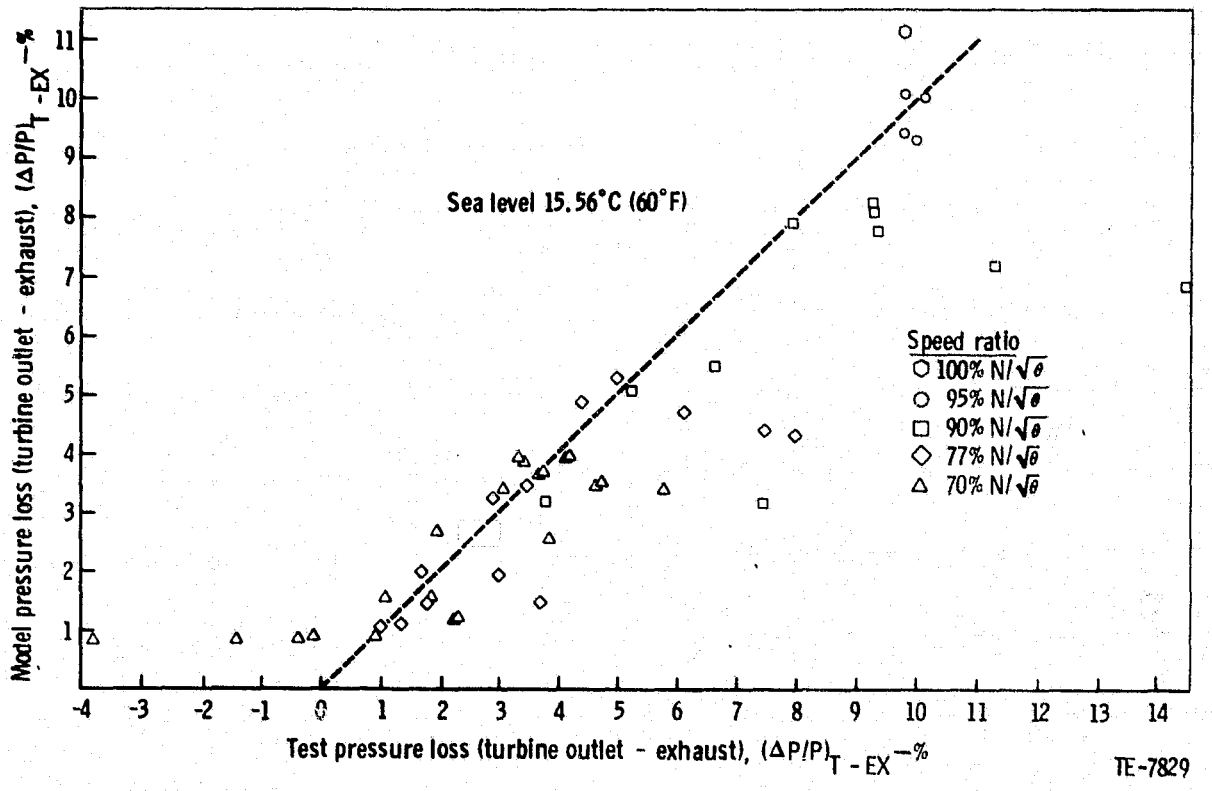

Figure 68. - Unadjusted Model Simulation vs Test Data.

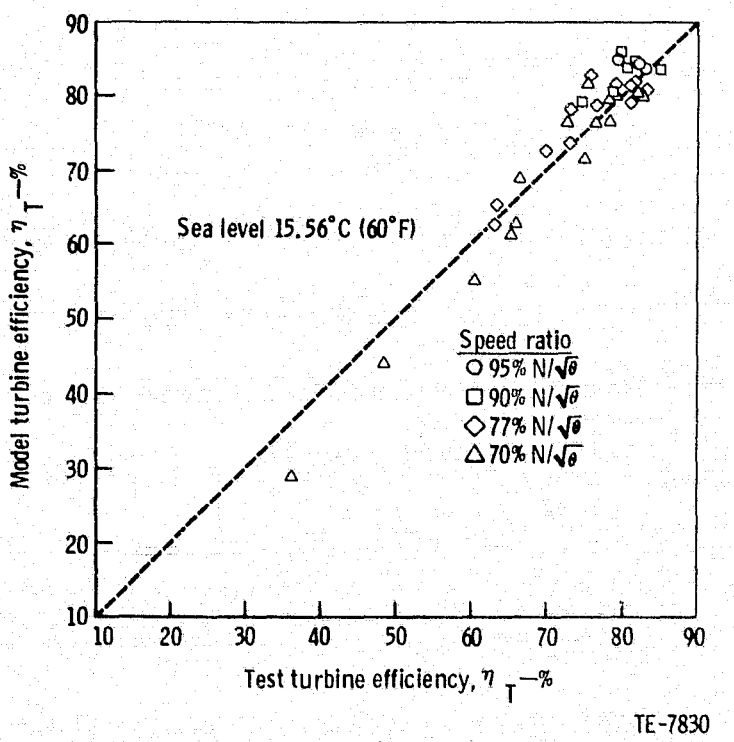

Figure 69. - Unadjusted Model Simulation vs Test Data.

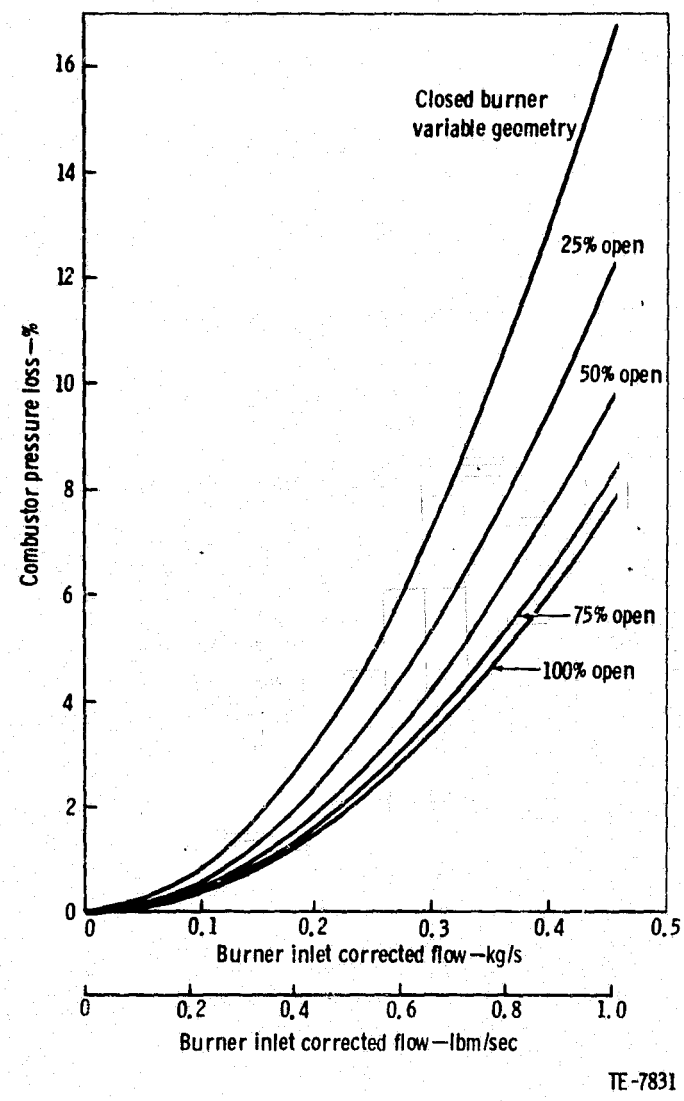

Figure 70. - AGT-2 Predicted Combustor Pressure Loss.

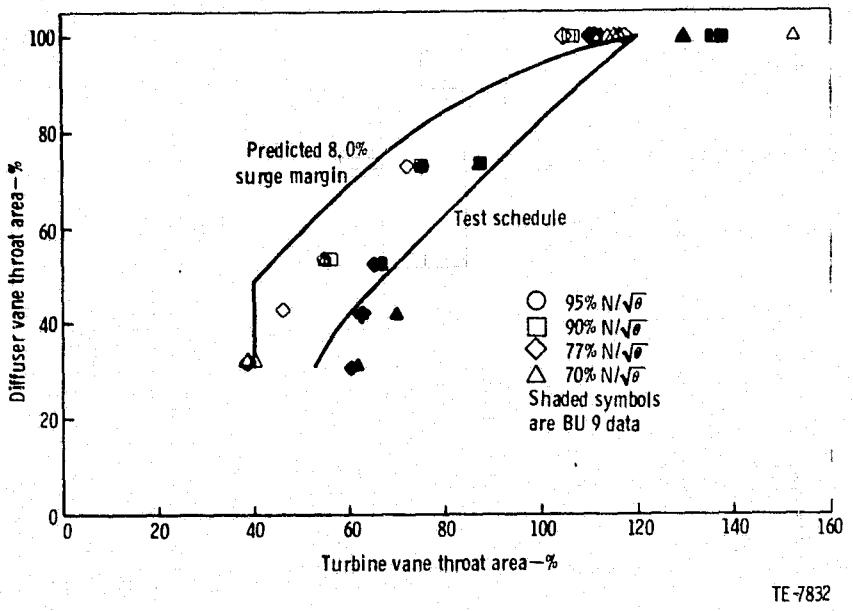

Figure 71. - Required Turbine Throat Area to Match Test Data.

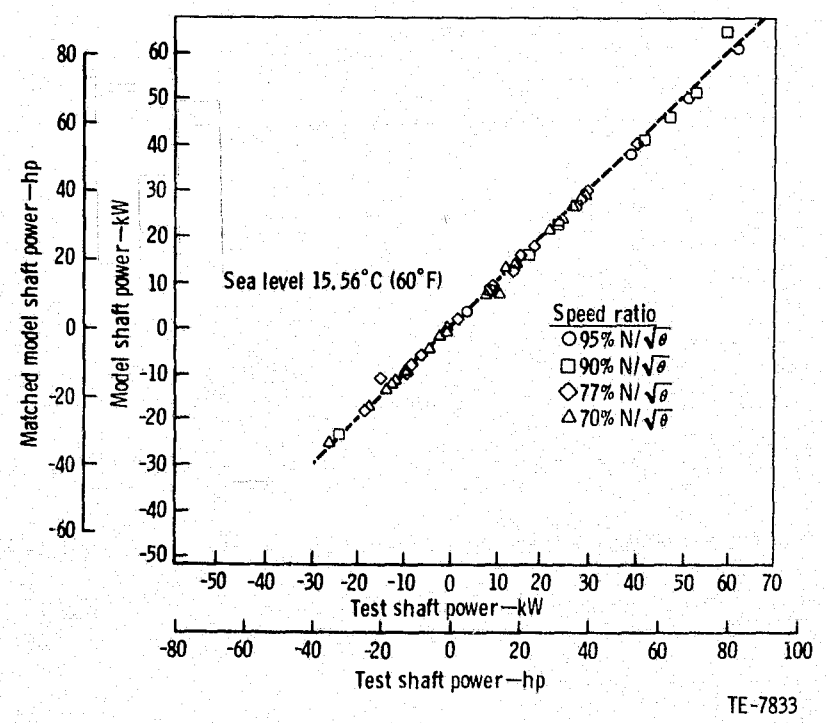

Figure 72. - Matched Model Simulation vs Test Data.

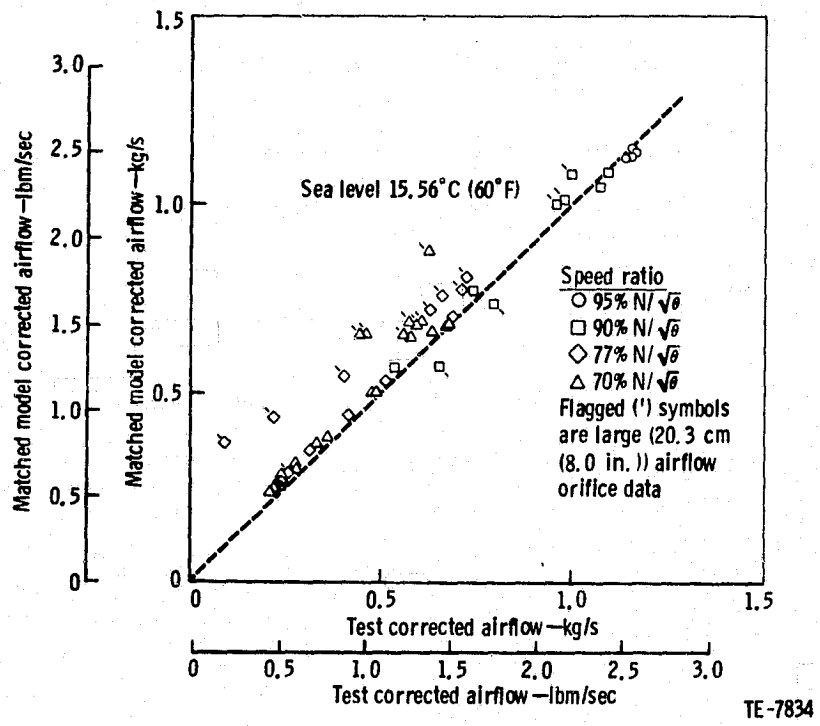

Figure 73. - Matched Model Simulation vs Test Data.

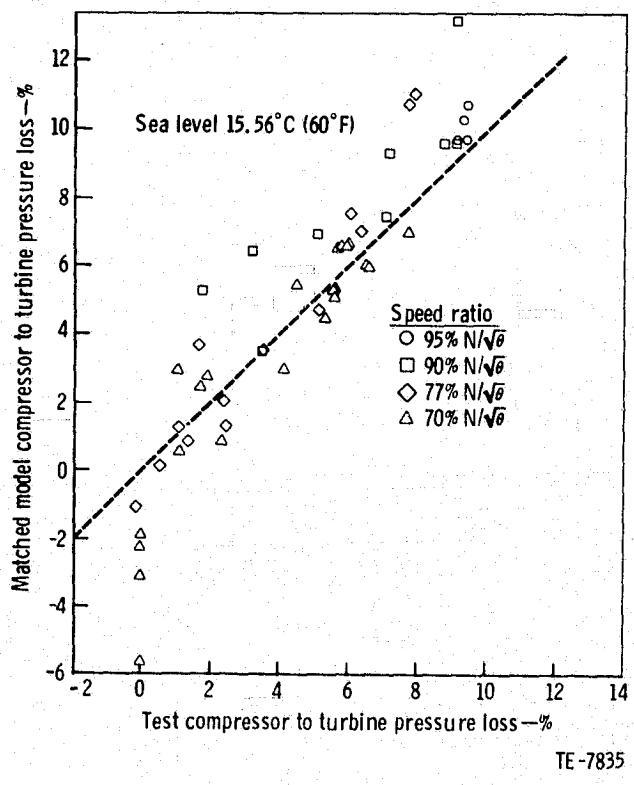

Figure 74. - Matched Model Simulation vs Test Data.

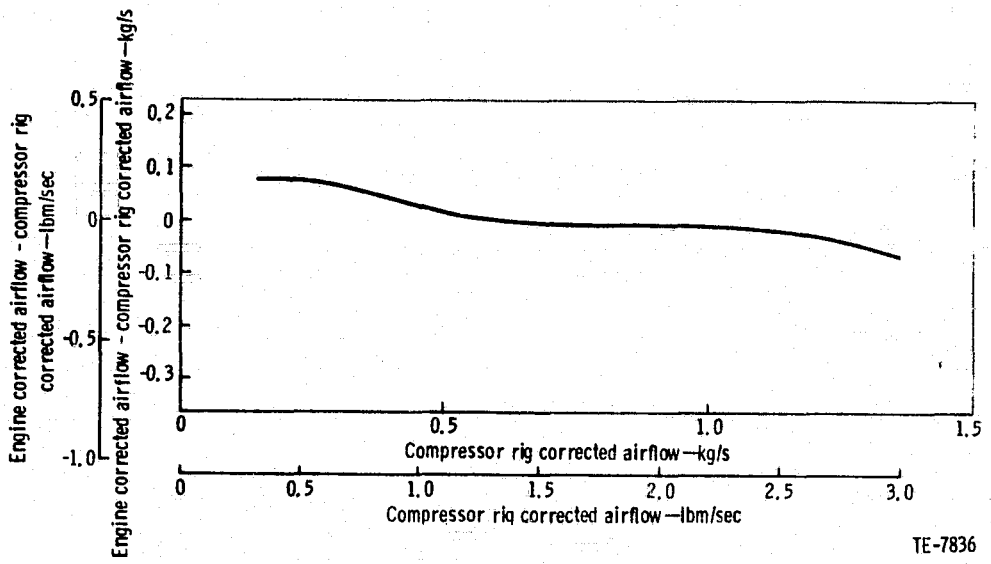

Figure 75. - Model Generalized Airflow Adjustments for All Diffuser Vane Settings.

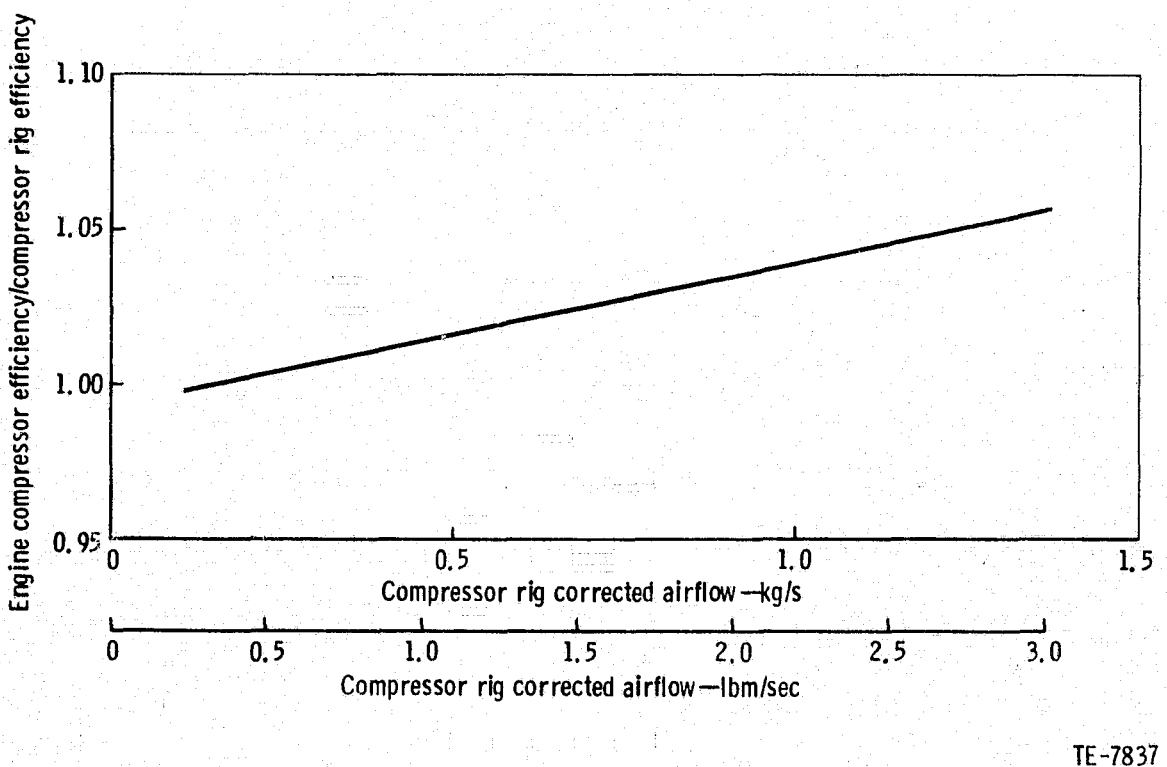

Figure 76. - Model Generalized Compressor Efficiency Adjustments for All Diffuser Vane Settings.

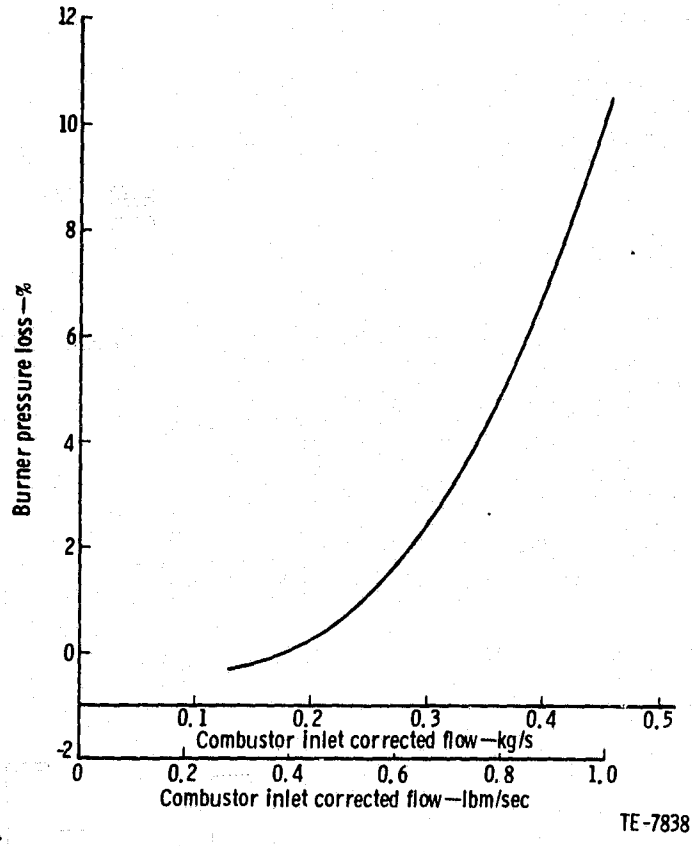

Figure 77. - Model Generalized Combustor Pressure Loss.

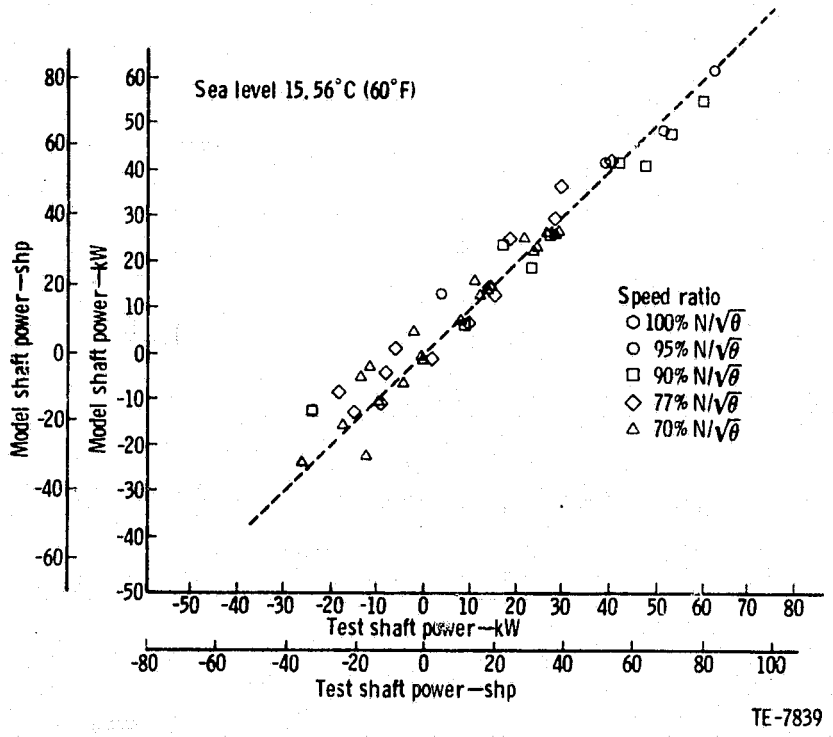

Figure 78. - Adjusted Model Simulation vs Test Data.

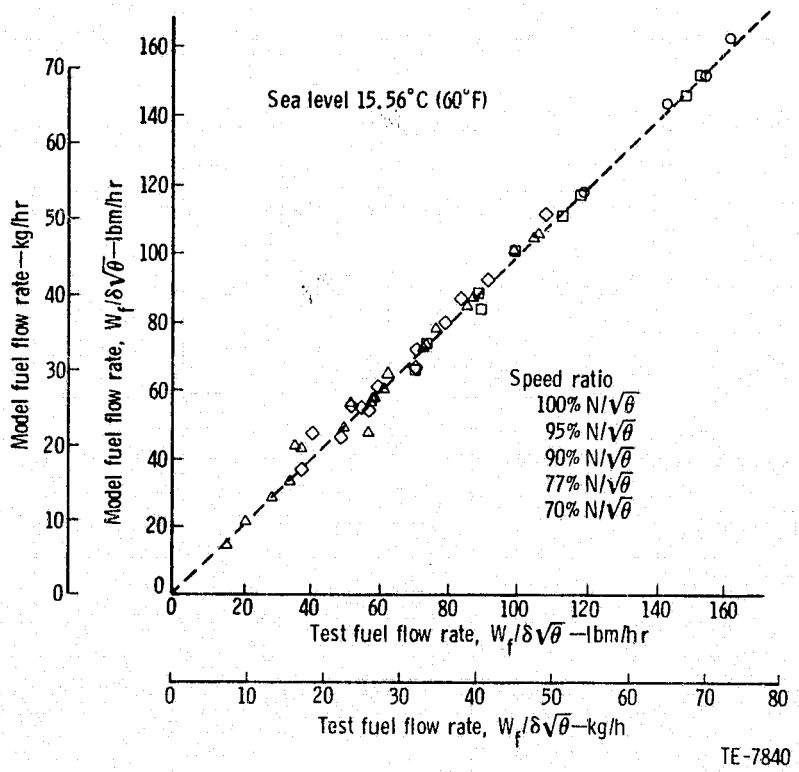

Figure 79. - Adjusted Model Simulation vs Test Data.

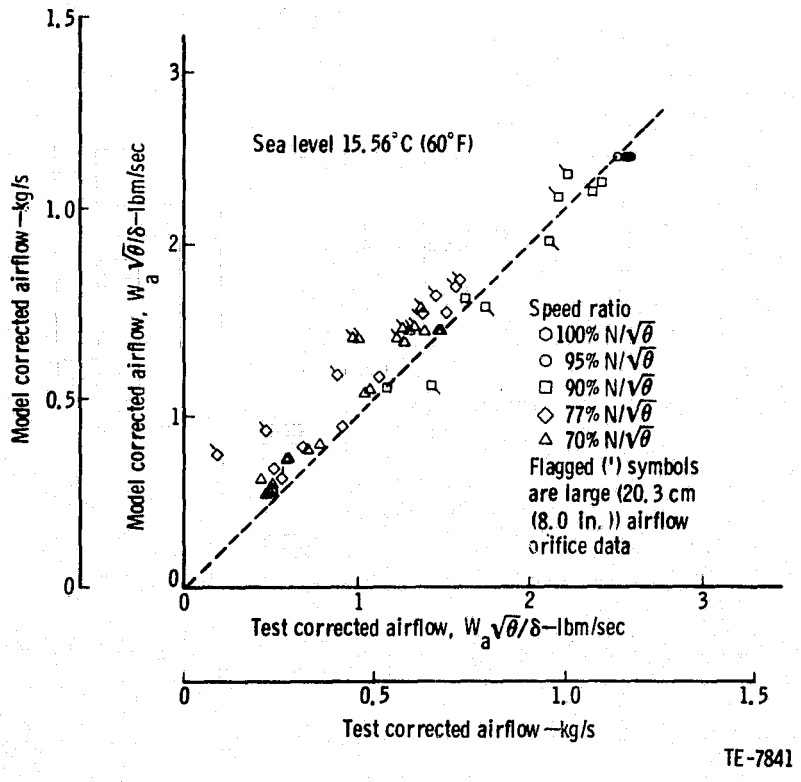

Figure 80. - Adjusted Model Simulation vs Test Data.

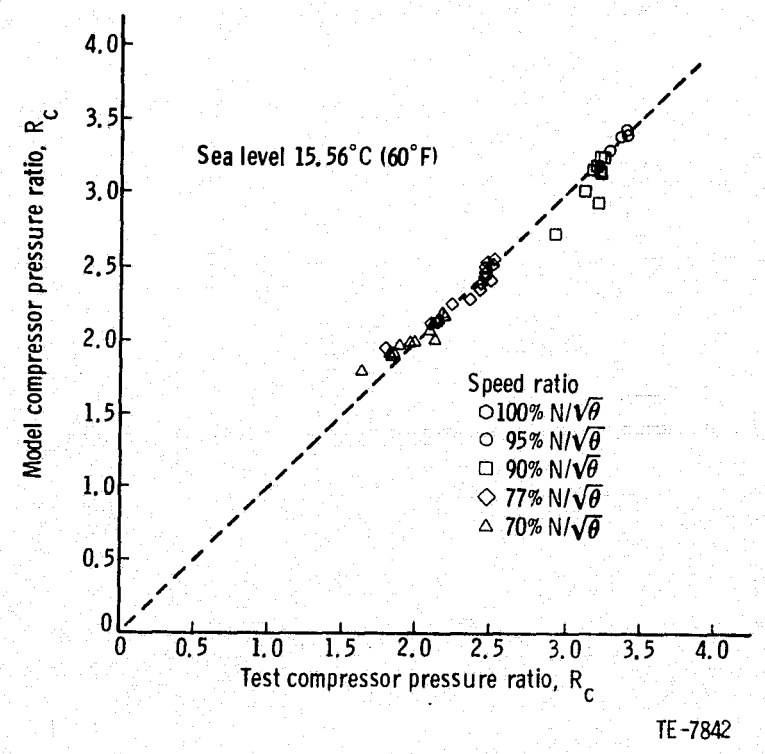

Figure 81. - Adjusted Model Simulation vs Test Data.

C - 2

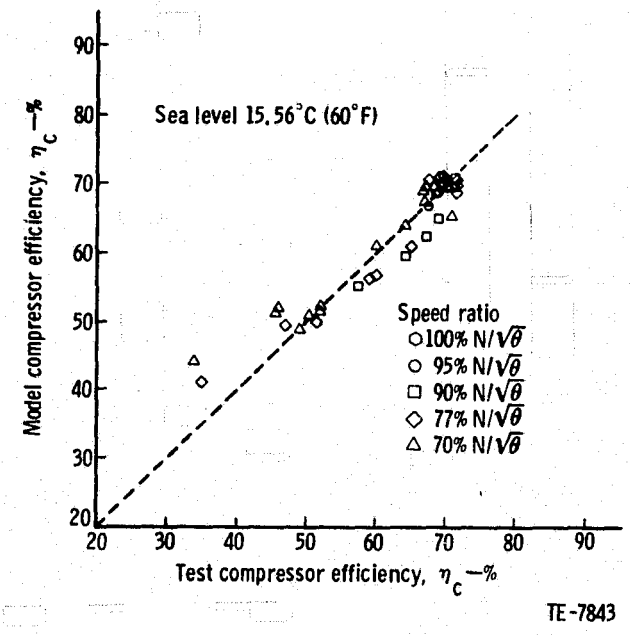

Figure 82. - Adjusted Model Simulation vs Test Data.

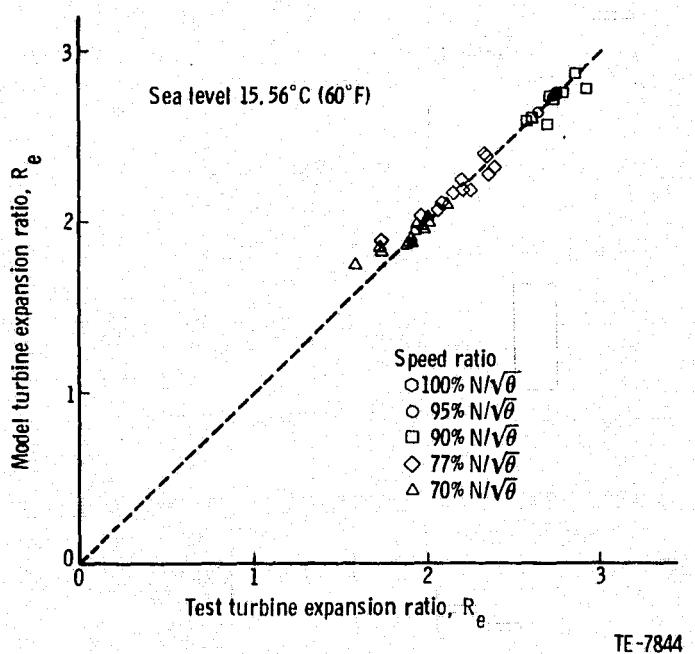

Figure 83. - Adjusted Model Simulation vs Test Data.

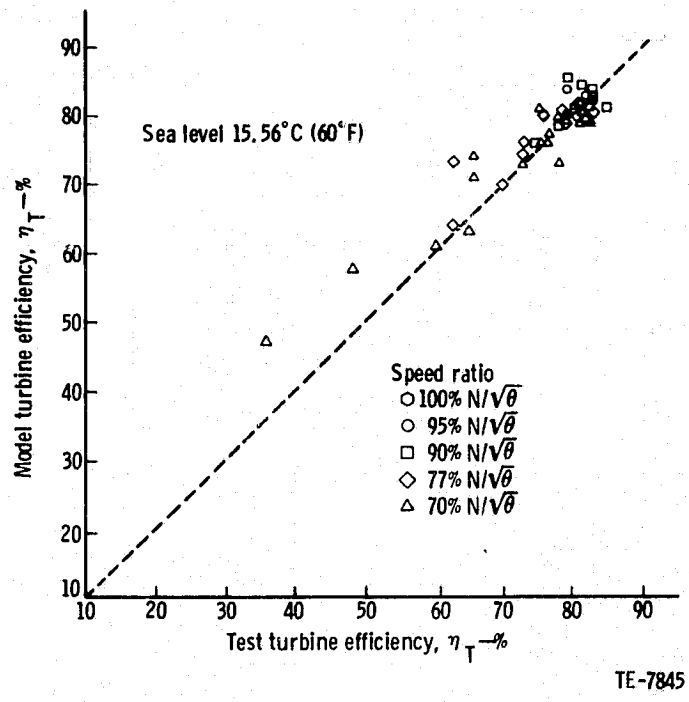

Figure 84. - Adjusted Model Simulation vs Test Data.

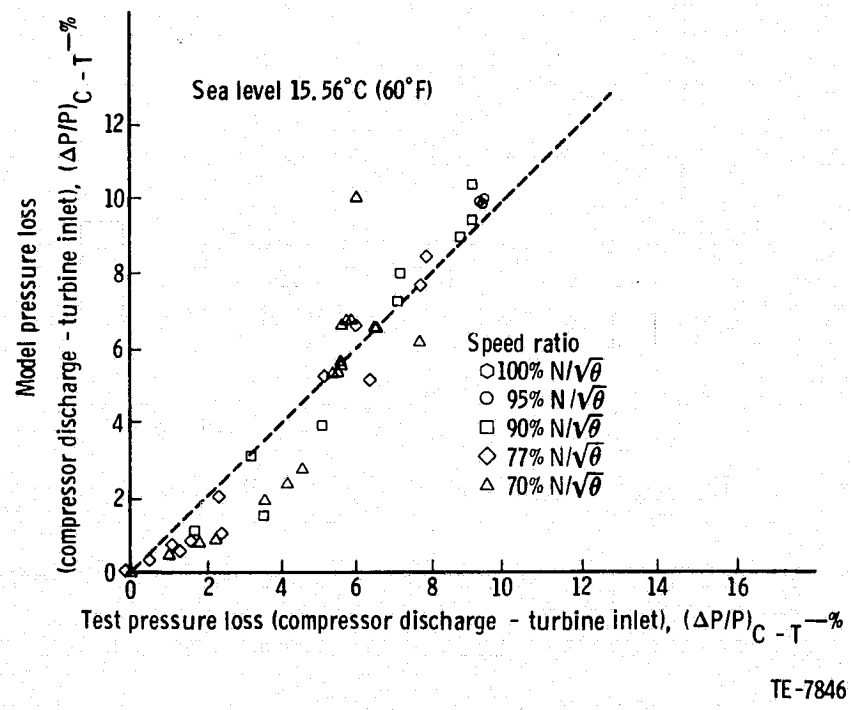

Figure 85. - Adjusted Model Simulation vs Test Data.

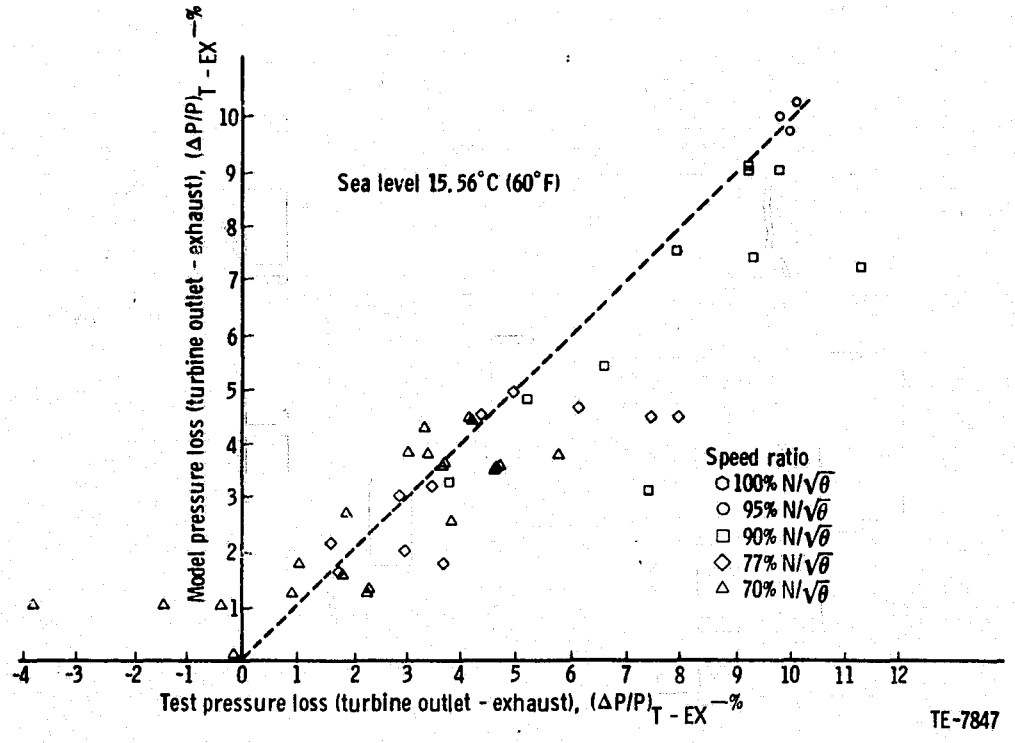

Figure 86. - Adjusted Model Simulation vs Test Data.

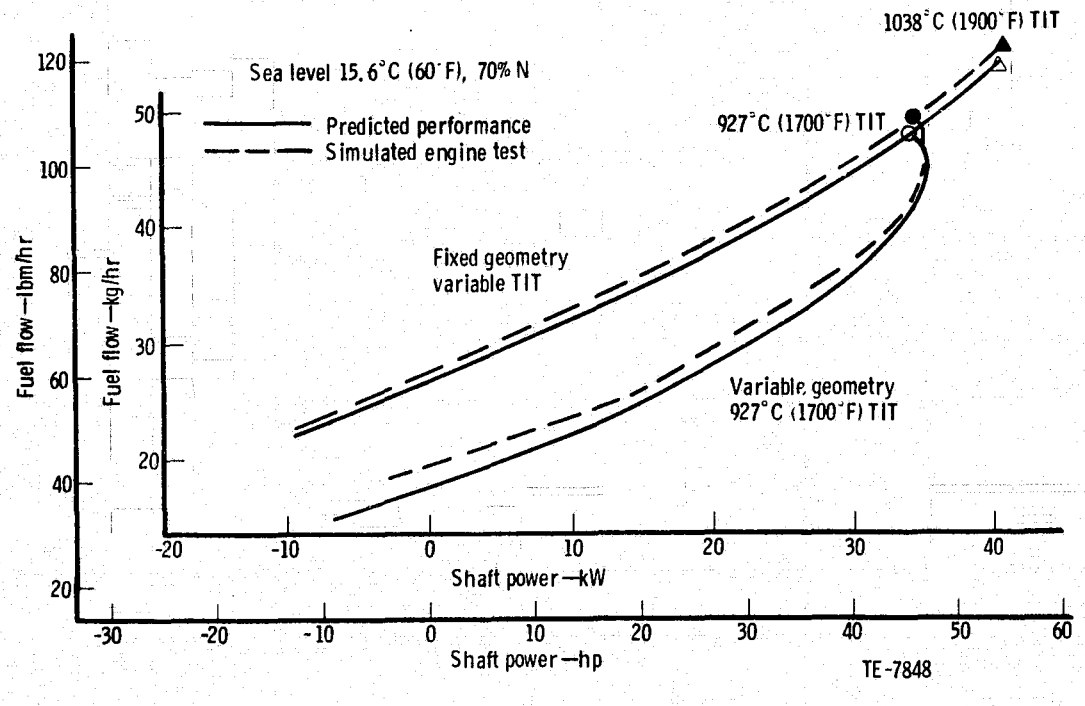

Figure 87. - AGT-2 Predicted Performance.

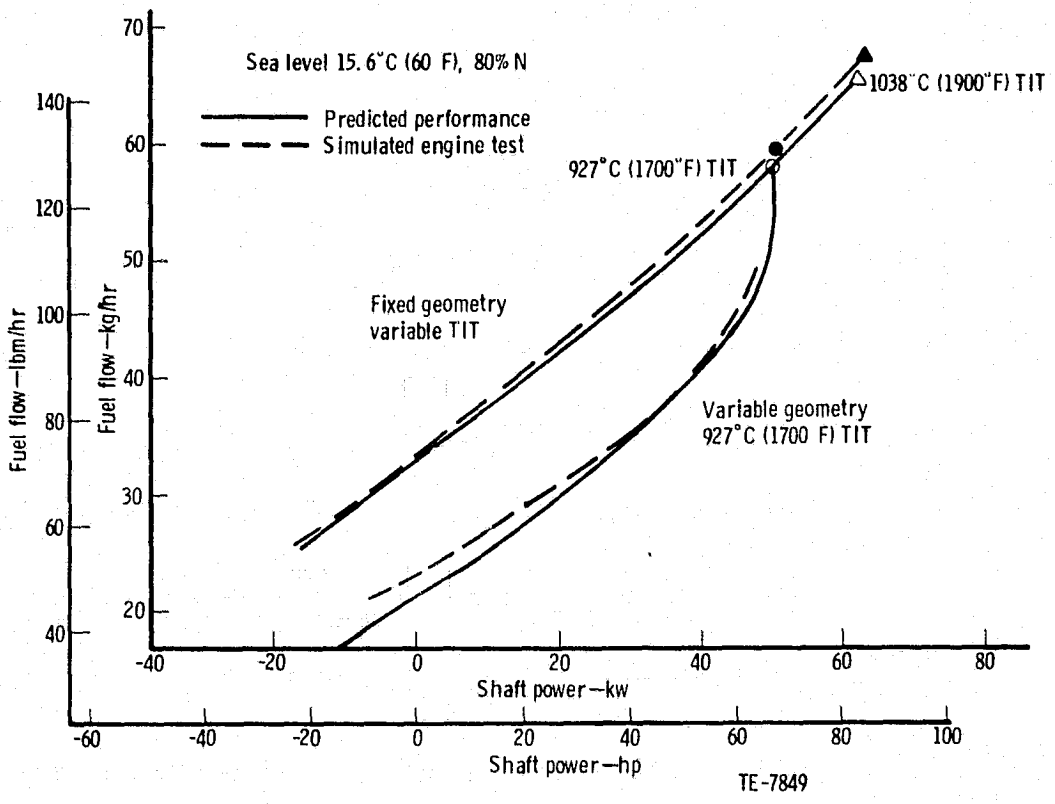

Figure 88. - AGT-2 Predicted Performance.

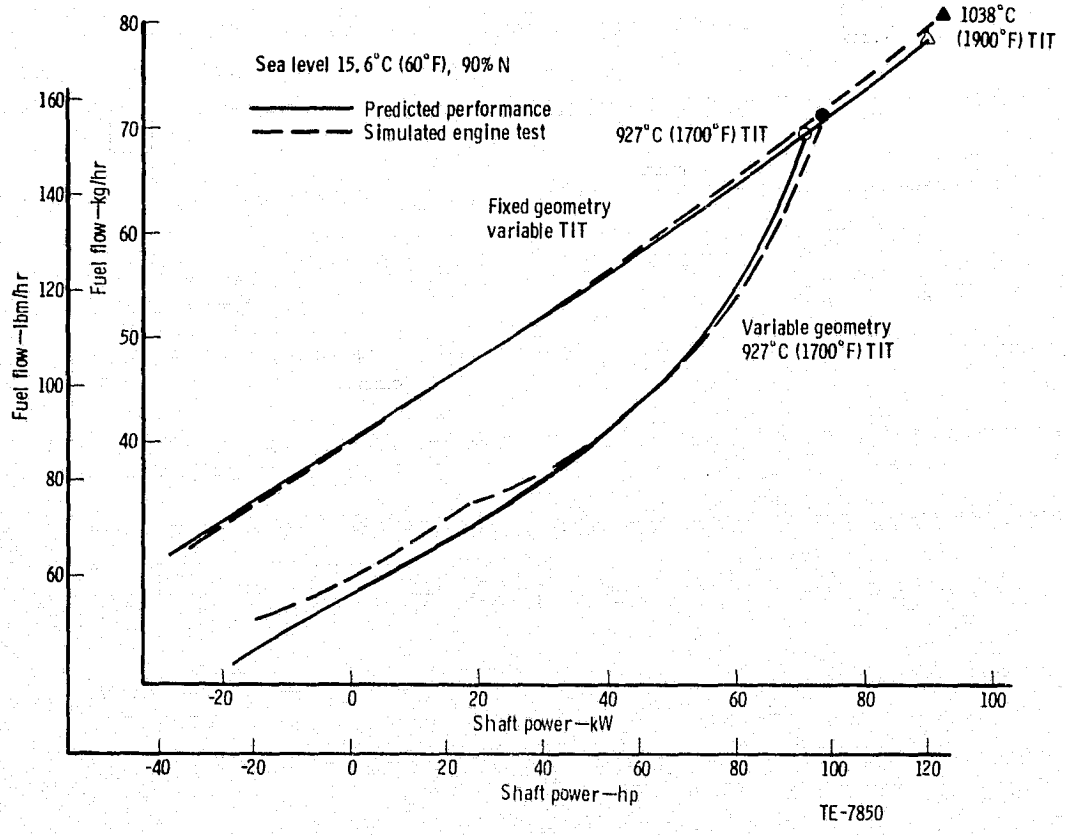

Figure 89. - AGT-2 Predicted Performance.

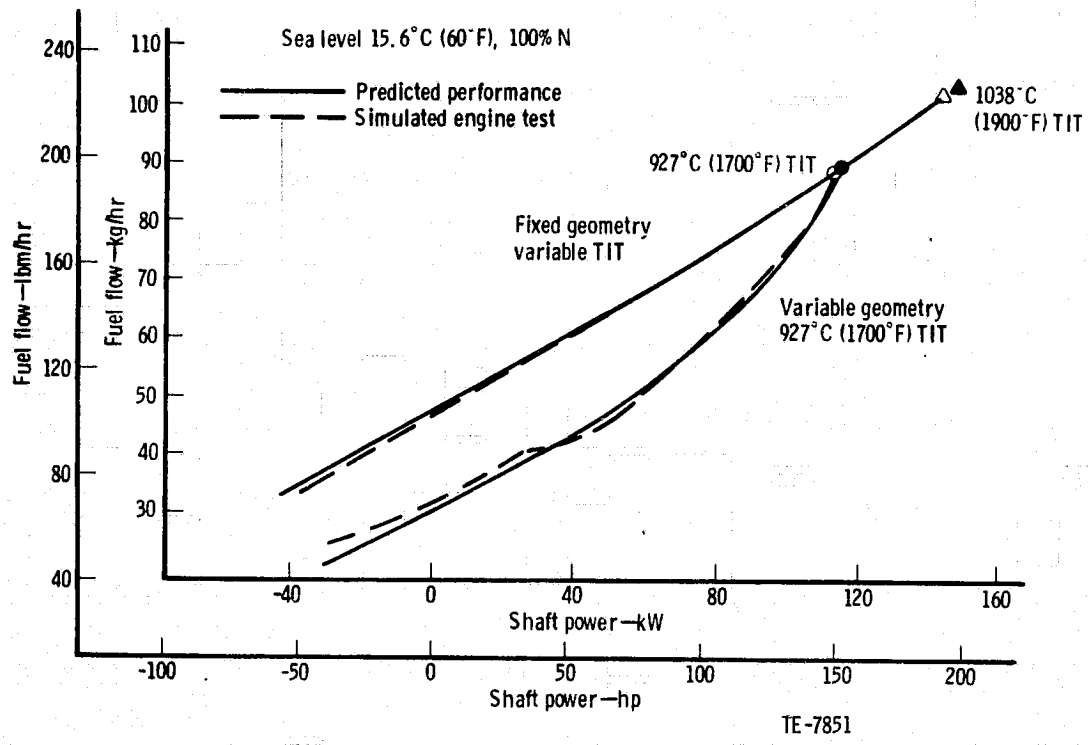

Figure 90. - AGT-2 Predicted Performance.

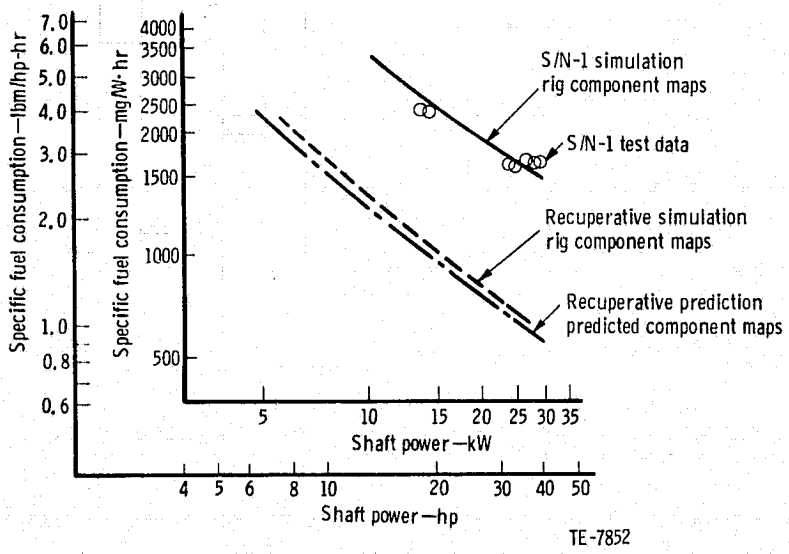

Figure 91. - AGT-2 Recuperative Performance.